NASA TECHNICAL NOTE

NASA TN D-3459

NASA TN D-3459

EFFECT OF THICKNESS AND SWEEP ANGLE ON THE LONGITUDINAL AERODYNAMIC CHARACTERISTICS OF SLAB DELTA PLANFORMS AT A MACH NUMBER OF 20

by Robert D. Witcofski and Don C. Marcum, Jr.

Langley Research Center
Langley Station, Hampton, Va.

NATIONAL AERONAUTICS AND SPACE ADMINISTRATION • WASHINGTON, D. C. • JUNE 1966

EFFECT OF THICKNESS AND SWEEP ANGLE ON THE LONGITUDINAL AERODYNAMIC CHARACTERISTICS OF SLAB DELTA PLANFORMS AT A MACH NUMBER OF 20

By Robert D. Witcofski and Don C. Marcum, Jr.

Langley Research Center
Langley Station, Hampton, Va.

NATIONAL AERONAUTICS AND SPACE ADMINISTRATION

For sale by the Clearinghouse for Federal Scientific and Technical Information
Springfield, Virginia 22151 – Price $3.00

EFFECT OF THICKNESS AND SWEEP ANGLE ON THE LONGITUDINAL AERODYNAMIC CHARACTERISTICS OF SLAB DELTA PLANFORMS AT A MACH NUMBER OF 20

By Robert D. Witcofski and Don C. Marcum, Jr.
Langley Research Center

SUMMARY

An investigation has been conducted at a free-stream Mach number of approximately 20 to determine the effects of sweep angle and thickness on the longitudinal aerodynamic characteristics of basic delta planforms. The sweep angles investigated were 45°, 60°, 70°, 80°, 85°, and 90°, and the ratio of thickness to root-chord length varied from 0 to 0.3. Reynolds number based on wing length varied from 1.4×10^6 to 6.6×10^6 and the angle-of-attack range was approximately from 0° to 30°. Within the limits of the investigation, experimental estimates of the optimum sweep angles for obtaining maximum lift-drag ratio for a given thickness ratio were made. Also obtained were experimental curves for determining the slopes of the normal-force curves and lift curves at zero angle of attack. Maximum lift-drag ratio exhibited a nearly linear decay as thickness ratio and volumetric coefficient were logarithmically increased. Angle of attack at maximum lift-drag ratio increased nearly exponentially with thickness ratio. Increasing wing thickness from zero shifted the center of pressure forward from the 2/3-root-chord point. Newtonian impact theory and a modified Newtonian impact theory plus skin-friction calculations were generally adequate for predicting trends only.

INTRODUCTION

The advantages in the ability of reentry or cruise vehicles to develop lifting capabilities at hypersonic speeds have been recognized for some time. Even small lifting capabilities tend to reduce entry deceleration and allow some range control, although some form of landing aid may be required. As lifting capabilities increase, deceleration loads are minimized, range control is greatly extended, and it is not at all unlikely that conventional landings could be executed. It was pointed out in reference 1, for instance, that the ability of glide vehicles to convert velocity to range is dependent to a large extent on their ability to develop sizable hypersonic lift-drag ratios. Increases in vehicle lifting capabilities tend to decrease the entry heating rate but may also increase the total heat absorbed. Reference 1 has also indicated that if hypersonic reentry vehicles are to

develop relatively high hypersonic lift-drag ratios and survive the high heating rates, the vehicles must have rounded noses and highly swept wings with rounded leading edges to reduce local heating problems while incurring minimum drag penalties. Of lifting configurations operating in high-speed ranges, the basic delta planform is of particular interest in that it has a relatively small movement of aerodynamic center with variations in Mach number (ref. 2).

The purpose of this paper is to present the results of an investigation conducted at a Mach number of approximately 20 to determine the effect of variation of sweep angle and thickness ratio on the longitudinal aerodynamic characteristics of basic delta planforms. Preliminary results of this investigation are presented in reference 3. The sweep angles investigated are 45°, 60°, 70°, 80°, 85°, and 90°. Wing leading edges were hemicylinders and the noses were spherical segments. The ratio of leading-edge diameter to root chord varied from 0 to 0.3. Reynolds number based on root-chord length varied from 1.4×10^6 to 6.6×10^6, but for wings having thickness ratios of 0.034 or less a constant Reynolds number of 3.7×10^6 was maintained to minimize possible Reynolds number effects. Angle of attack was approximately from 0° to 30°. Particular emphasis is placed on maximum lift-drag ratio, and the experimental results are compared with those obtained from Newtonian impact theory and a combination of modified Newtonian impact theory and skin-friction calculations.

SYMBOLS

Measurements for this investigation were taken in the U.S. Customary Units but are also given parenthetically in the International System of Units (SI). To promote use of this system in future NASA reports, details concerning the use of SI units, together with physical constants and conversion factors, are given in reference 4.

c wing root-chord length, inches (meters)

C_A axial-force coefficient, $\frac{F_A}{q_\infty S}$

C_D drag coefficient, $\frac{\text{Drag}}{q_\infty S}$

C_L lift coefficient, $\frac{\text{Lift}}{q_\infty S}$

C_{L_α} lift-curve slope at $\alpha = 0^{\circ}$, per degree

$C_{L,(L/D)_{max}}$ lift coefficient at maximum lift-drag ratio

C_m pitching-moment coefficient about a point two-thirds of model length rearward from nose on model center line, $\frac{M_Y}{q_\infty Sc}$

C_N normal-force coefficient, $\frac{F_N}{q_\infty S}$

C_{N_α} normal-force-curve slope at $\alpha = 0^o$, per degree

$C_{p,max}$ maximum pressure coefficient, $\frac{p - p_\infty}{q_\infty}$

F_A axial force, pounds force (newtons)

F_N normal force, pounds force (newtons)

L/D lift-drag ratio, C_L/C_D

M_Y pitching moment about a point two-thirds of model length rearward from nose on model center line, inch-pounds force (meter-newtons)

M_∞ free-stream Mach number

p pressure

p_∞ free-stream static pressure

q_∞ free-stream dynamic pressure, pounds force/inch^2 (newtons/meter^2)

r wing leading-edge radius and nose radius, inches (meters)

r_b base radius of balance-housing body, inches (meters) (see fig. 1)

R Reynolds number, based on root-chord length

S planform area, inches^2 (meters^2)

t wing thickness, inches (meters)

t/c thickness ratio

V volume of wing or of wing and balance-housing body, inches^3 (meters^3)

$V^{2/3}/S$	volumetric coefficient
x	distance along wing longitudinal axis, measured from nose of wing, inches (meters)
x_{cp}/c	location of center of pressure
α	angle of attack, degrees
$\alpha_{(L/D)_{max}}$	angle of attack at maximum lift-drag ratio, degrees
γ	ratio of specific heats
Λ	wing sweep angle, degrees (fig. 1)

Subscript:

max	maximum

MODELS, FACILITY, AND TESTS

Models and Wind Tunnel

The basic configuration (fig. 1(a)) consisted of slab delta planforms with sweep angles of 45°, 60°, 70°, 80°, 85°, and 90°. The thickness ratio t/c varied from 0 to 0.3. The models had either hemicylindrical leading edges and spherical-segment noses or sharp leading edges and noses. A sketch of the basic configuration with a balance-housing body is shown in figure 1(b). Figure 1(c) is a sketch of the wings used to simulate zero leading-edge thickness and of the balance-housing bodies associated with them. A photograph of the 80° sweep-angle wings is figure 3. Basic dimensions for all models tested are given in table I.

All tests were conducted in the Langley 22-inch helium tunnel (fig. 2) by utilizing a contoured nozzle to obtain Mach numbers on the order of 20. A detailed description of the tunnel characteristics is given in reference 5. The free-stream Mach number for the present investigation was 20.3 for all but the zero-leading-edge-thickness wings, for which, to maintain a constant Reynolds number, stagnation pressures were selected based on the results of reference 5. Reynolds number based on wing length was approximately 3.7×10^6 for wings which had thickness ratios of 0.034 or less and ranged from 1.43×10^6 to 6.60×10^6 for the entire investigation. The free-stream Mach numbers and the Reynolds numbers are given in table I. Stagnation temperature decreased about 20° F (11° K) during each test because of decreasing reservoir pressure; however, an average stagnation temperature of 70° F (294° K) would be representative. The angle-of-attack range was approximately from 0° to 30°.

Instrumentation

The optical system described in reference 6 was utilized to measure pitch attitude. Data were obtained by the use of five different strain-gage balances. Because of the physical size of the strain-gage balances used to measure forces and moments in this investigation it was impossible to house the strain-gage balances completely within the more slender wings, that is, wings having thickness ratios of 0.034 or less. Balance-housing bodies were therefore necessary on the leeward surfaces of the more slender wings. A sketch of the balance-housing body on the basic configuration and a table containing pertinent information on the geometry of the balance-housing bodies are shown in figure 1(b). At the time the zero-leading-edge-thickness wings were tested, a new external strain-gage balance became available and made possible the use of a much smaller balance-housing body, as seen in figure 1(c). The effect of the balance-housing body on the validity of the data was determined by retesting the wing having a thickness ratio of 0.01 and a sweep angle of 80° by utilizing the external balance which required a balance-housing body having only 18 percent as much volume as the balance-housing body used when the wing was first tested. Results from tests on both bodies, the large balance-housing body and the small balance-housing body, are presented in figure 4. As can be seen in the figure, the reduction in body size, as well as a reduction in the angle of attack at which the balance-housing body was hidden from the flow, resulted in only small changes in the basic force data and about a 3-percent increase in $(L/D)_{max}$, which is believed to be within the accuracy of the data. As a result of these tests, it is believed, at least for the wings having sweep angles of 80° or less, that the balance housing had no significant effect on the wing characteristics.

An additional test of the same wing with the large balance-housing body was made to determine the possible presence of Reynolds number effects. These data at a Reynolds number of 6.60×10^6 are compared with those at a Reynolds number of 3.66×10^6 in figure 4. The data show that the change in Reynolds number produced only small differences in the force and moment data.

Base pressures were not measured for the present investigation and therefore the data have not been corrected to a condition where free-stream pressures would exist on the base. However, base pressures were measured on delta-wing—half-cone bodies of reference 7, and from the results of reference 7 it is thought that base pressures in the range of three times free-stream static pressure should be realistic. When applied to the present data, base pressures of this magnitude would result in corrections to the axial force which were smaller than the inaccuracy of the strain-gage balances used for the present investigation.

Accuracy

Tabulated estimations of the accuracy of the data are shown in coefficient form in table I. These estimations were computed by using the quoted accuracy of static-balance calibrations.

The estimated pitching-moment accuracy includes the possible error incurred when pitching-moment reference center is transferred from the moment reference center of the balance to the moment reference center selected on the models. This transfer introduces the inaccuracy in the normal-force component into the inaccuracy already present in the balance pitching-moment component. The moment reference center for all wings was at a point two-thirds the chord length from the nose. Angle of attack is believed to be accurate to at least $\pm 0.2^{\circ}$.

RESULTS AND DISCUSSION

The pertinent results from this investigation are shown in summary plots in figures 5 to 11 and in basic-data plots in figures 12 to 42.

Maximum Lift-Drag Ratio

Maximum lift-drag ratios obtained in the present investigation are shown in figure 5 as a function of thickness ratio. The abscissa scale has arbitrarily been extrapolated to zero to present the data from the wings used to simulate zero leading-edge radius. It is noted that $(L/D)_{max}$ exhibited a nearly linear decay as thickness ratio was increased logarithmically. Included along with the experimental results of the present investigation are the results obtained from both Newtonian impact theory and a modified Newtonian impact theory by utilizing the method described in reference 8.

The two theories are represented in figure 5, Newtonian impact theory $\left(C_{p,max} = 2\right)$ for wings having $t/c > 0.04$ and modified Newtonian theory plus skin friction for $t/c < 0.04$ (skin friction calculated by the method described in ref. 9). In the modified theory a maximum stagnation pressure coefficient given by reference 8 as

$$\frac{\gamma + 3}{\gamma + 1}\left[1 - \left(\frac{2}{\gamma + 3}\right)\frac{1}{M_{\infty}^{2}}\right]$$

was used on the cylindrical leading edges and spherical-segment nose sections, whereas $\gamma + 1$ was used on the flat-plate portions of the wings. The force and moment contributions of the balance housings, as well as the dihedral on the leeward surface of the zero-leading-edge-radius wings, have been neglected and the theoretical calculations have been made on the basic wings only.

Wings having thickness ratios less than about 0.10 (fig. 5) were seen to achieve higher values of $(L/D)_{max}$ when the wings had 80^{o} sweep angles, whereas wings having thickness ratios greater than 0.10 had higher values of $(L/D)_{max}$ when the wings had sweep angles of 70^{o}. The optimum sweep angles for obtaining maximum values of $(L/D)_{max}$, for the basic type of configuration considered in this investigation, can be more easily ascertained from figure 6. Figure 6 indicates that as thickness ratio increased from a value of zero the optimum sweep angle for maximum lift-drag ratio decreased from an angle slightly larger than 80^{o} to 70^{o} or less for the highest thickness ratio. The peak in $(L/D)_{max}$ for each curve suggests that as sweep angle decreases from 90^{o}, the increased lifting surface more than offsets the increase in drag initially; whereas at sweep angles less than optimum the converse is true. Unfortunately, the angle-of-attack range did not permit many of the higher thickness-ratio wings to obtain a maximum lift-drag ratio and the optimum sweep angles for the higher thickness-ratio bodies could not be ascertained. Newtonian theory is in fairly good agreement with experiment for the higher thickness-ratio wings and is thus useful in determining the optimum sweep angle for these cases.

Figure 7(a) indicates the large penalty in lift coefficient at $(L/D)_{max}$ that is accrued as thickness ratio is decreased. The angle of attack at which $(L/D)_{max}$ occurs is seen, in figure 7(b), to increase nearly exponentially with thickness ratio. Drag polars were useful in ascertaining lift coefficient and angle of attack at $(L/D)_{max}$. Included in figure 7(b) are the predictions of angle of attack at $(L/D)_{max}$ given by the method of reference 10 and expressed in degrees herein:

$$\alpha_{(L/D)_{max}} = \frac{57.3^{o}}{2(L/D)_{max}} \tag{1}$$

In the present paper experimental values of $(L/D)_{max}$ are used in this equation to predict angle of attack at $(L/D)_{max}$.

Volumetric Coefficient

In figure 8 $(L/D)_{max}$ is presented as a function of the volumetric coefficient $V^{2/3}/S$. The solid symbols denote results in which the volume of the balance-housing bodies have been included. However, since the balance-housing bodies have very little effect on the wing characteristics (see fig. 4), the data are also representative of wing-alone data. Therefore the volumetric coefficients have also been computed for the wings alone by subtracting the volume of the balance-housing bodies and are shown in the figure as flagged symbols. When the wings alone (all open symbols) are considered, $(L/D)_{max}$ exhibits a nearly linear decrease as volumetric coefficient is increased logarithmically, the slope of this trend depending on wing sweep angle. This analysis

indicates that considerable volume may be discretely added to delta planforms without incurring serious losses in $(L/D)_{max}$.

Normal-Force-Curve and Lift-Curve Slopes

As can be seen in figure 9 the slopes of the normal-force curves and lift curves at zero angle of attack increase nearly linearly with thickness ratio. As sweep angle increases, C_{N_α} and C_{L_α} decrease, a trend previously obtained on slender wings at lower hypersonic speeds (ref. 11). Because the presence of balance-housing bodies would tend to introduce negative normal and lift forces at and near zero angle of attack, initial slopes for only the wings which had no balance-housing bodies were presented. Within the limitations of the data in figure 9, values of C_{L_α} may be interpolated for various combinations of thickness ratio and sweep angle. The following empirical expression was found for determining C_{N_α}:

$$C_{N_\alpha} = 0.016667(t/c) + 0.000240(90^o - \Lambda) + 0.000718$$

$$(0.08 \leqq t/c \leqq 0.30; \quad 60^o \leqq \Lambda \leqq 85^o) \quad (2)$$

The values of C_{N_α} as predicted by this equation are shown in figure 9 as straight lines. Equation (2) was found to be inadequate in predicting values of C_{N_α} at lower Mach numbers, when compared with data obtained on similar wings from reference 12.

Center of Pressure

Figures 10 and 11 contain the center-of-pressure data as given in root-chord lengths from the nose and as plotted as a function of angle of attack. The initial forward shift of the center of pressure occurring at low angles of attack on some of the wings is attributed to the presence of the balance-housing bodies. Included in figure 10 are curves representing Newtonian impact theory. For the sake of clarity, Newtonian impact theory is presented for only a representative number of wings. Also indicated on the plots is the location of the center of pressure for zero-leading-edge-thickness wings as predicted by Newtonian impact theory. In figure 10, each set of data represents a particular sweep angle and the data within each set represent the different thickness ratios investigated at these respective sweep angles. The experimental data indicate that as thickness ratio t/c increases from zero, the center of pressure moves forward from the 2/3-root-chord point. In figure 11, each set of data represents a particular thickness ratio and the data within each set represent different sweep angles. Center of pressure of the wings having higher thickness ratios is seen to move rearward as sweep angle is decreased. Center of pressure is also seen to move rearward as angle of attack increases from zero. The rate of rearward shift of the center of pressure increases with increasing sweep angle.

BASIC DATA

Presentation of the basic data (figs. 12 to 42) is made in order of decreasing thickness ratio and, for each thickness ratio, in order of increasing sweep angle. Arrows on the abscissa of the plots (figs. 30 to 42) indicate the approximate angle of attack at which the balance-housing bodies were geometrically hidden from the flow by the wings. The Newtonian impact theory calculations are shown as solid lines (figs. 12 to 42) and the results of the modified Newtonian impact theory plus calculated skin friction (figs. 30 to 42) are shown as broken lines. In general, it will be observed that the theoretical predictions are good for predicting trends, but are inadequate for predicting experimental values.

CONCLUDING REMARKS

An investigation has been conducted to determine the effects of sweep angle and thickness ratio on the longitudinal aerodynamic characteristics of a series of delta planforms having hemicylinder leading edges and spherical-segment noses. The sweep angles investigated were 45°, 60°, 70°, 80°, 85°, and 90°, and the thickness ratio varied from 0 to 0.3 for each sweep angle. The investigation was conducted at a Mach number of approximately 20 in helium flow and the angle-of-attack range was approximately from 0° to 30°.

Maximum lift-drag ratio exhibited a nearly linear decay as thickness ratio and volumetric coefficient were logarithmically increased. The angle of attack at which maximum lift-drag ratio occurred exhibited a nearly exponential increase with thickness ratio. The data indicated that it may be possible to discretely add a considerable volume to delta planforms without incurring serious penalities in maximum lift-drag ratio. Normal-force-curve and lift-curve slopes generally increased linearly with thickness ratio. Center of pressure moved forward from the 2/3-root-chord point as thickness ratio increased from zero. Center of pressure also moved rearward with decreasing sweep angle for the thicker wings. Newtonian impact theory and a modified Newtonian impact theory plus skin-friction calculations were generally adequate for predicting trends only.

Langley Research Center,
National Aeronautics and Space Administration,
Langley Station, Hampton, Va., February 8, 1966.

REFERENCES

1. Eggers, Alfred J., Jr.; Allen, H. Julian; and Neice, Stanford E.: A Comparative Analysis of the Performance of Long-Range Hypervelocity Vehicles. NACA Rept. 1382, 1958.

2. Fetterman, David E.; and Neal, Luther, Jr.: An Analysis of the Delta-Wing Hypersonic Stability and Control Behavior at Angles of Attack Between 30^{o} and 90^{o}. NASA TN D-1602, 1963.

3. Witcofski, Robert D.; and Marcum, Don C., Jr.: Wing Sweep and Blunting Effects on Delta Planforms at M = 20. AIAA J., vol. 3, no. 3, Mar. 1965, pp. 547-548.

4. Mechtly, E. A.: The International System of Units – Physical Constants and Conversion Factors. NASA SP-7012, 1964.

5. Arrington, James P.; Joiner, Roy C., Jr.; and Henderson, Arthur, Jr.: Longitudinal Characteristics of Several Configurations at Hypersonic Mach Numbers in Conical and Contoured Nozzles. NASA TN D-2489, 1964.

6. Johnston, Patrick J.; and Snyder, Curtis D.: Static Longitudinal Stability and Performance of Several Ballistic Spacecraft Configurations in Helium at a Mach Number of 24.5. NASA TN D-1379, 1962.

7. Johnston, Patrick J.; Snyder, Curtis D.; and Witcofski, Robert D.: Maximum Lift-Drag Ratios of Delta-Wing—Half-Cone Combinations at a Mach Number of 20 in Helium. NASA TN D-2762, 1965.

8. Olstad, Walter B.: Theoretical Evaluation of Hypersonic Forces, Moments, and Stability Derivatives for Combinations of Flat Plates, Including Effects of Blunt Leading Edges, by Newtonian Impact Theory. NASA TN D-1015, 1962.

9. Bertram, Mitchel H.: Boundary-Layer Displacement Effects in Air at Mach Numbers of 6.8 and 9.6. NASA TR R-22, 1959.

10. Maslen, S. H.: Considerations in the Design of Vehicles Capable of Substantial Hypersonic Lift-Drag Ratios. Trans. Ninth Symposium on Ballistic Missile and Space Technology, Vol. II, U.S. Air Force and Aerospace Corp., Aug. 1964, pp. 117-158.

11. Bertram, Mitchel H.; and McCauley, William D.: Investigation of the Aerodynamic Characteristics at High Supersonic Mach Numbers of a Family of Delta Wings Having Double-Wedge Sections With the Maximum Thickness at 0.18 Chord. NACA RM L54G28, 1954.

12. Olstad, Walter B.: Longitudinal Aerodynamic Characteristics of Several Thick-Slab Delta Wings at Mach Numbers of 3.00, 4.50, and 6.00 and Angles of Attack to 95°. NASA TM X-742, 1963.

TABLE I.- PERTINENT MODEL DIMENSIONS, TEST PARAMETERS, AND ACCURACY

Figure	Λ, deg	t/c	t		c		M_∞	R	Accuracy of –		
			in.	cm	in.	cm			C_N	C_A	C_m
12	45	0.299	1.250	3.175	4.183	10.625	20.3	1.53×10^6	±0.0026	±0.0065	$\pm 0.62 \times 10^{-3}$
13	60	.299	1.250	3.175	4.183	10.625	↓	↓	±.0025	±.0025	±.37
14	70	.299	1.250	3.175	4.183	10.625	↓	↓	±.0032	±.0032	±.48
15	80	.299	1.250	3.175	4.183	10.625	↓	↓	±.0026	±.0009	±.45
16	85	.299	1.250	3.175	4.183	10.625	↓	↓	±.0031	±.0010	±.52
17	[b]90	.299	2.000	5.080	6.693	17.000	↓	2.45	±.0094	±.0013	±.12
18	45	.205	.800	2.032	3.902	9.911	↓	1.43	±.0031	±.0079	±.81
19	60	.205	1.250	3.175	6.100	15.494	↓	2.23	±.0043	±.0006	±.61
20	70	.205	1.250	3.175	6.098	15.489	↓	↓	±.0017	±.0017	±.17
21	80	.205	1.250	3.175	6.098	15.489	↓	↓	±.0026	±.0026	±.27
22	85	.205	1.250	3.175	6.098	15.489	↓	↓	±.0032	±.0032	±.39
23	[b]90	.205	2.000	5.080	9.756	24.780	↓	3.57	±.0054	±.0008	±.48
24	45	.143	.598	1.519	4.183	10.625	↓	1.53	±.0027	±.0067	±.91
25	70	.132	1.255	3.188	9.500	24.130	↓	3.48	±.0027	±.0004	±.25
26	60	.098	.600	1.524	6.098	15.489	↓	2.23	±.0022	±.0056	±.36
27	80	.083	1.250	3.175	15.000	38.100	↓	5.49	±.0020	±.0003	±.11
28	85	.083	1.250	3.175	15.000	38.100	↓	↓	±.0031	±.0004	±.18
29	[b]90	.083	1.250	3.175	15.000	38.100	↓	↓	±.0028	±.0069	±.31
[a]30	70	.033	.333	.846	10.000	25.400	↓	3.66	±.0029	±.0004	±.36
[a]31	80	.033	.333	.846	10.000	25.400	↓	↓	±.0054	±.0008	±.67
[a]32	85	.033	.333	.846	10.000	25.400	↓	↓	±.0095	±.0013	±1.17
[a]33	70	.020	.200	.508	10.000	25.400	↓	↓	±.0031	±.0004	±.48
[a]34	80	.020	.200	.508	10.000	25.400	↓	↓	±.0059	±.0008	±.94
[a]35	85	.020	.200	.508	10.000	25.400	↓	↓	±.0095	±.0013	±1.20
[a]36	70	.010	.100	.254	10.000	25.400	↓	↓	±.0030	±.0004	±.48
[a]4 and 37	80	.010	.100	.254	10.000	25.400	↓	↓	±.0061	±.0009	±.98
[a]38	85	.010	.100	.254	10.000	25.400	↓	↓	±.0116	±.0016	±1.06
[a]39	60	0	0	0	5.200	13.208	21.7	3.83	±.0027	±.0003	±2.20
[a]40	70	0	0	0	8.150	20.701	20.6	3.67	±.0026	±.0003	±.96
[a]41	80	0	0	0	11.340	28.804	19.9	3.80	±.0037	±.0005	±.55
[a]42	85	0	0	0	11.380	28.905	19.9	3.80	±.0073	±.0009	±1.10
[a]4 and 37	80	.010	.100	.254	10.000	25.400	20.3	3.66	±.0041	±.0005	±.89
[a]4	80	.010	.100	.254	10.000	25.400	21.6	6.60	±.0036	±.0005	±.57

[a]Balance-housing bodies are on model.

[b]Hemisphere-cylinder.

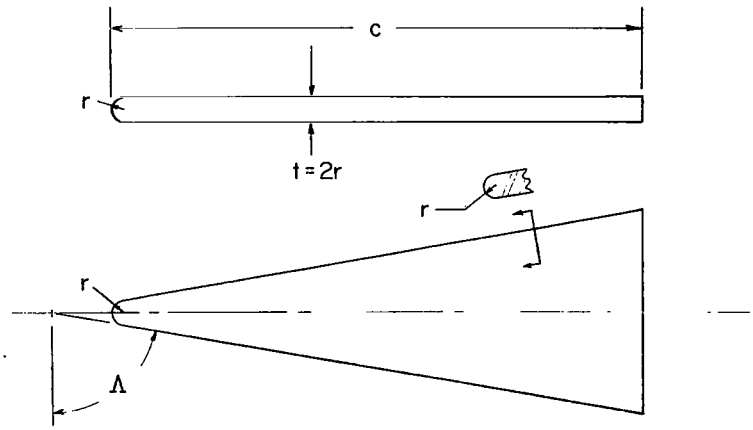

(a) Basic configuration.

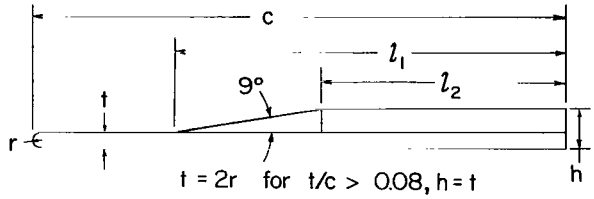

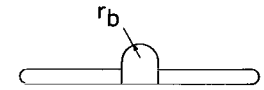

t/c	l_1/c	l_2/c	h/c	r_b/c
0.010	0.88	0.46	0.081	0.037
.020	.84	.46	.081	.037
.033	.75	.51	.066	.035

(b) Wing balance-housing bodies.

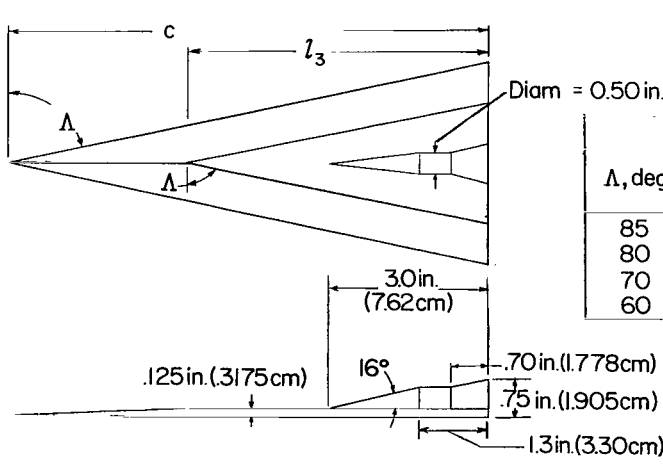

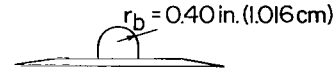

Λ, deg	l_3/c	r/c = 0, c, in.	r/c = 0, c, cm
85	0.77	11.38	28.90
80	.65	11.34	28.80
70	.77	8.15	20.70
60	.77	5.20	13.21

(c) Wings used to simulate zero leading-edge radius.

Figure 1.- Model sketches.

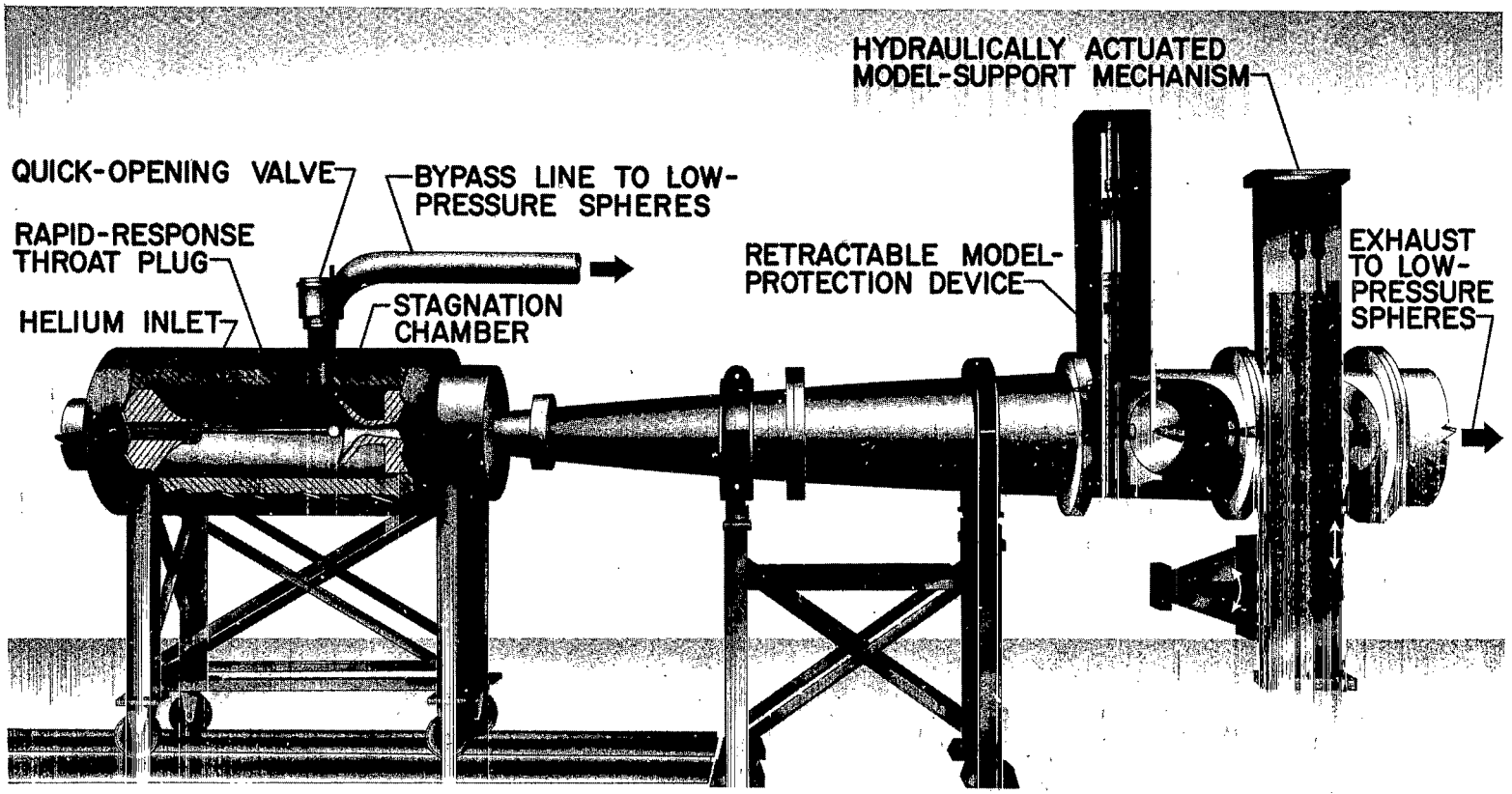

Figure 2.- Perspective drawing of Langley 22-inch helium tunnel.

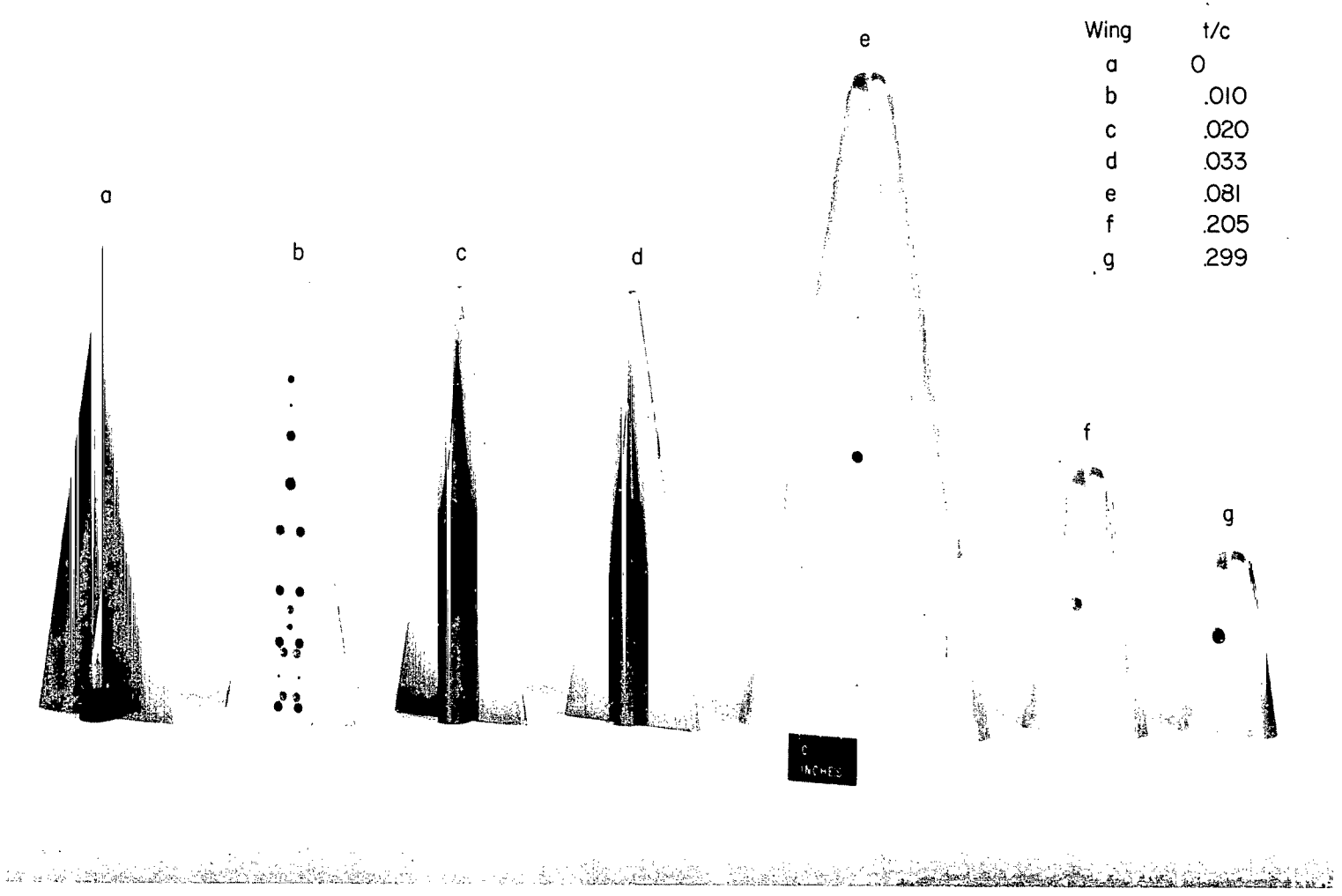

Figure 3.- Photograph of $\Lambda = 80^{0}$ wings. The balance-housing bodies shown on wing a and wing c were used on wing b. L-65-7778.1

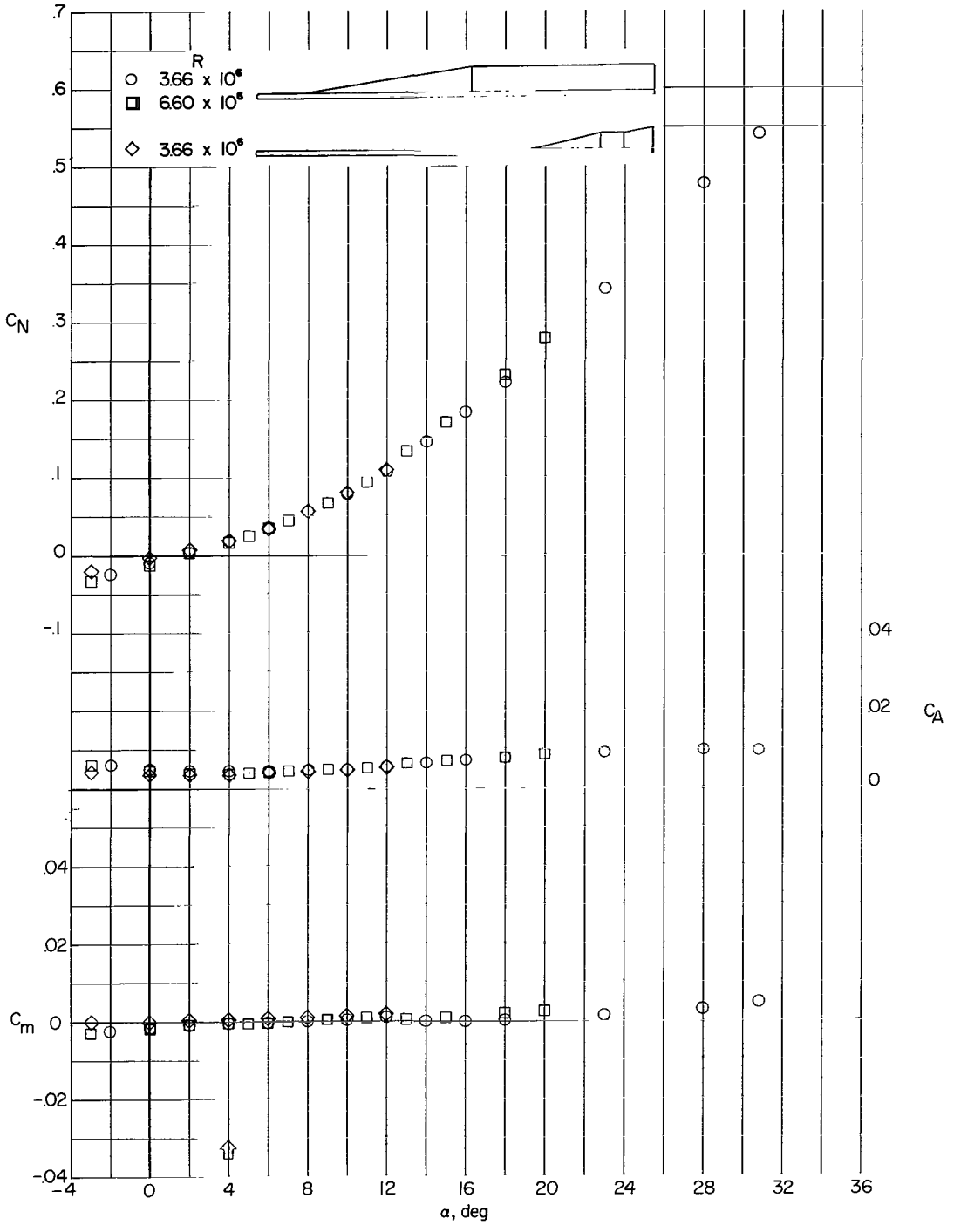

(a) Variation of C_N, C_A, and C_m with α.

Figure 4.- Effect of Reynolds number and balance-housing bodies on aerodynamic characteristics.

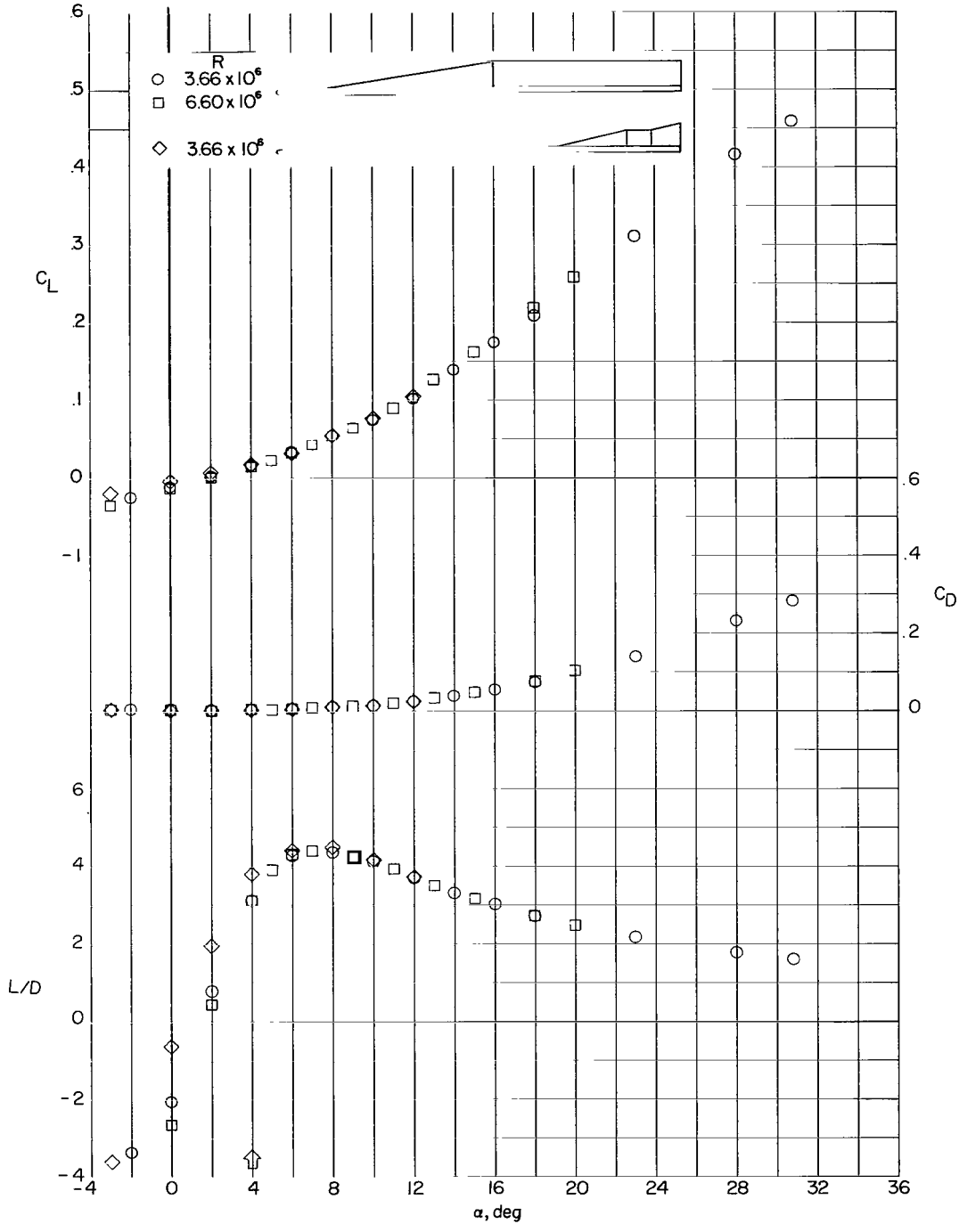

(b) Variation of C_L, C_D, and L/D with α.

Figure 4.- Concluded.

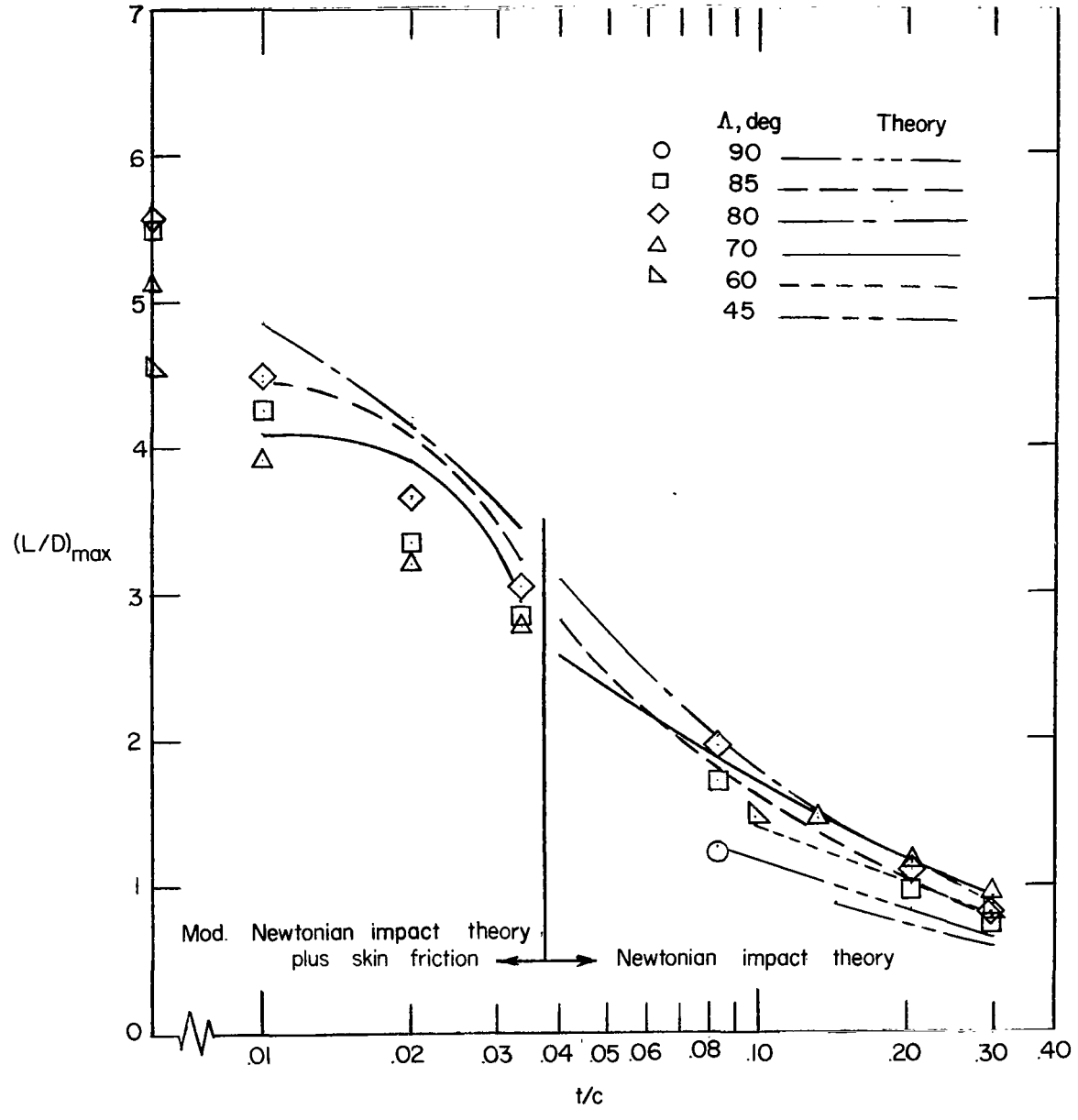

Figure 5.- Maximum lift-drag ratio as a function of thickness ratio.

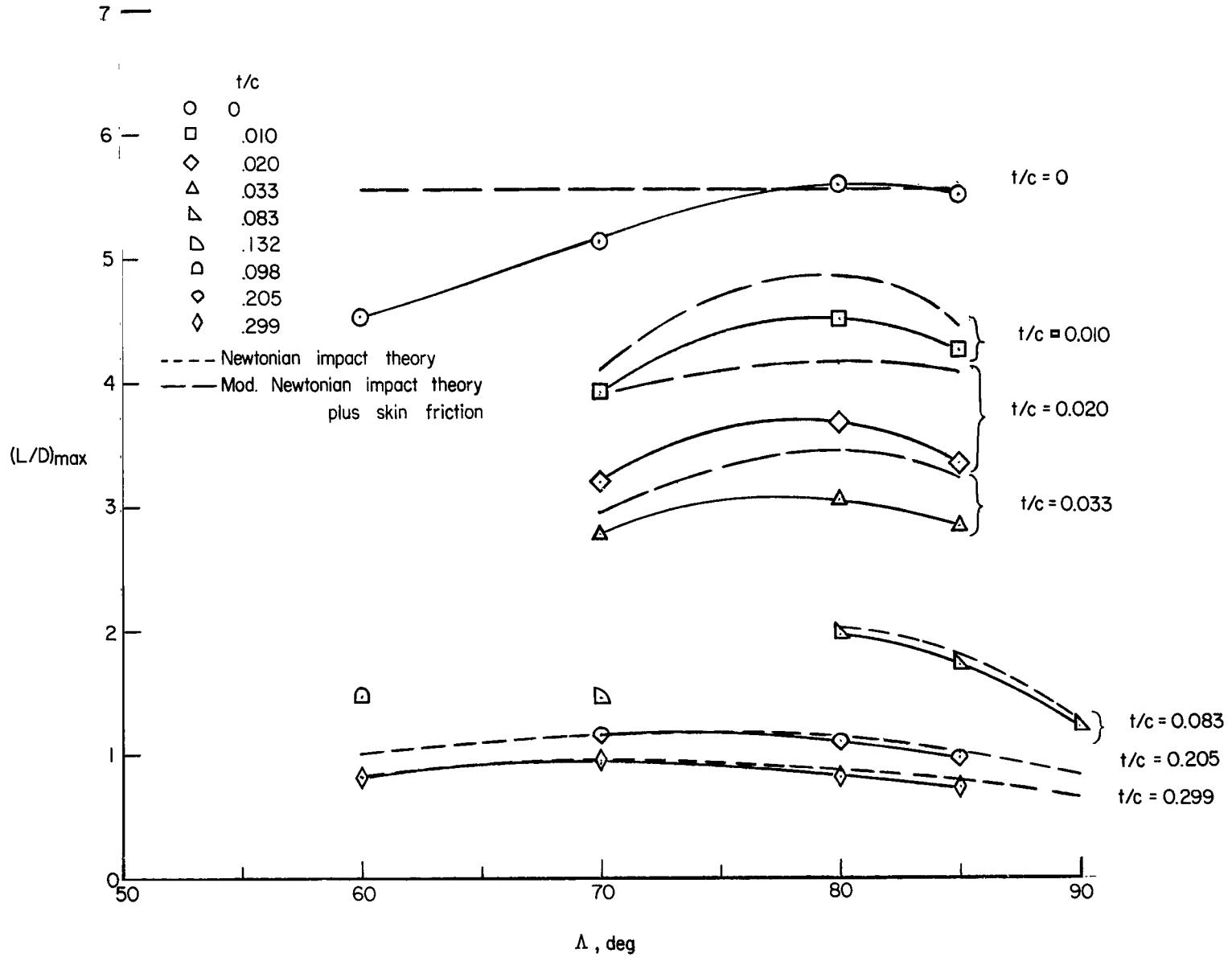

Figure 6.- Variation of $(L/D)_{max}$ with sweep angle.

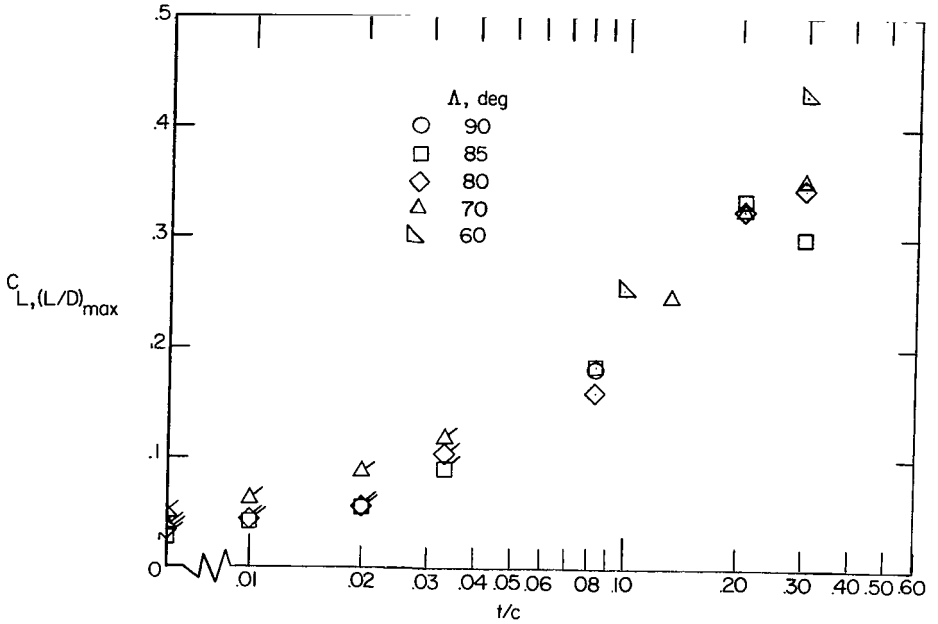

(a) Lift coefficient at $(L/D)_{max}$. Flags indicate presence of balance-housing bodies.

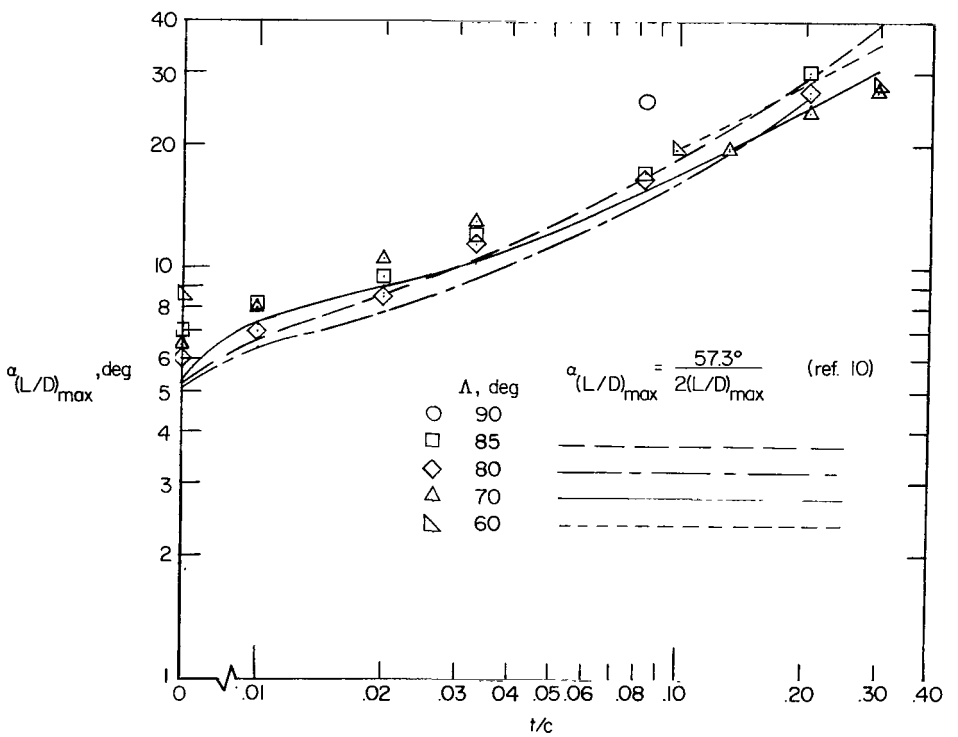

(b) Angle of attack at $(L/D)_{max}$.

Figure 7.- Lift and angle of attack at $(L/D)_{max}$ as a function of thickness ratio.

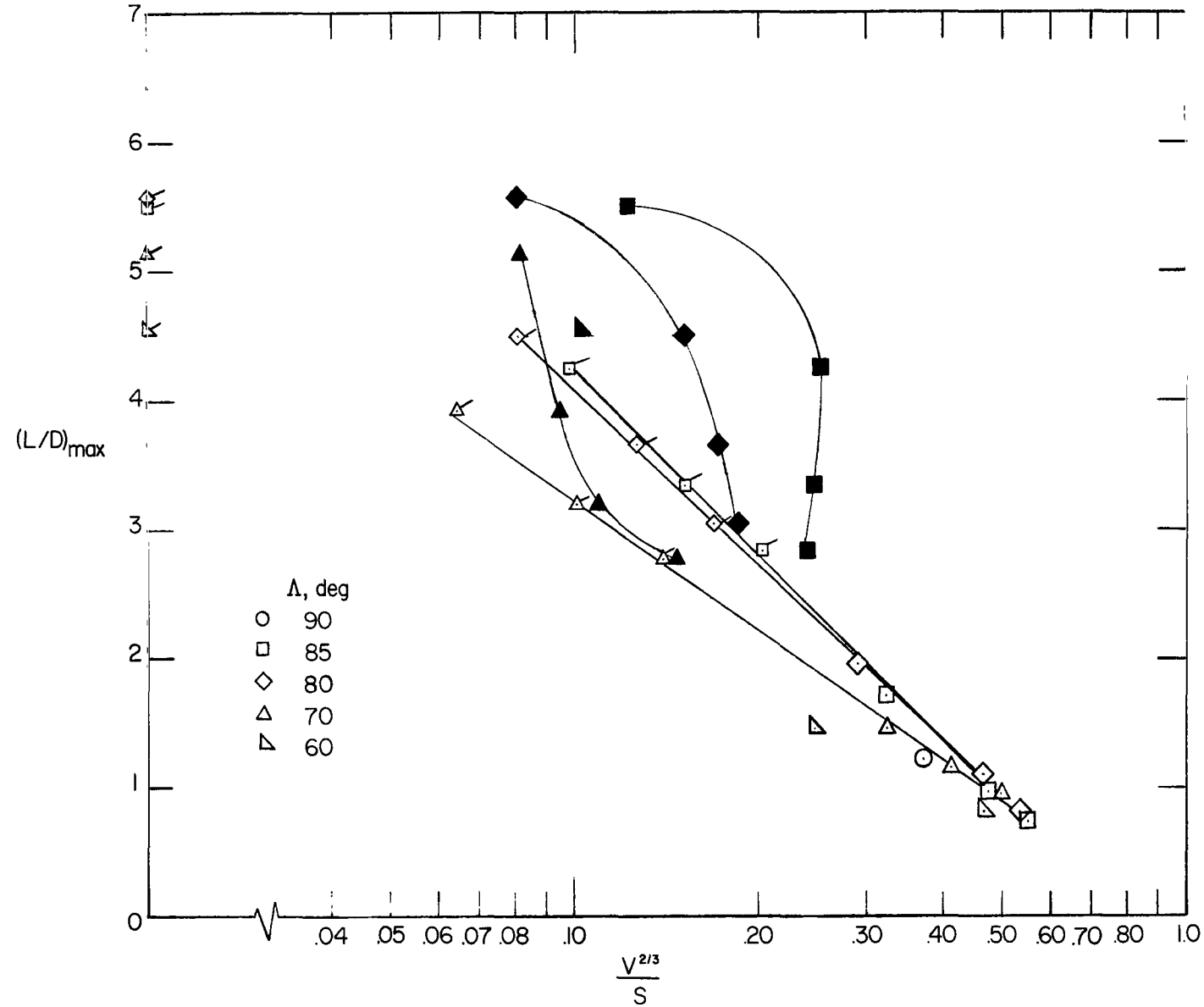

Figure 8.- $(L/D)_{max}$ as a function of volumetric coefficient. Solid symbols denote inclusion of balance-housing-body volume; flagged symbols denote inclusion of wing volume only. Unflagged symbols denote wings which required no balance-housing bodies.

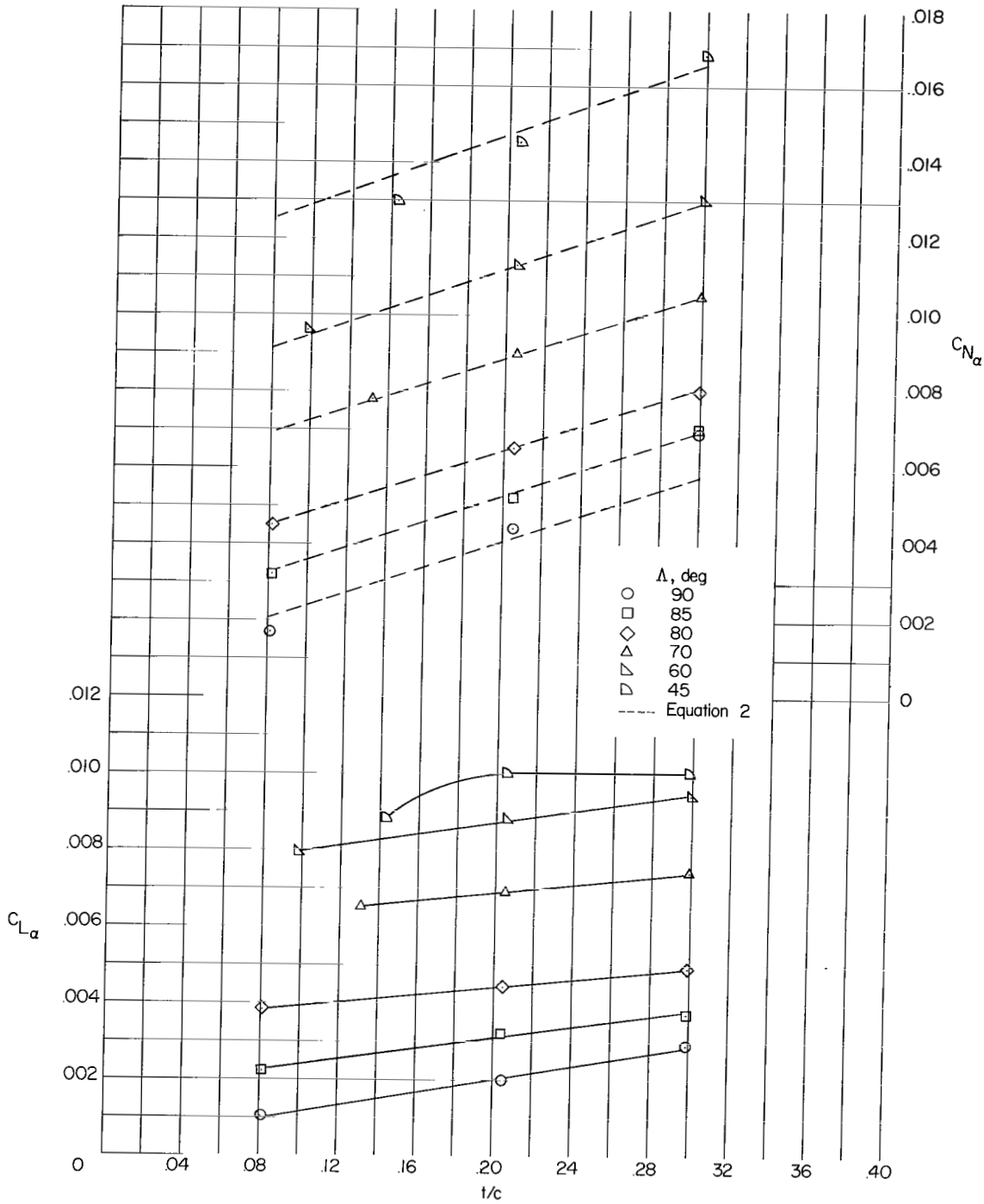

Figure 9.- Slopes of normal-force curves and lift curves at zero angle of attack as a function of thickness ratio.

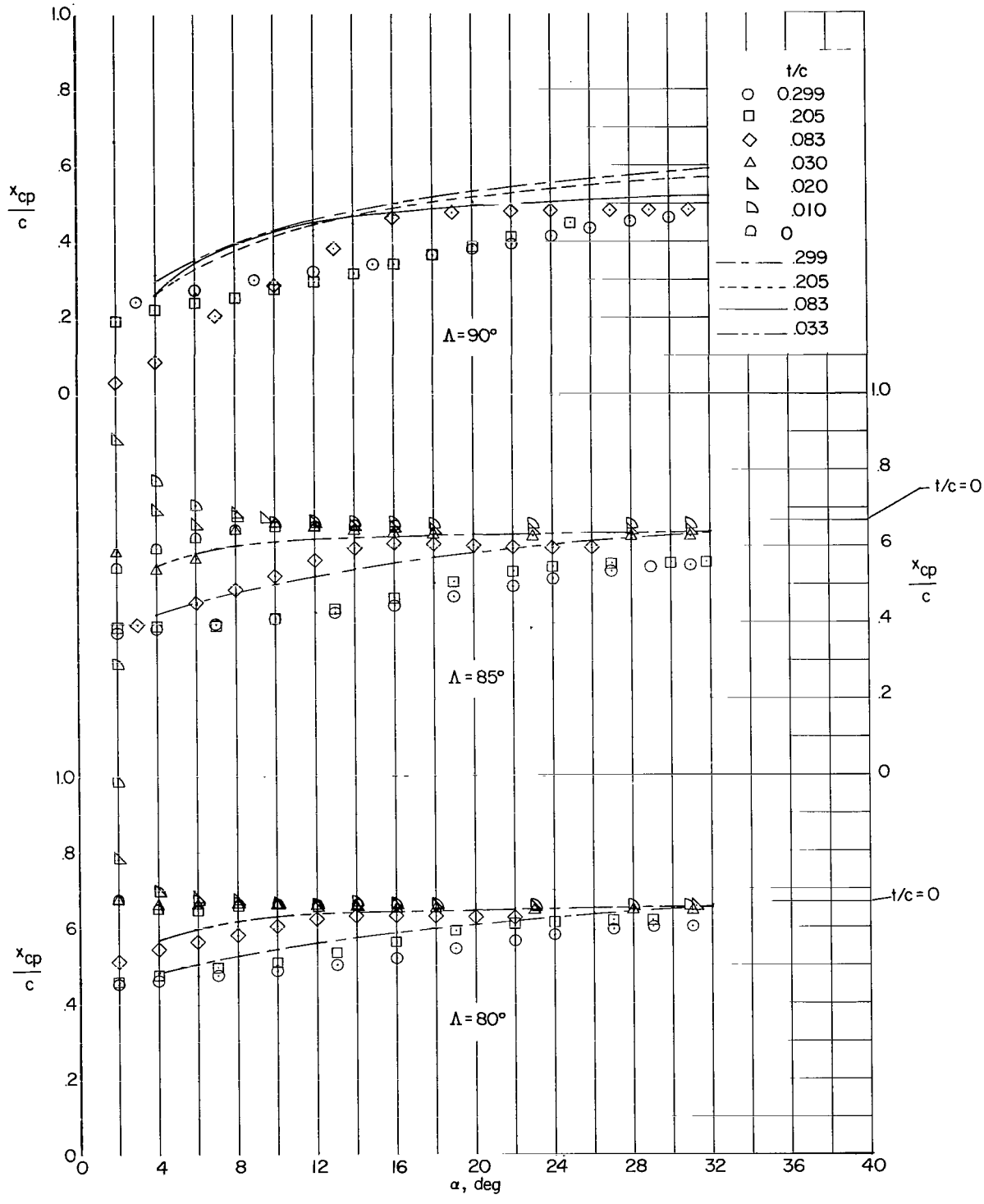

Figure 10.- Variation of center of pressure with angle of attack. Curves denote Newtonian impact theory.

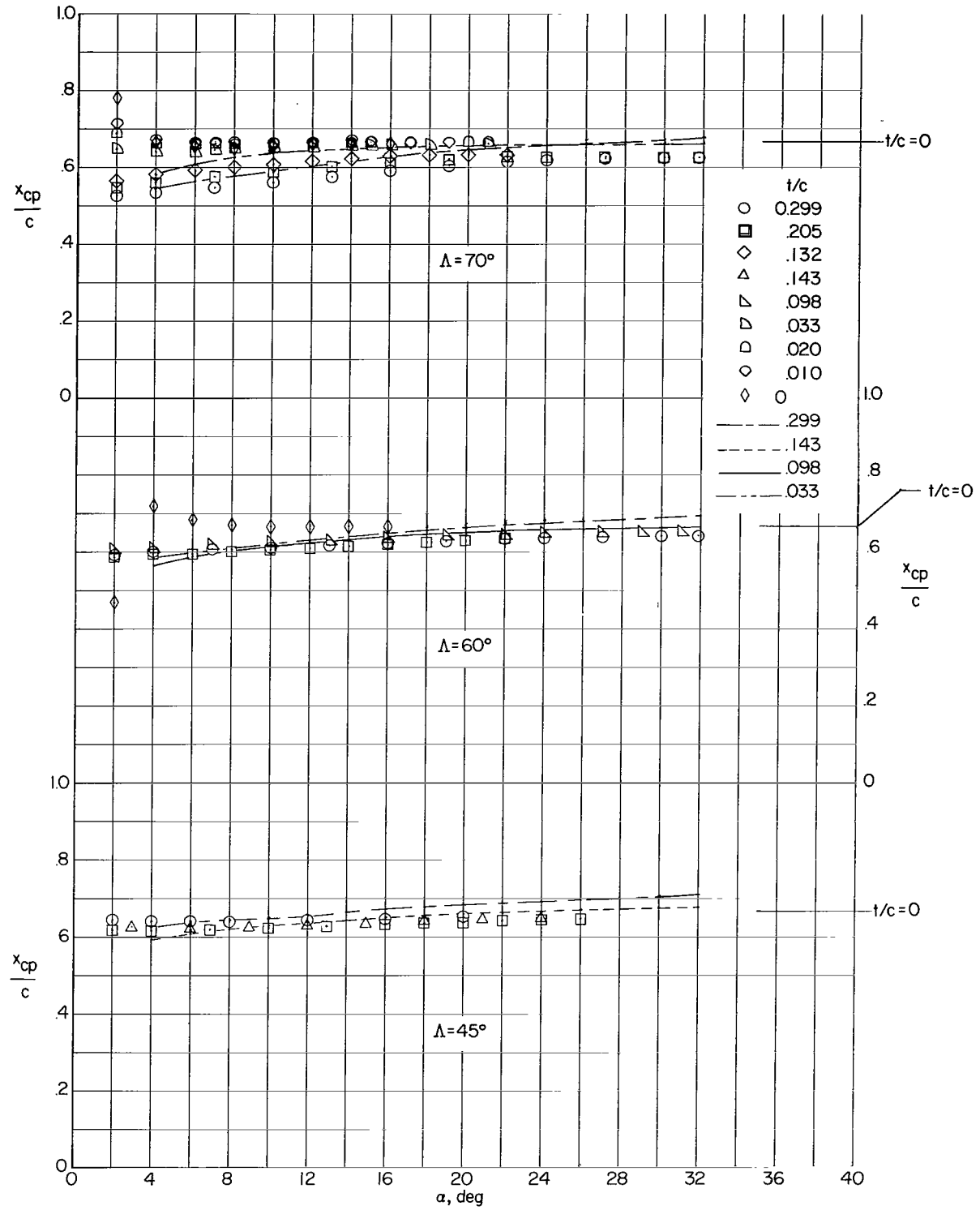

Figure 10.- Concluded.

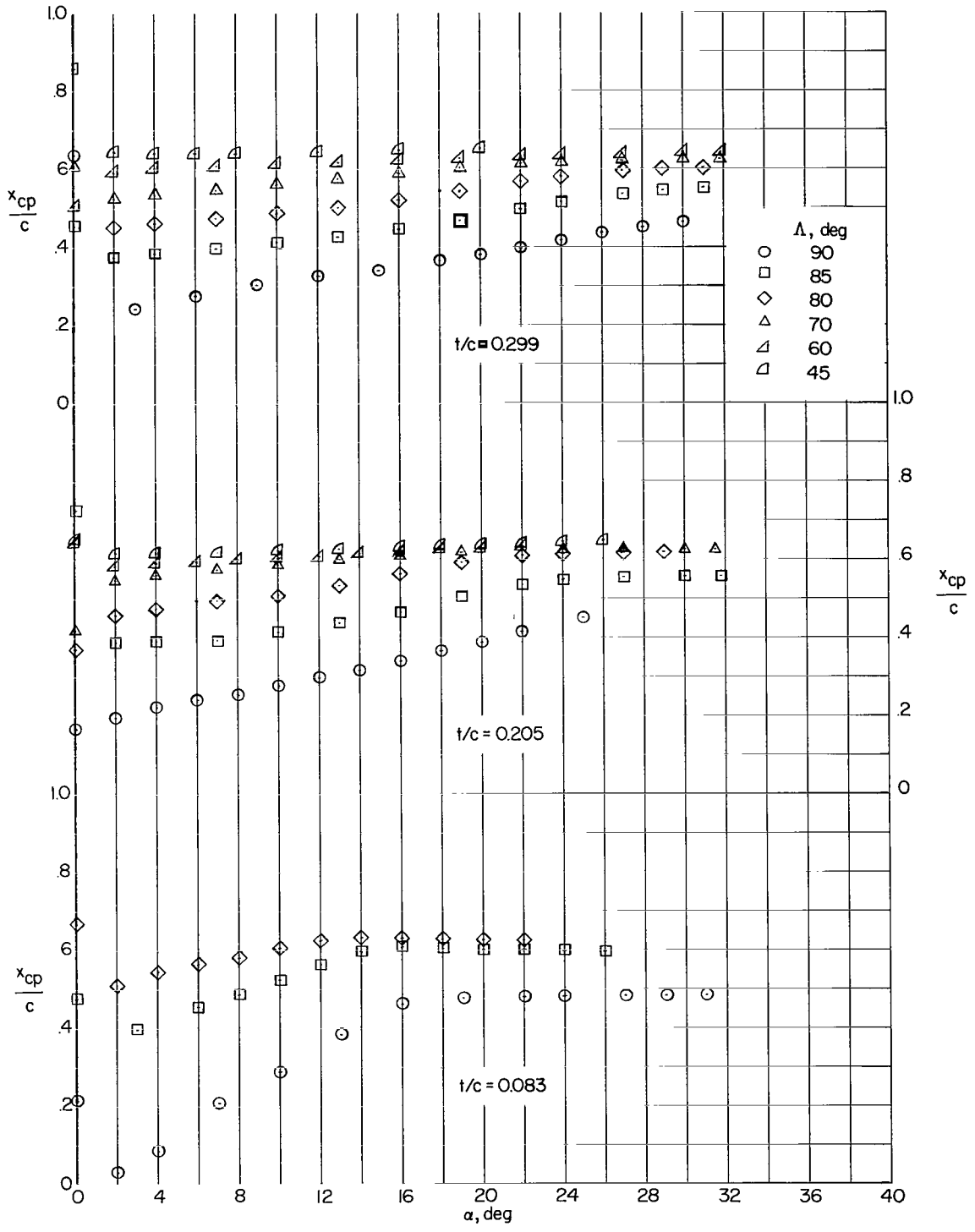

Figure 11.- Variation of center of pressure with angle of attack.

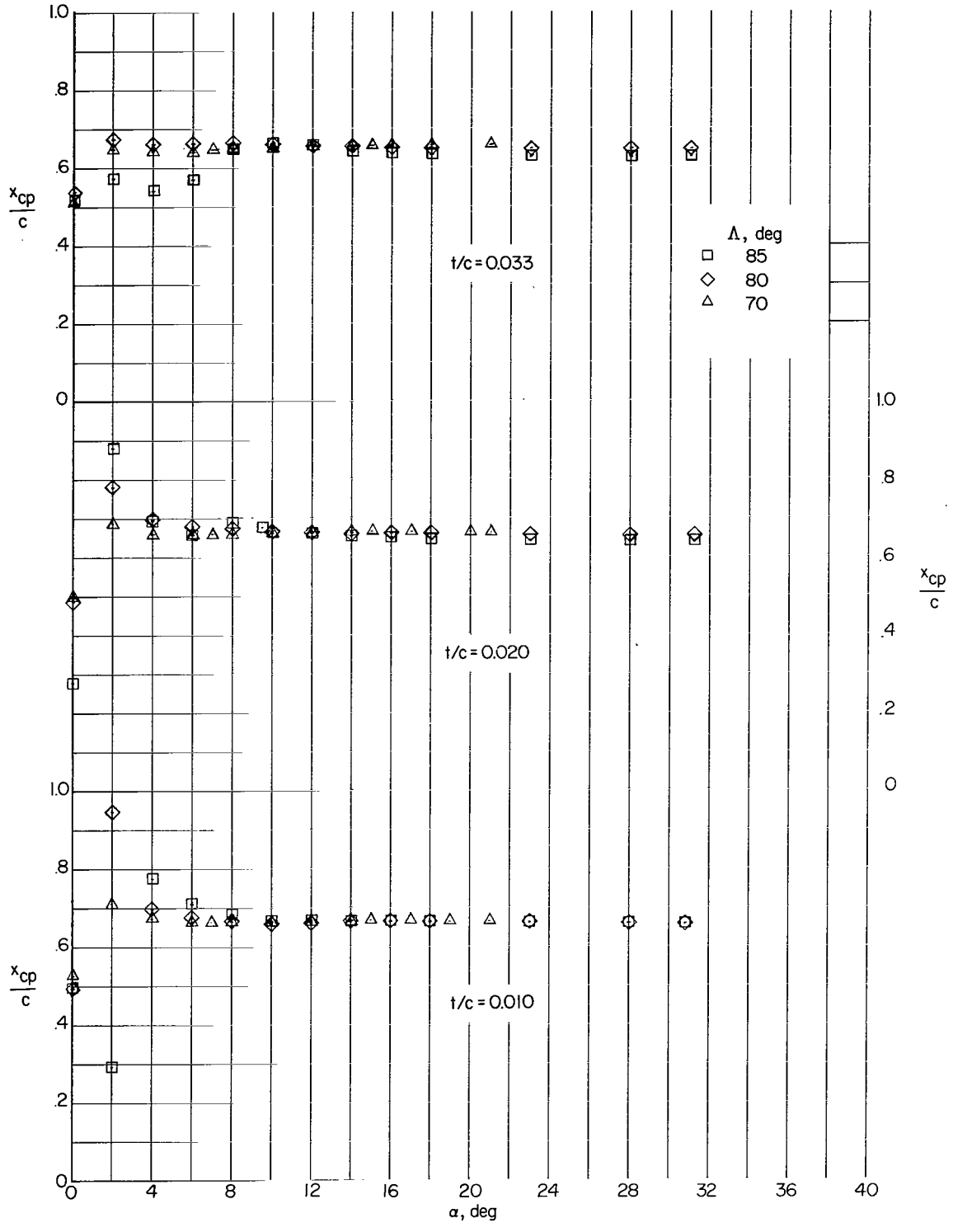

Figure 11.- Concluded.

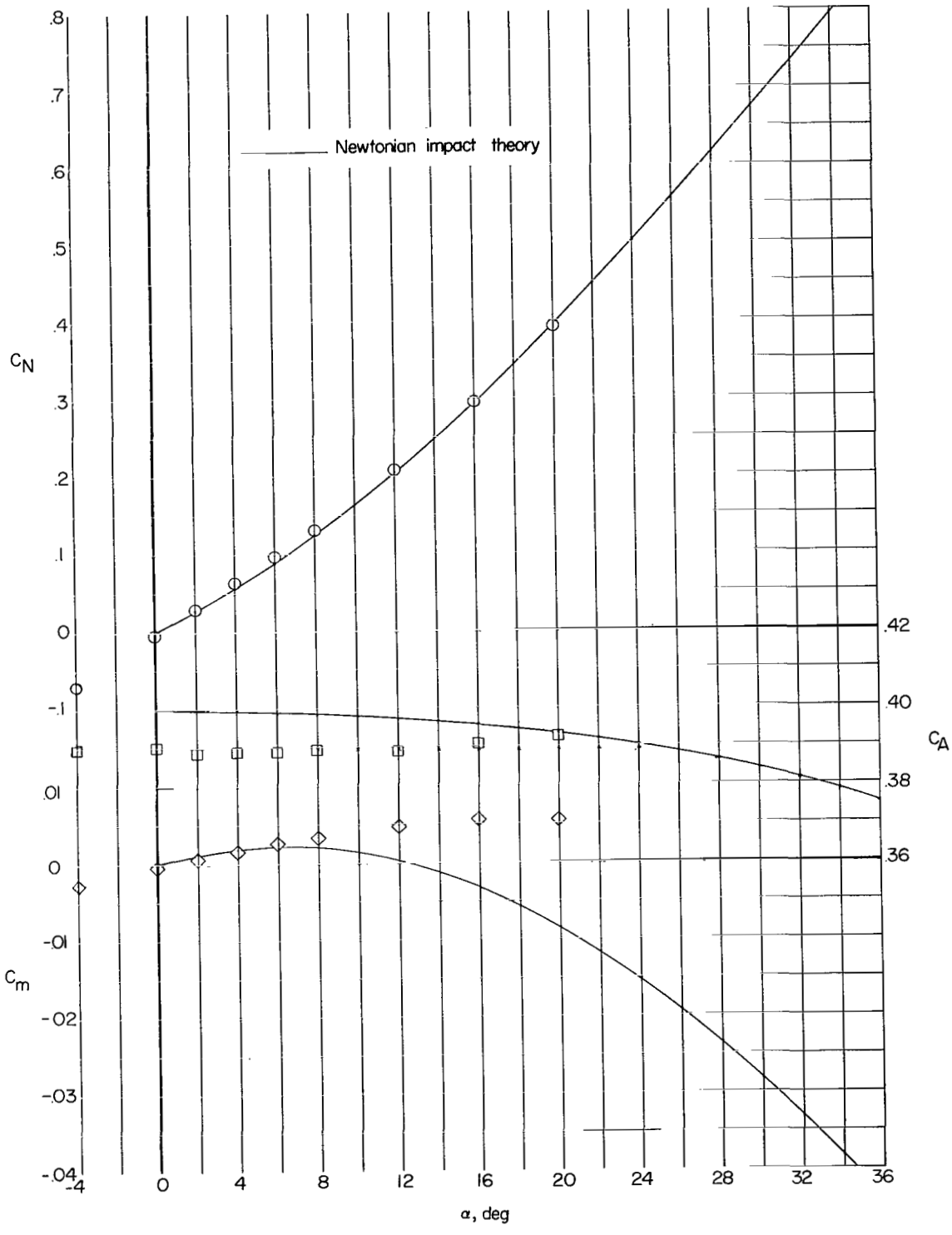

Figure 12.- Basic aerodynamic characteristics. t/c = 0.299; $\Lambda = 45^0$.

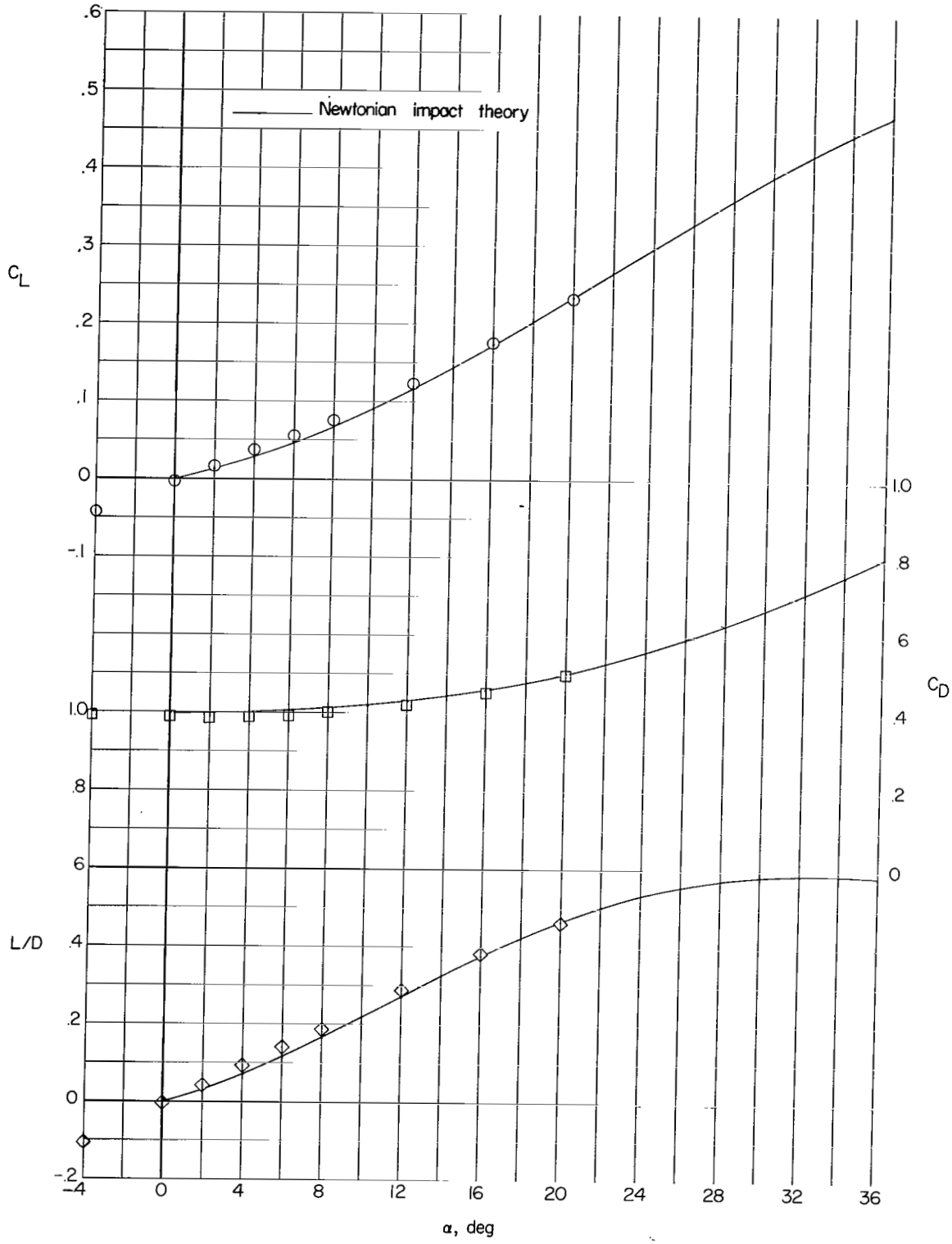

Figure 12.- Concluded.

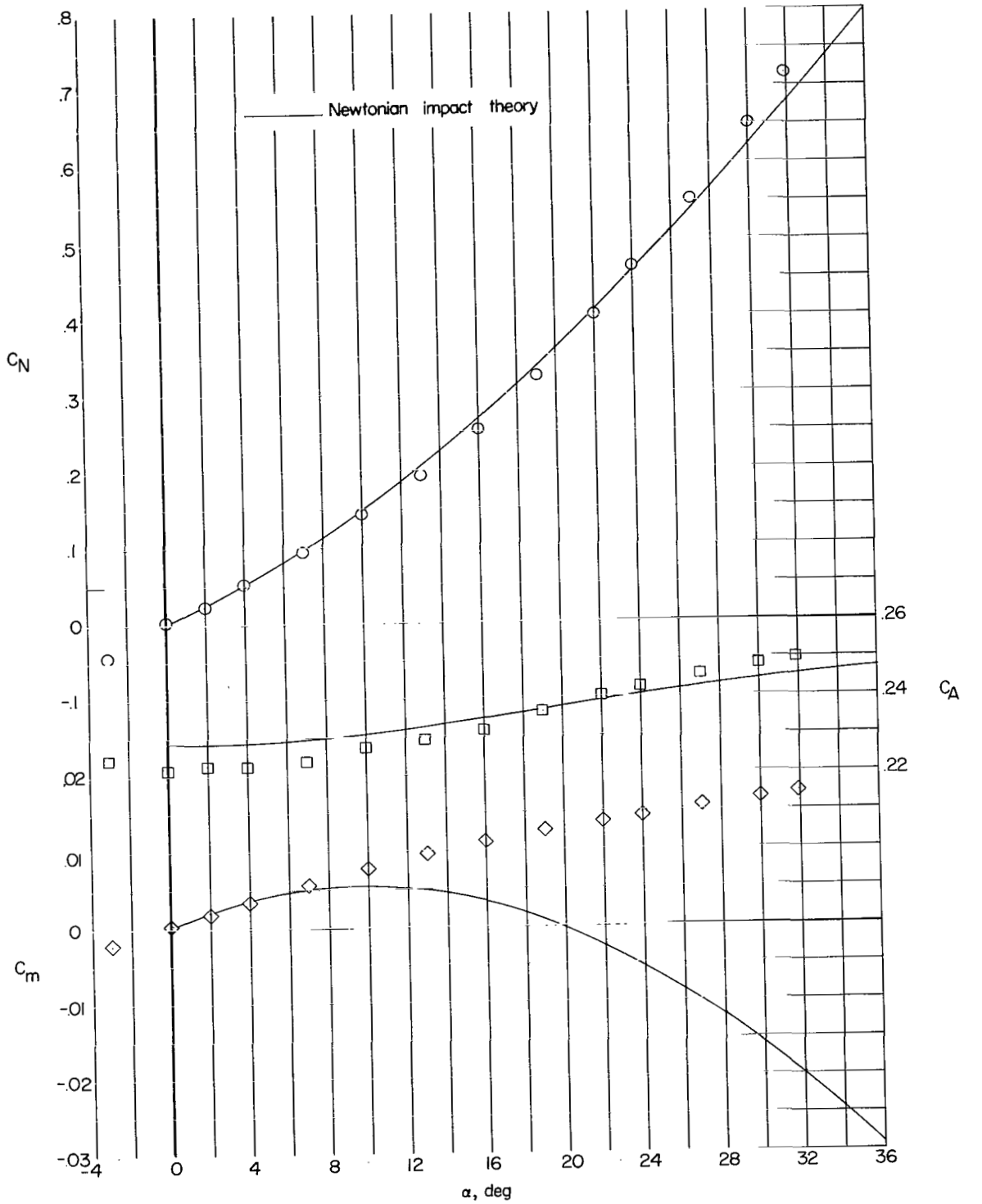

Figure 13.- Basic aerodynamic characteristics. t/c = 0.299; Λ = 60°.

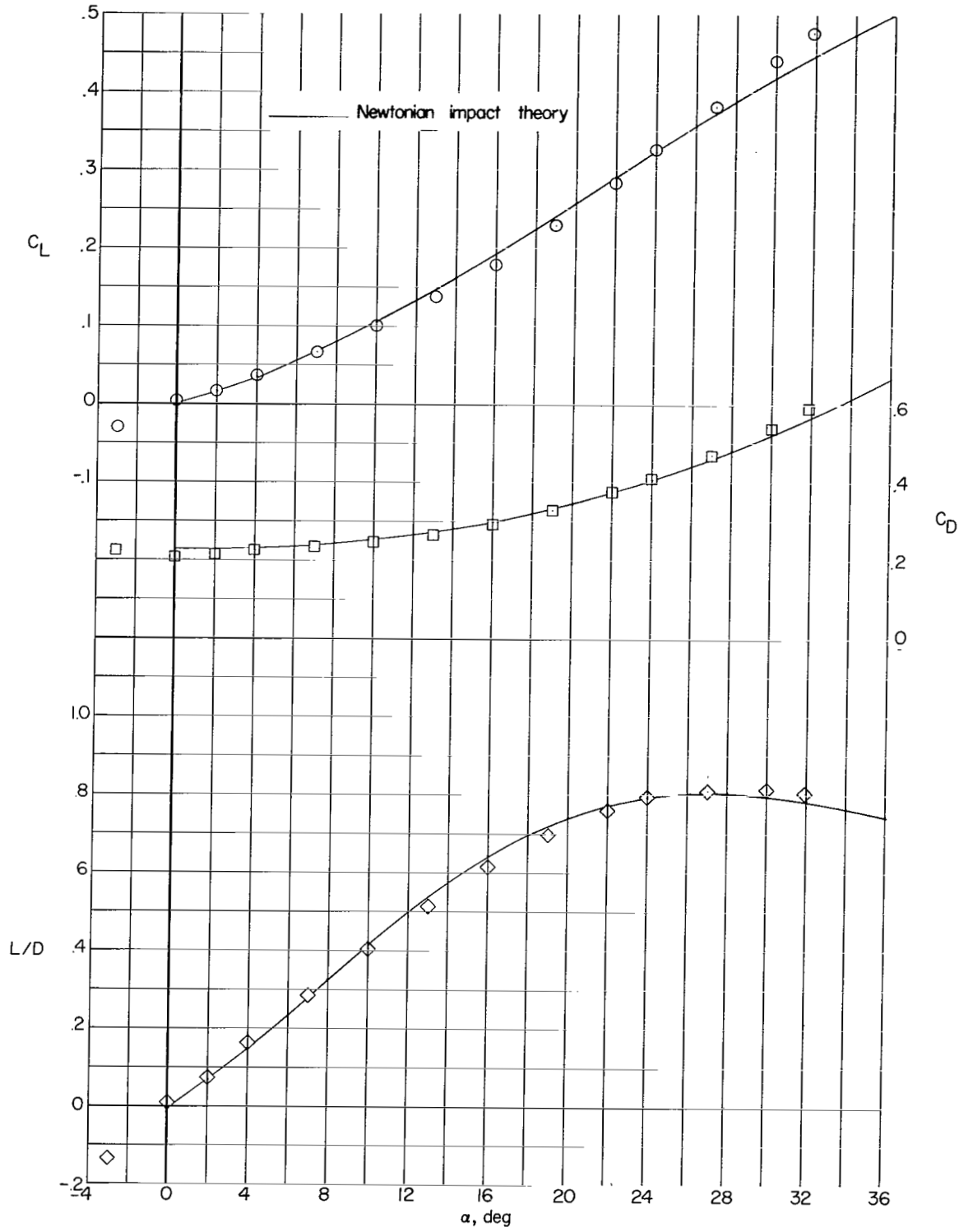

Figure 13.- Concluded.

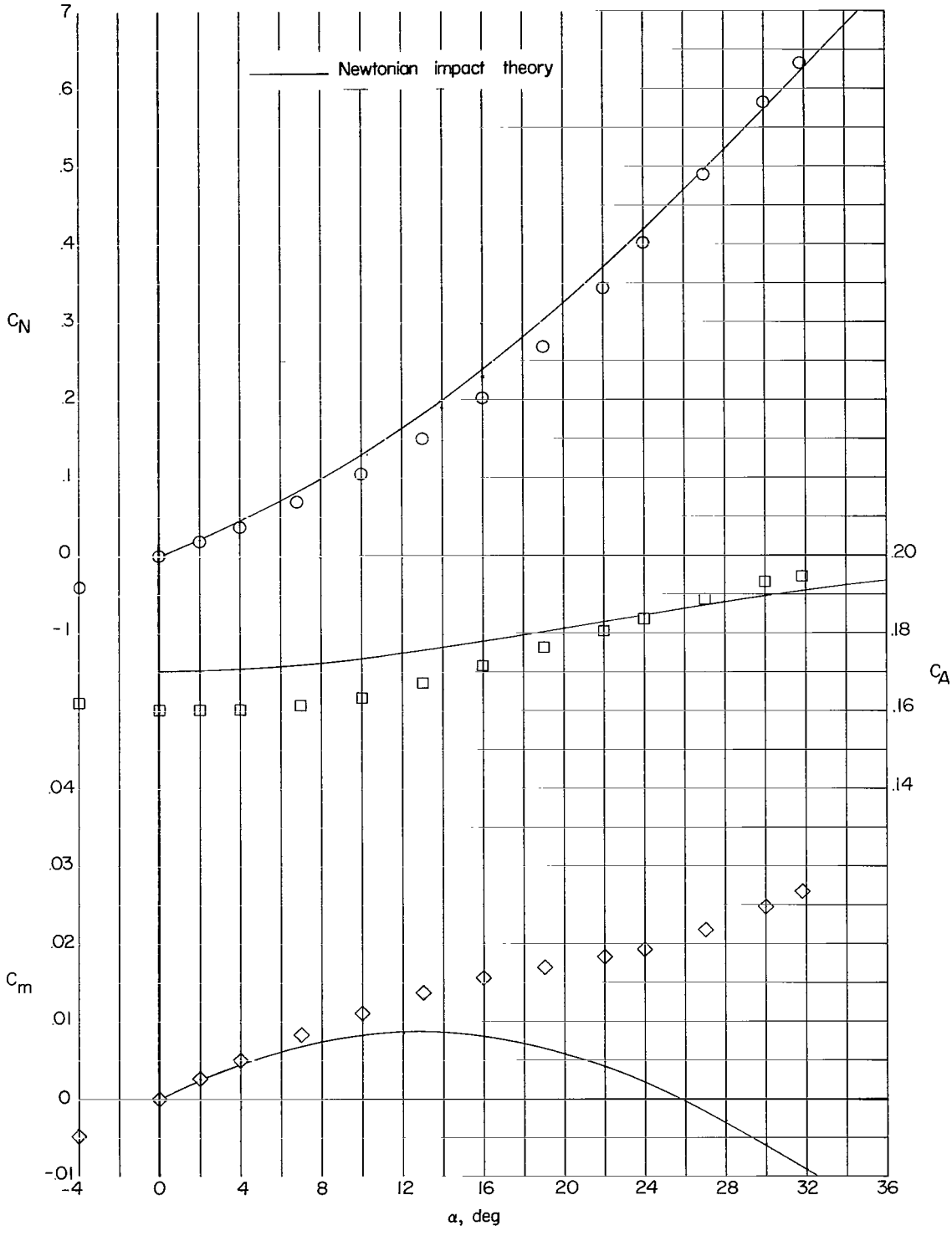

Figure 14.- Basic aerodynamic characteristics. t/c = 0.299; Λ = 70°.

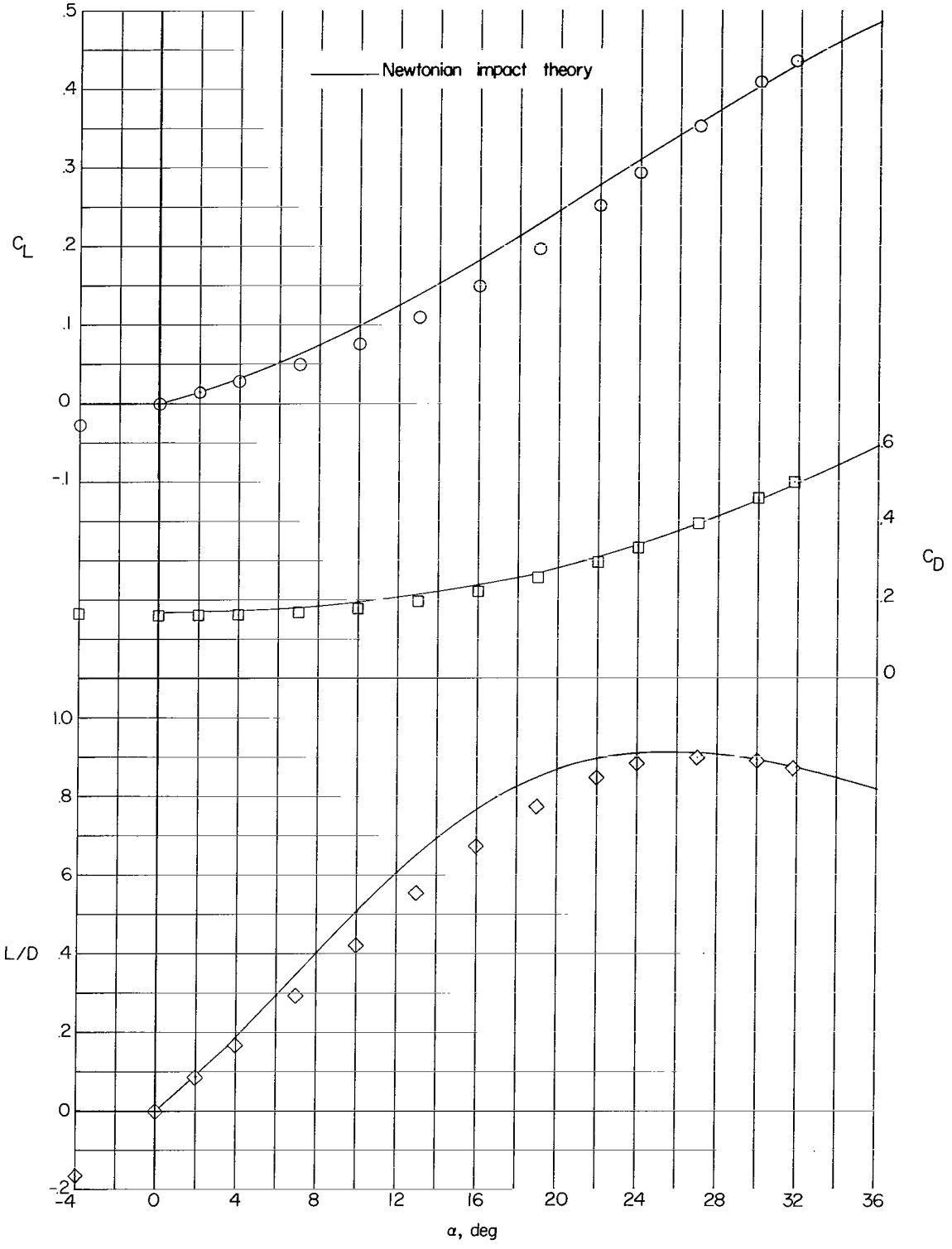

Figure 14.- Concluded.

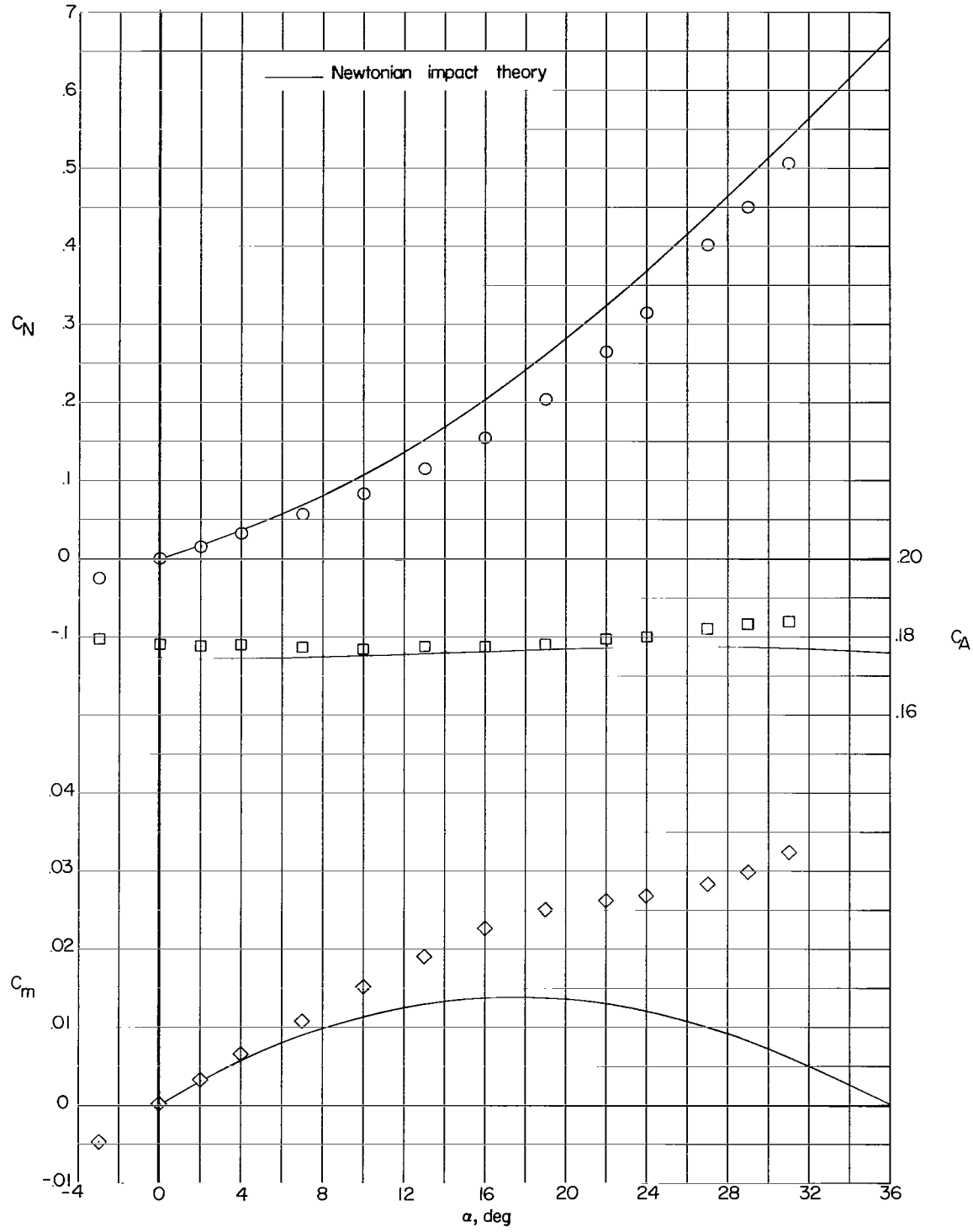

Figure 15.- Basic aerodynamic characteristics. t/c = 0.299; Λ = 80°.

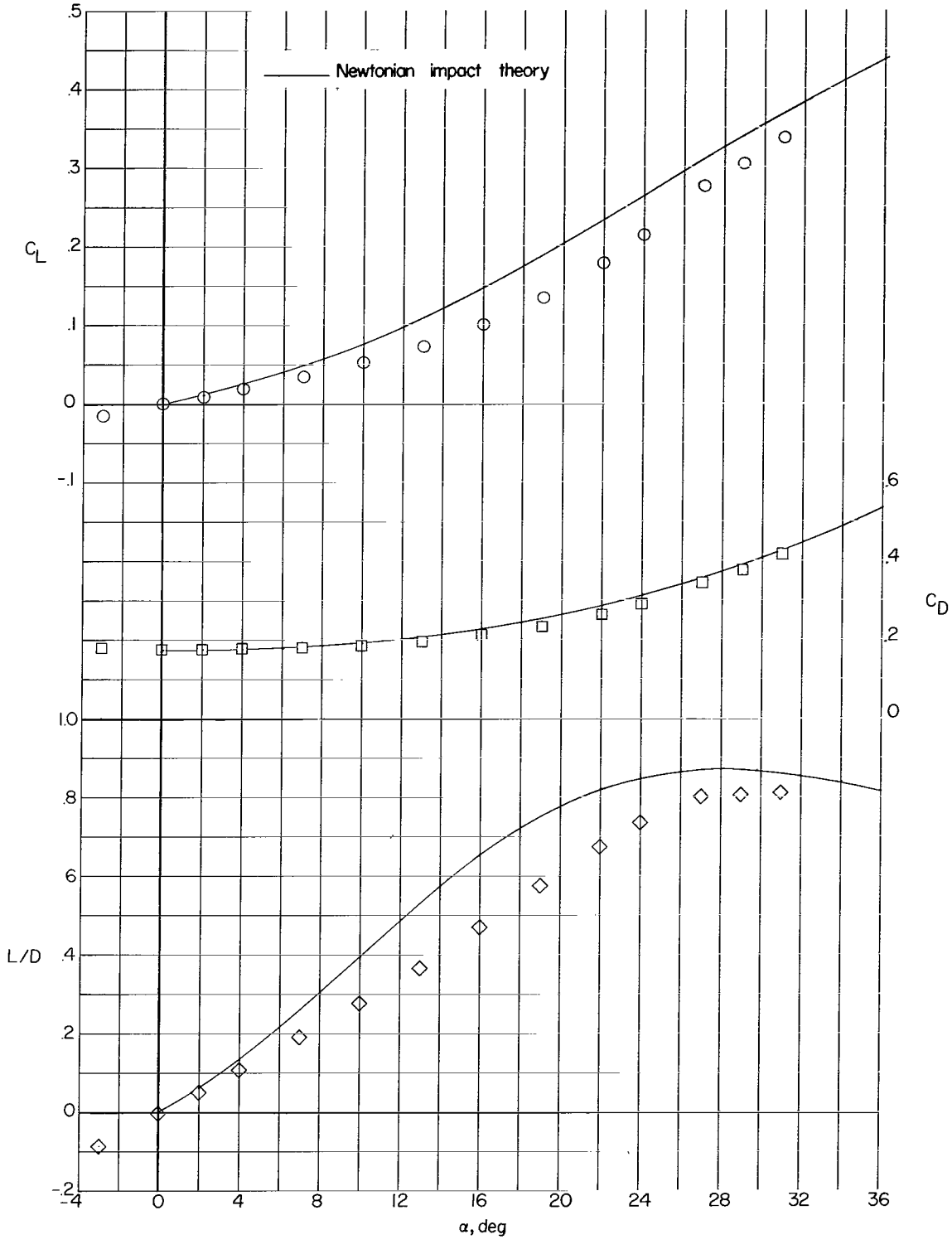

Figure 15.- Concluded.

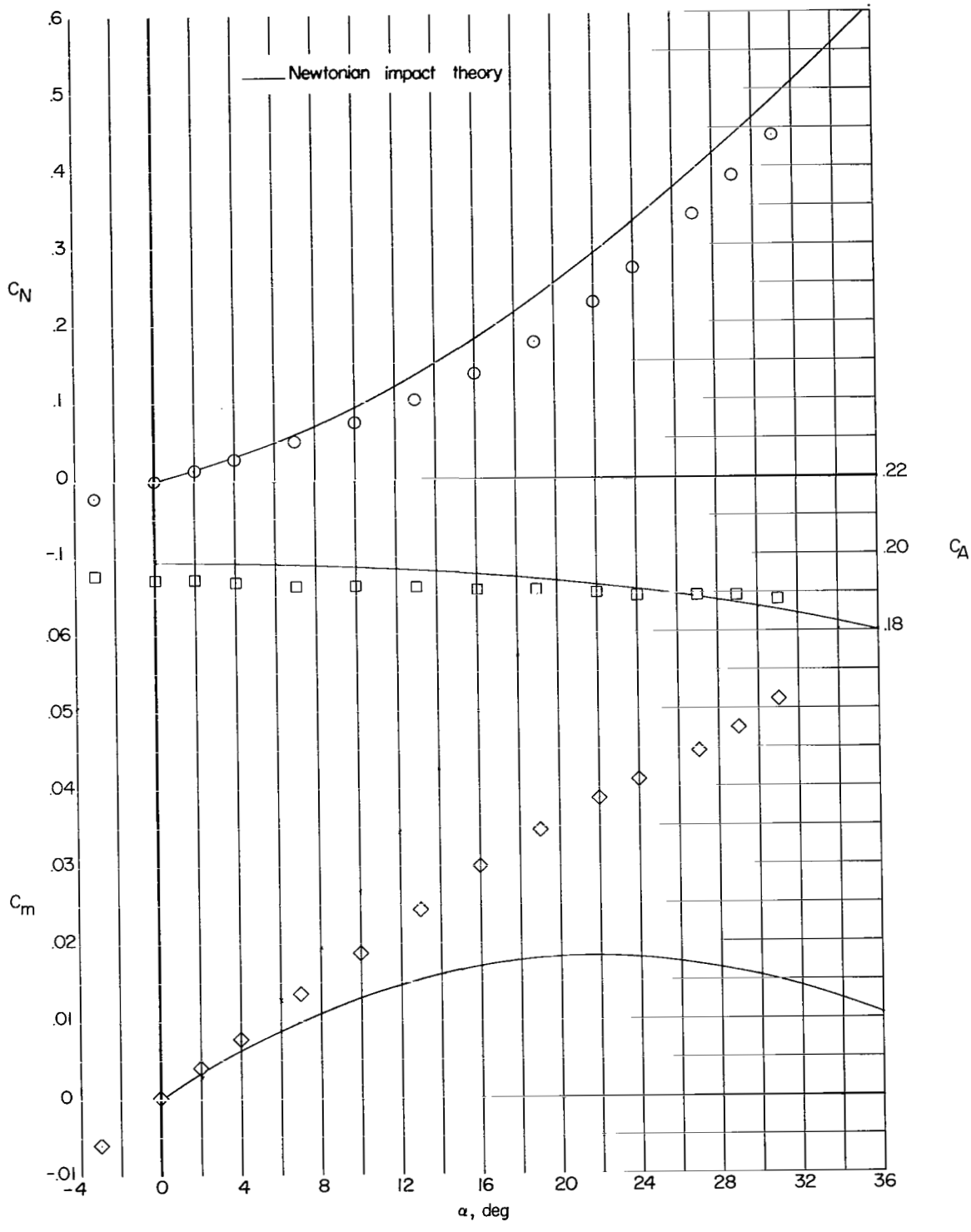

Figure 16.- Basic aerodynamic characteristics. t/c = 0.299; $\Lambda = 85^0$.

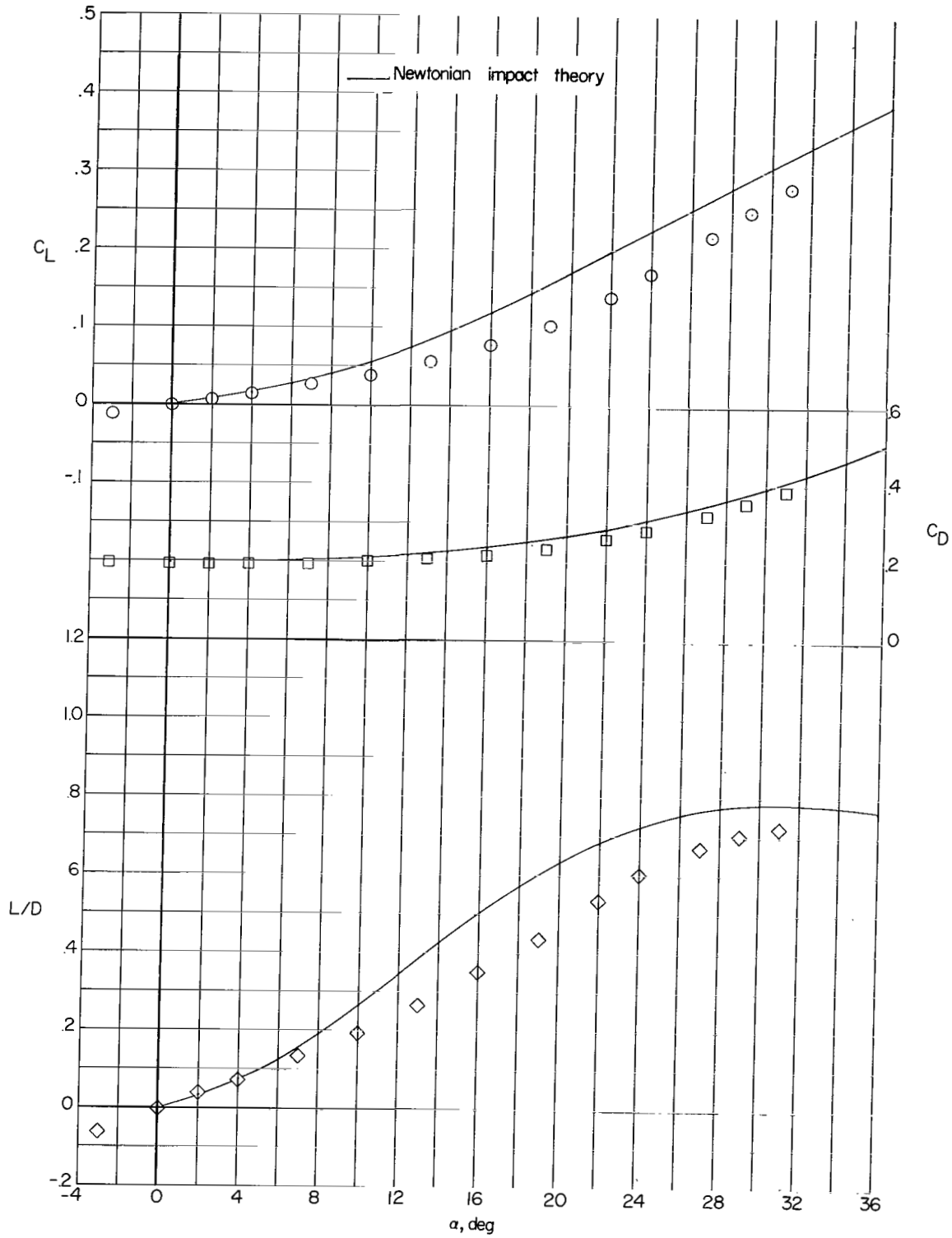

Figure 16.- Concluded.

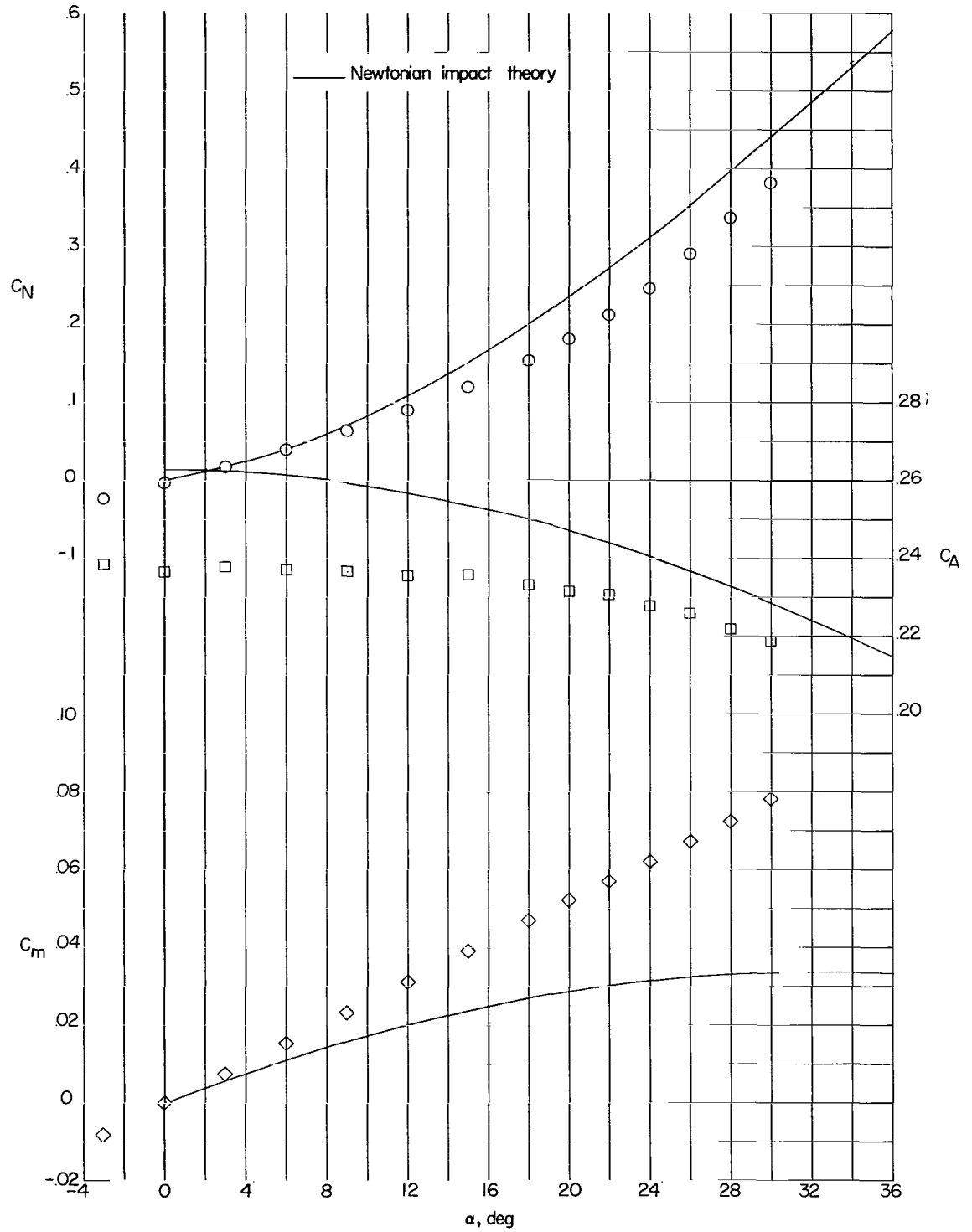

Figure 17.- Basic aerodynamic characteristics $t/c = 0.299$; $\Lambda = 90^0$.

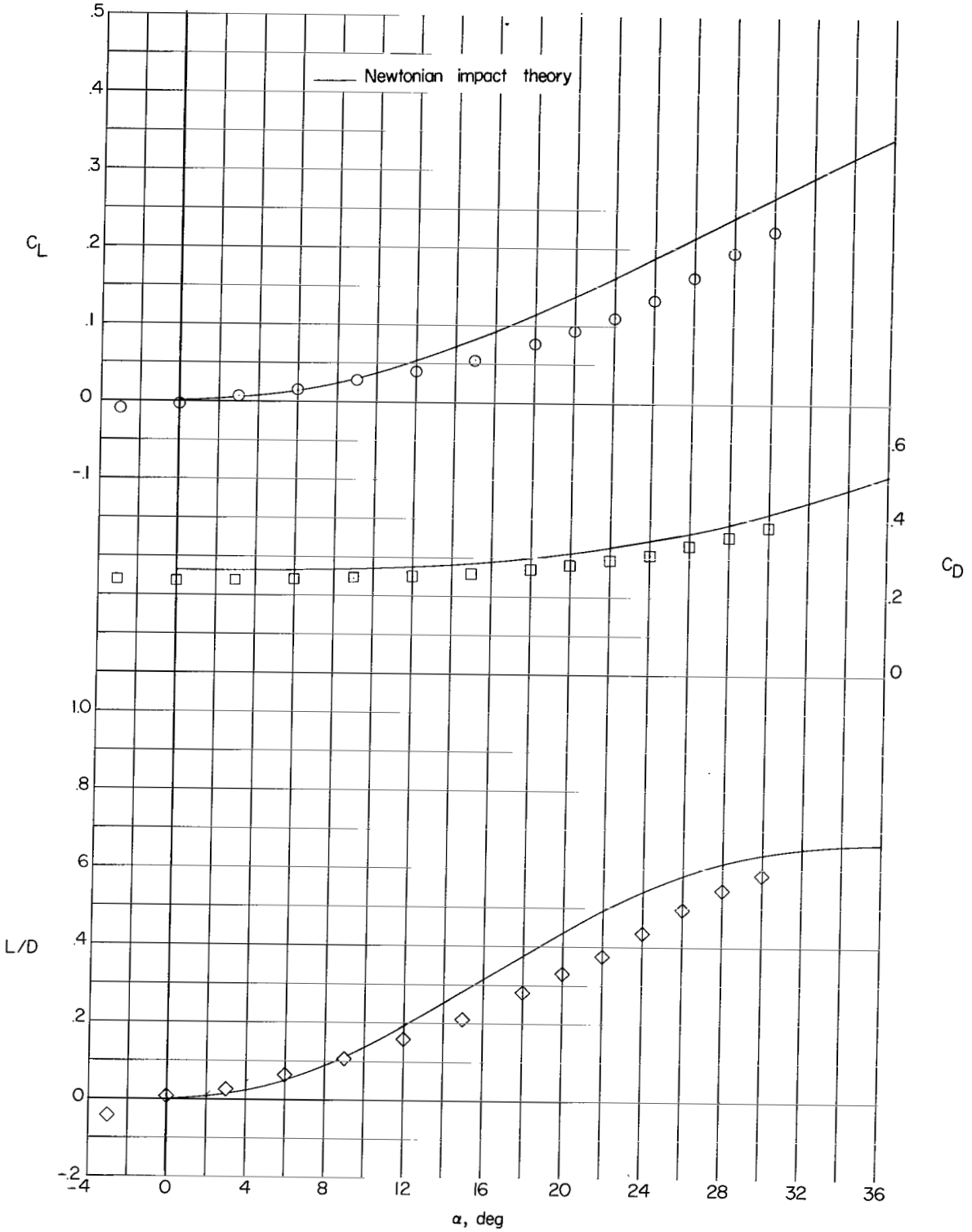

Figure 17.- Concluded.

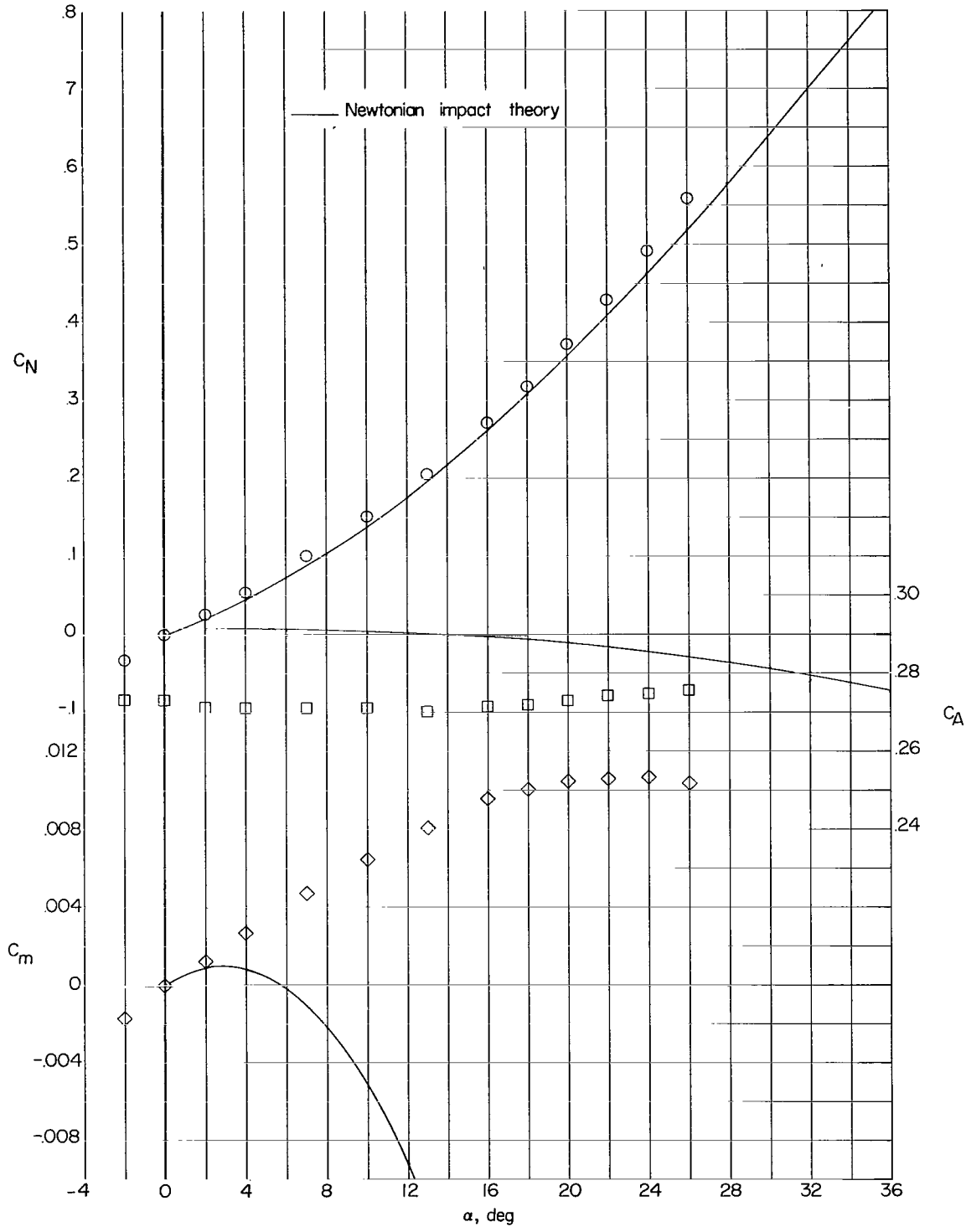

Figure 18.- Basic aerodynamic characteristics. t/c = 0.205; Λ = 45°.

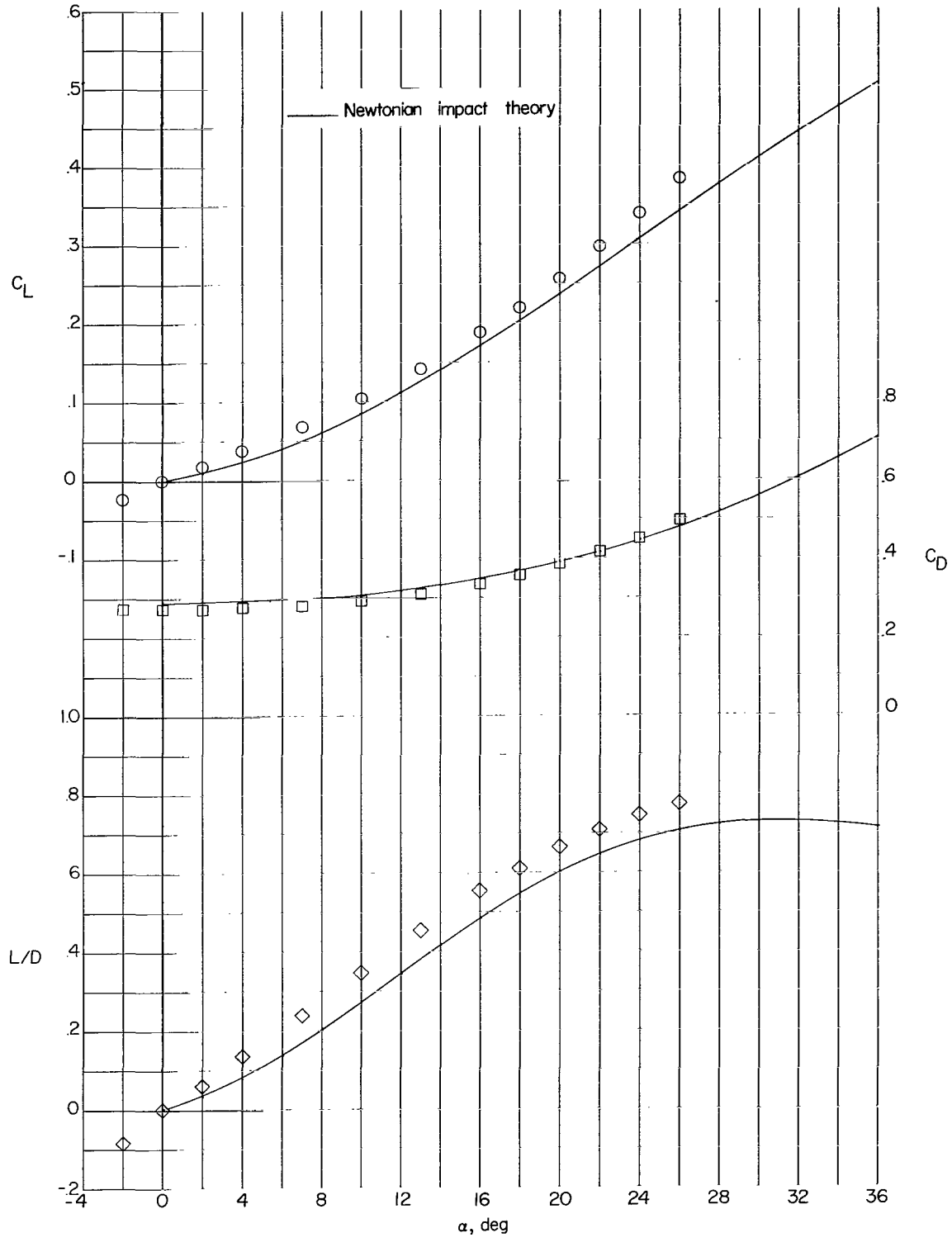

Figure 18.- Concluded.

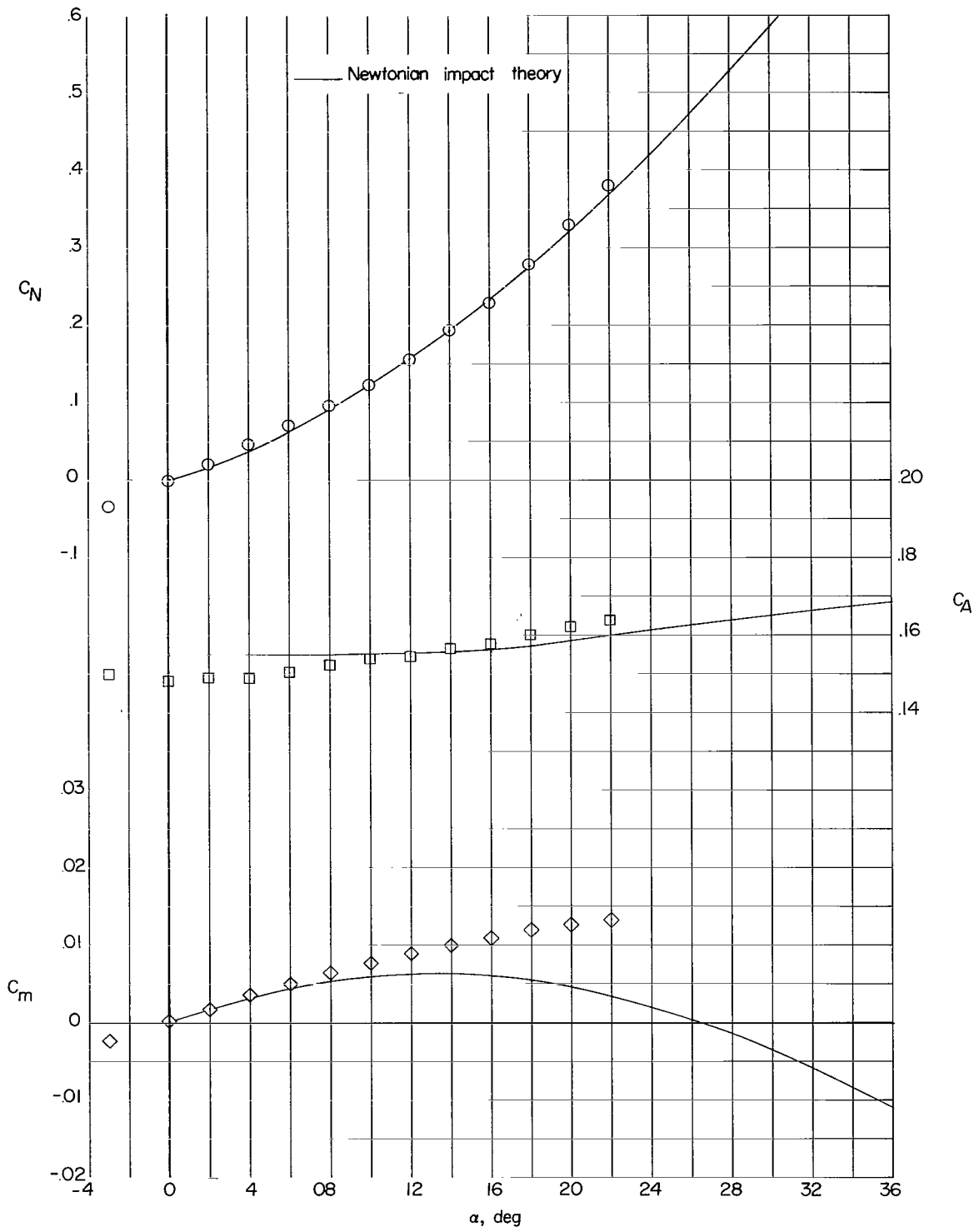

Figure 19.- Basic aerodynamic characteristics. t/c = 0.205; Λ = 60°.

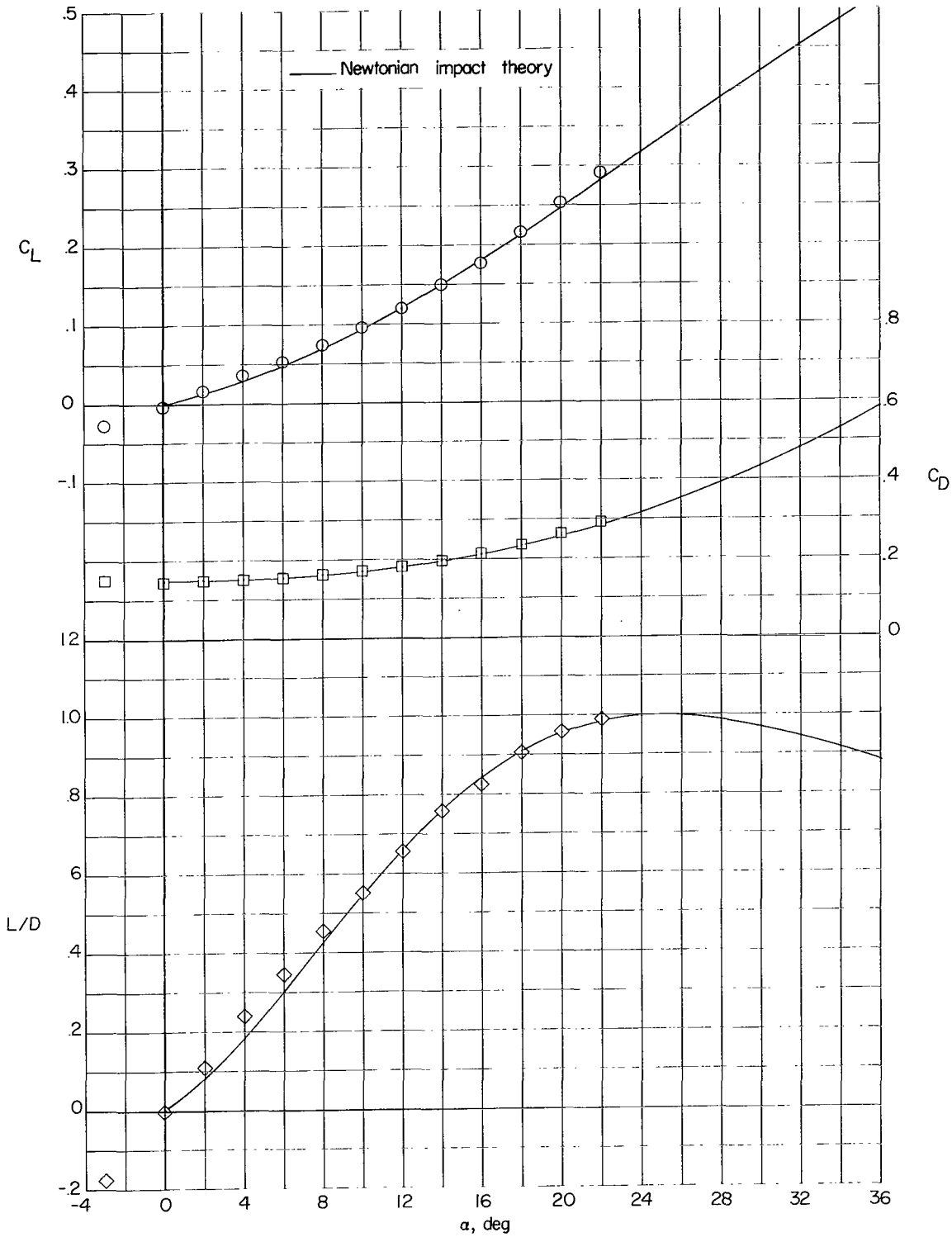

Figure 19.- Concluded.

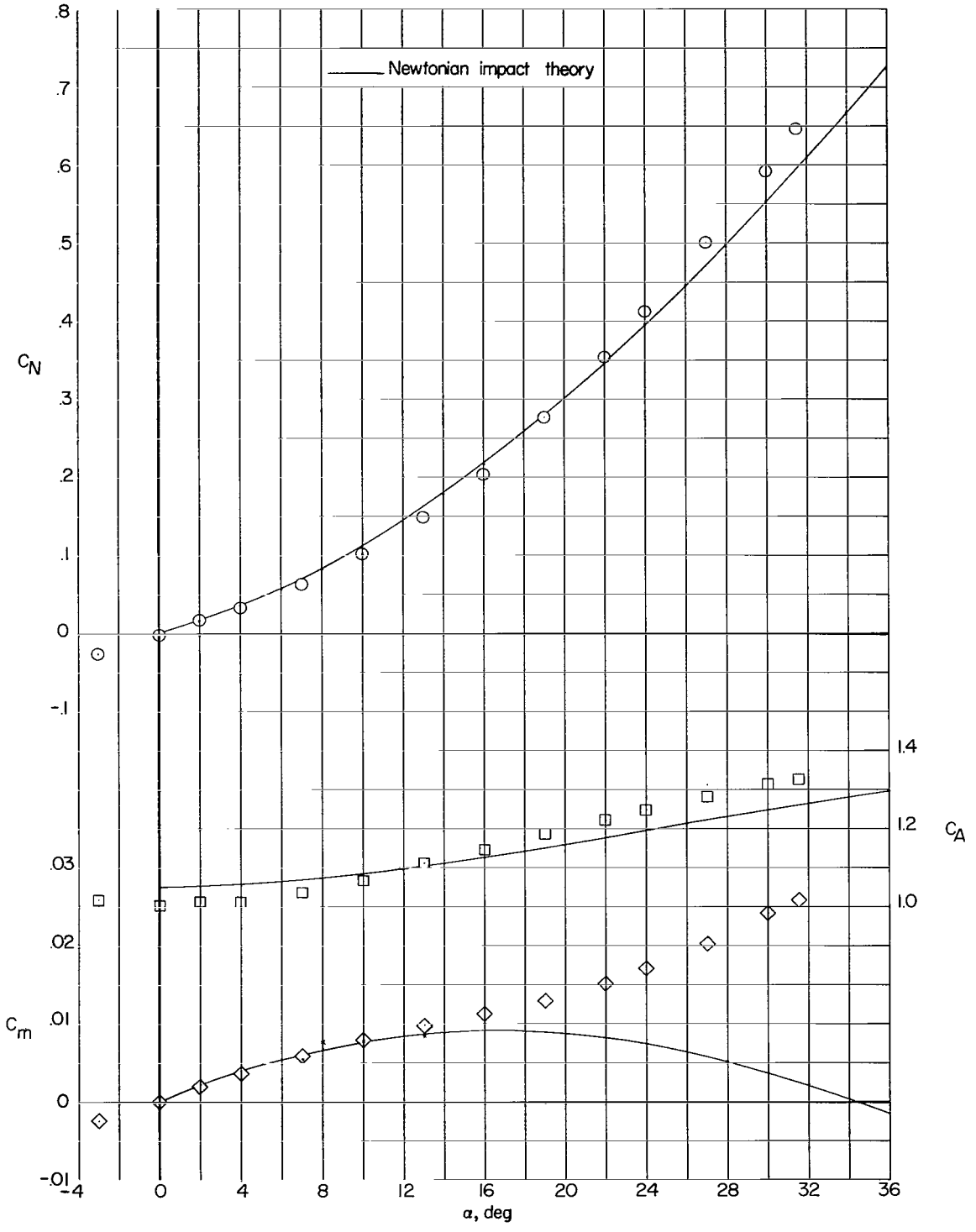

Figure 20.- Basic aerodynamic characteristics. t/c = 0.205; $\Lambda = 70^0$.

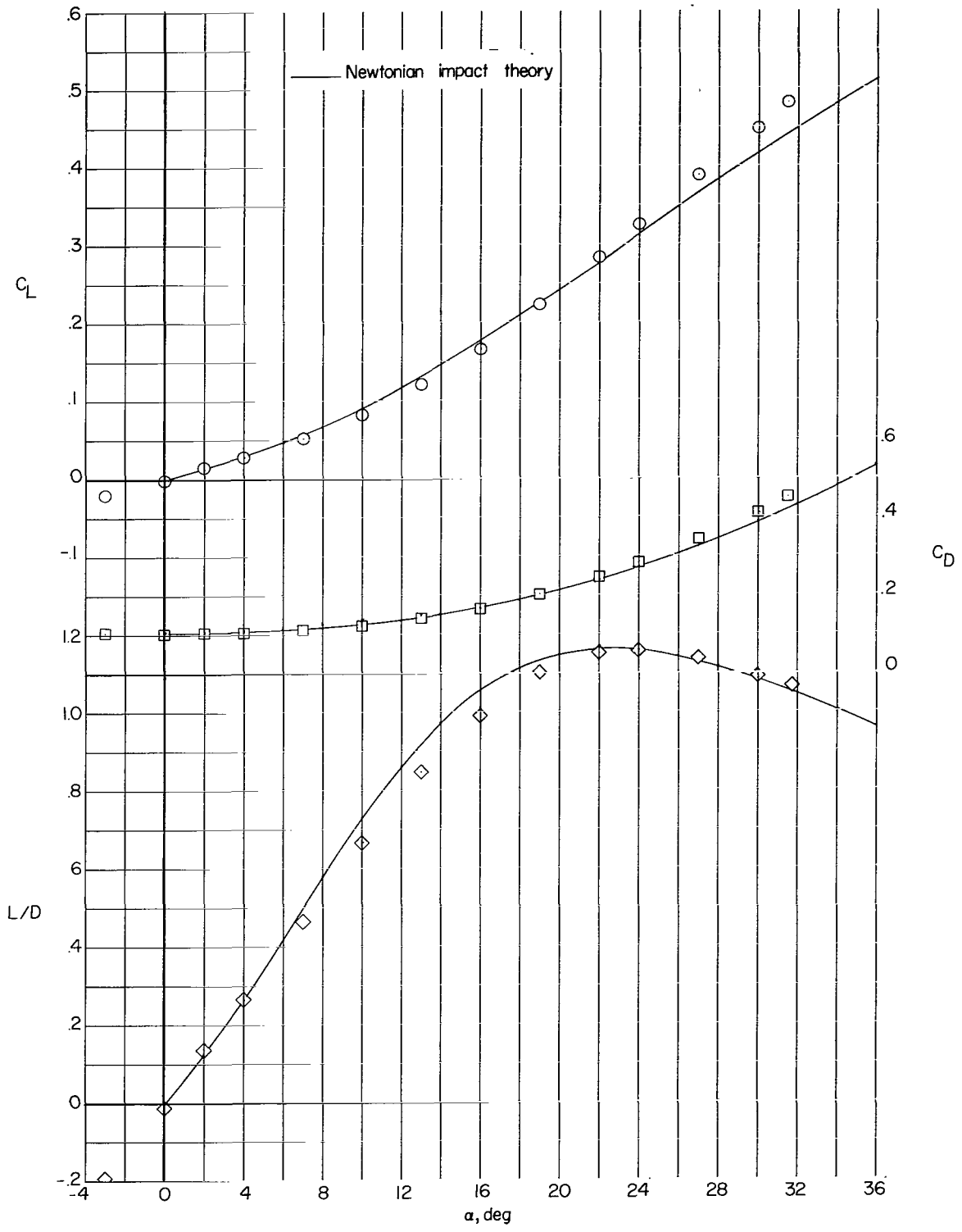

Figure 20.- Concluded.

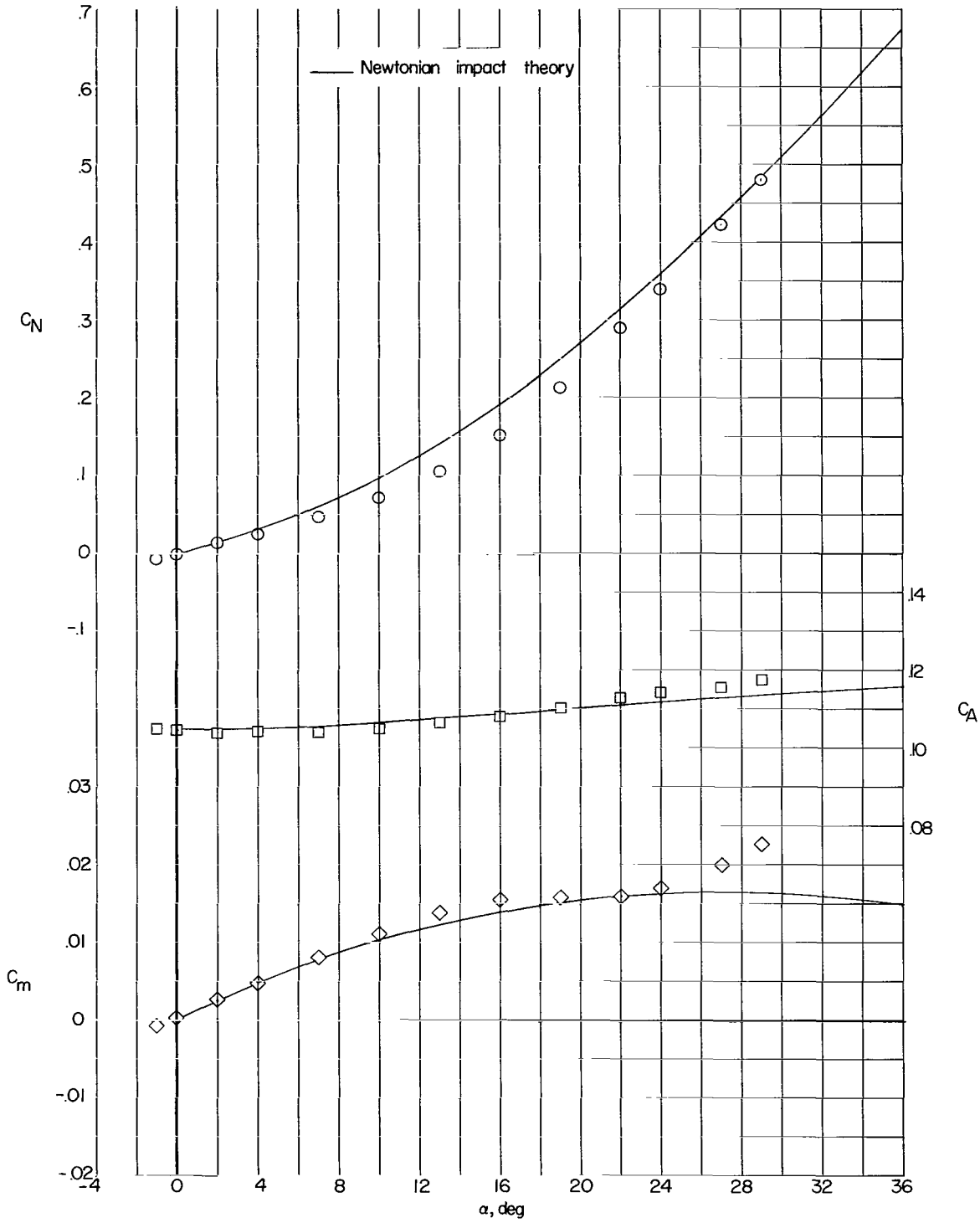

Figure 21.- Basic aerodynamic characteristics. t/c = 0.205; Λ = 80°.

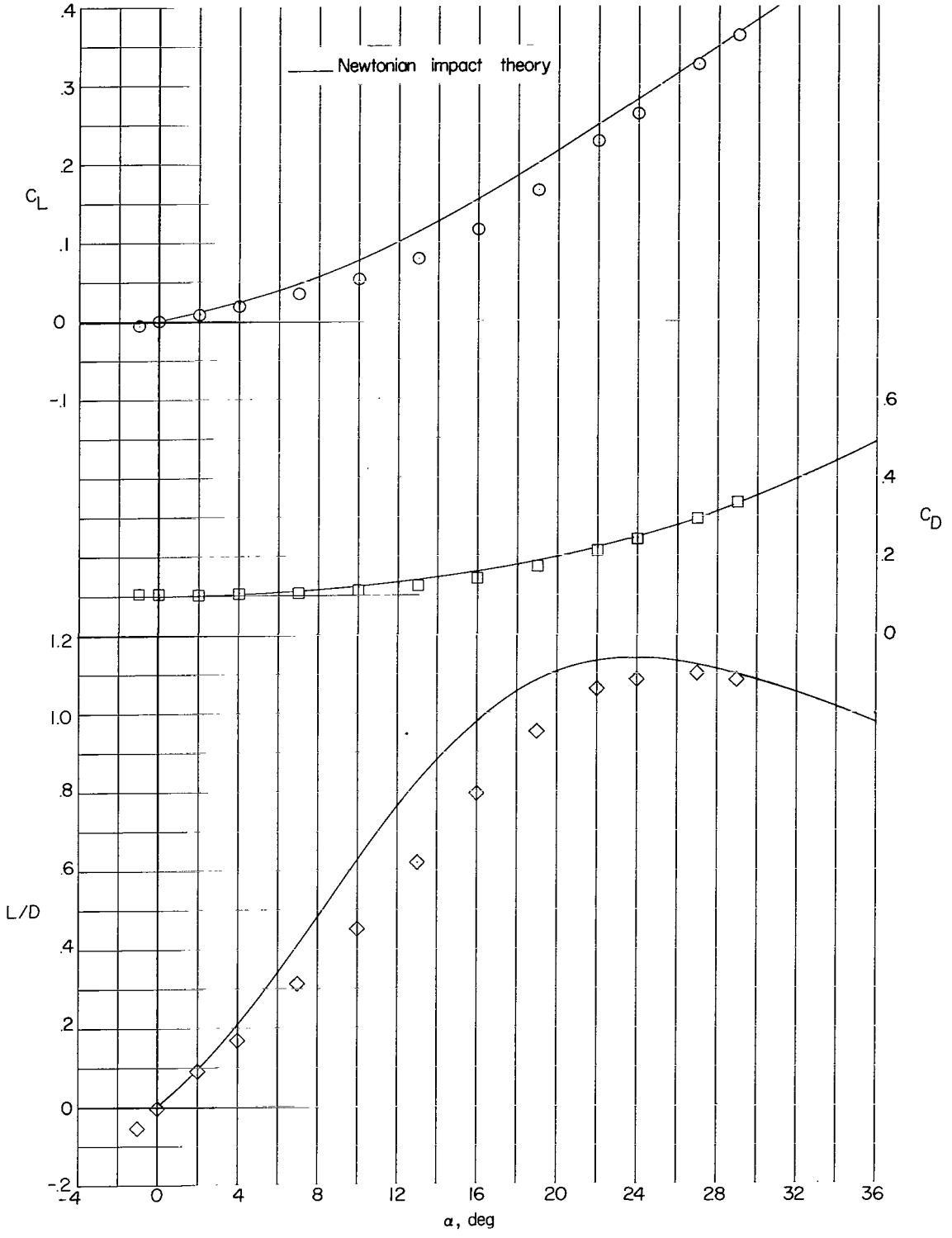

Figure 21.- Concluded.

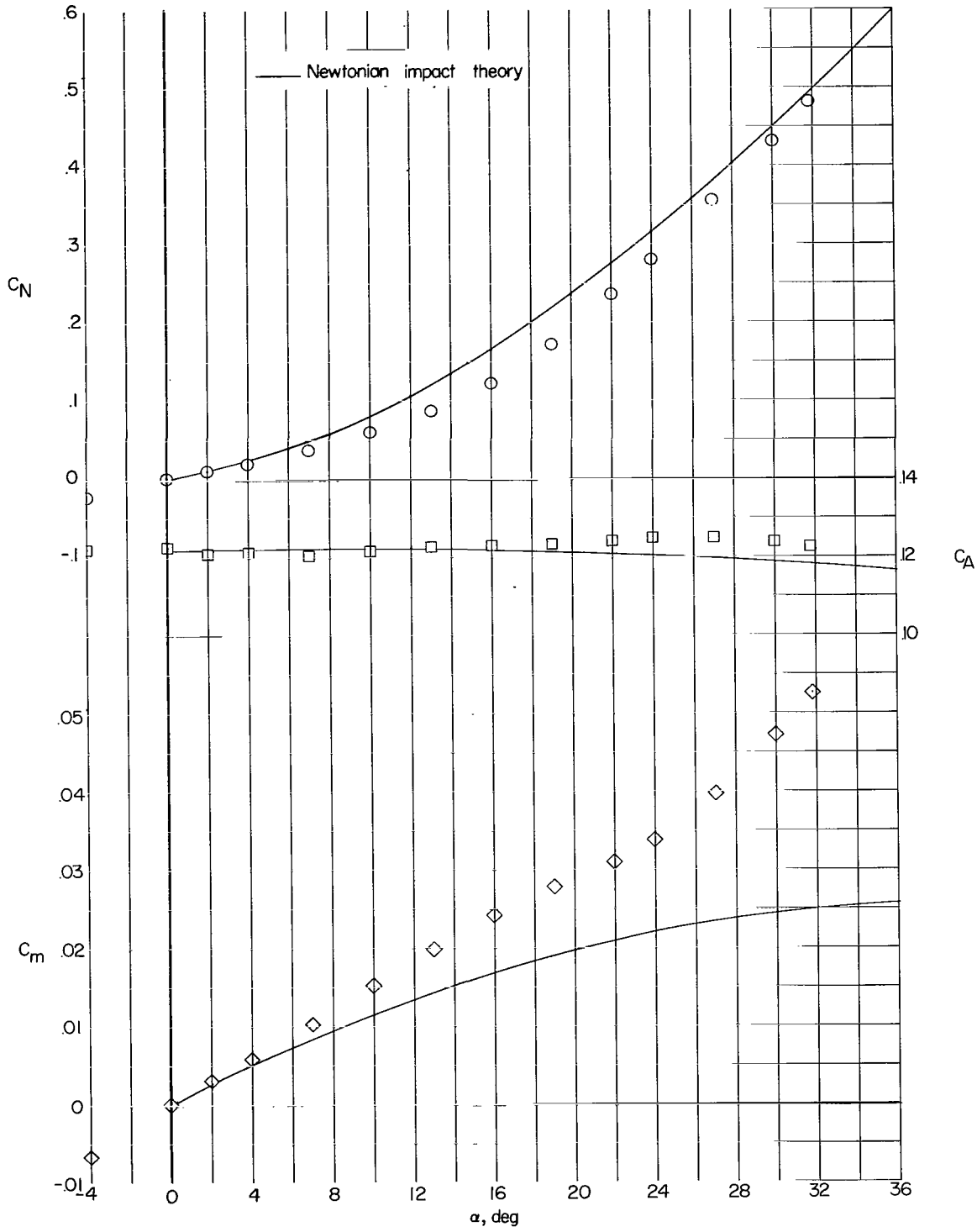

Figure 22.- Basic aerodynamic characteristics. t/c = 0.205; Λ = 85°.

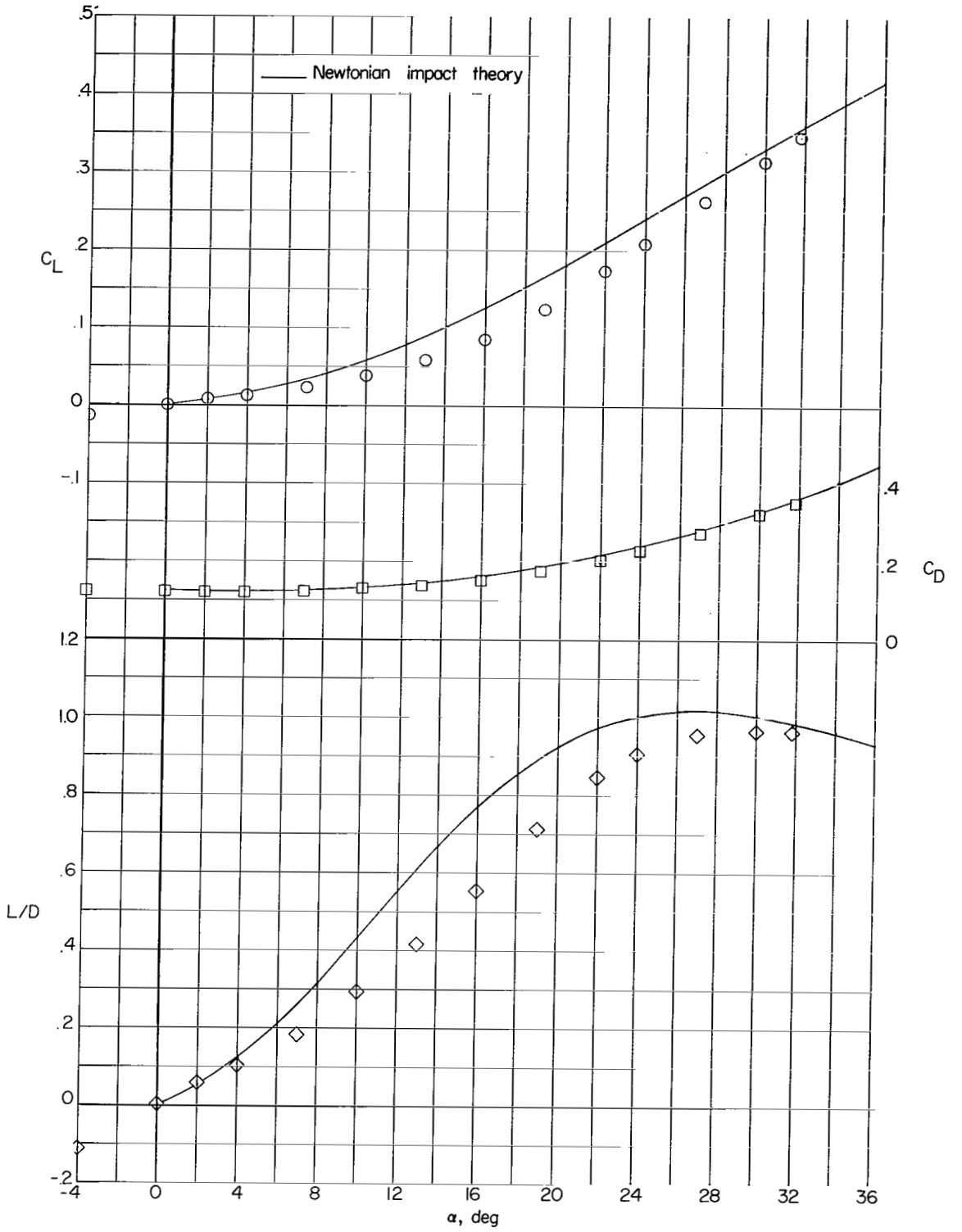

Figure 22.- Concluded.

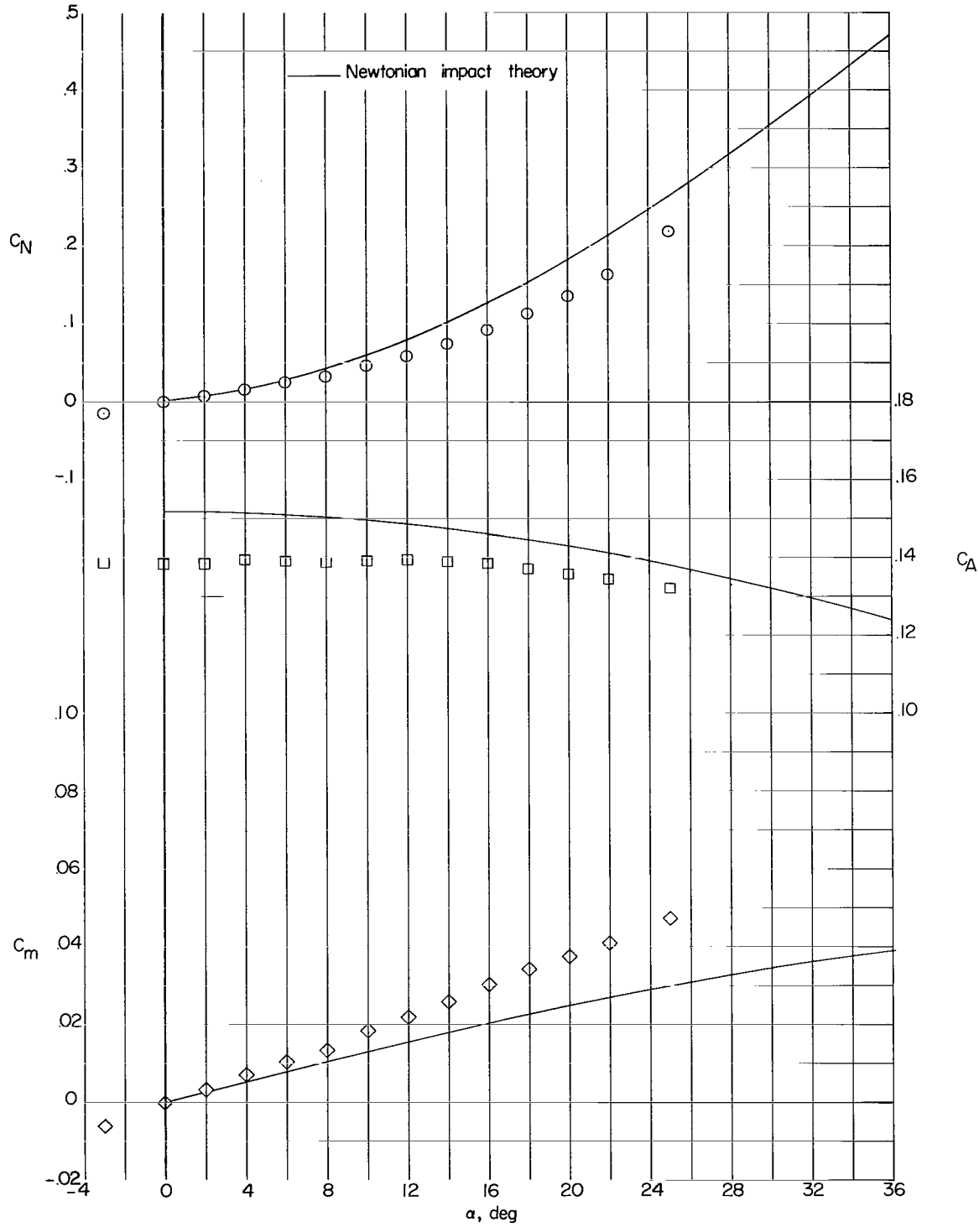

Figure 23.- Basic aerodynamic characteristics. t/c = 0.205; Λ = 90°.

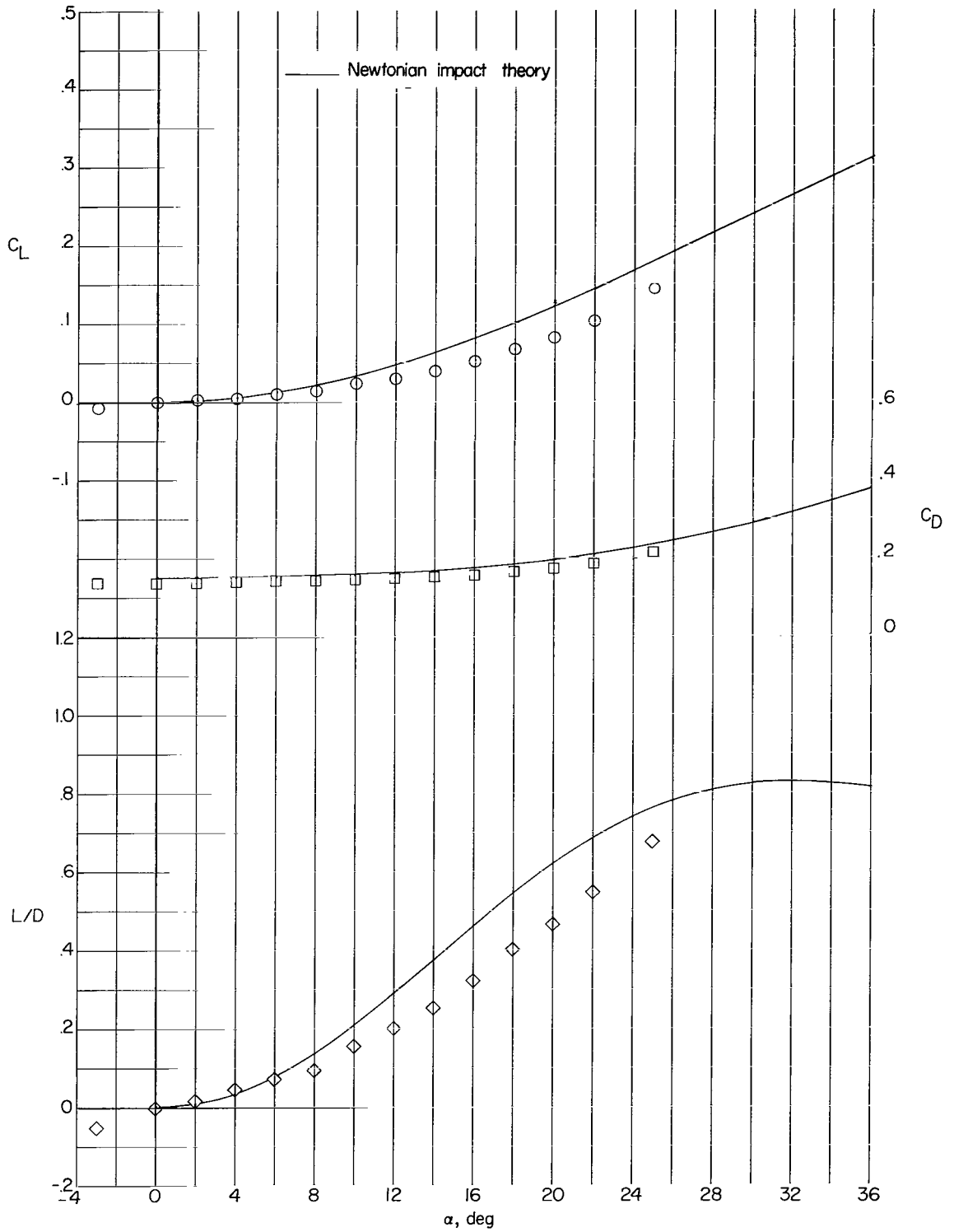

Figure 23.- Concluded.

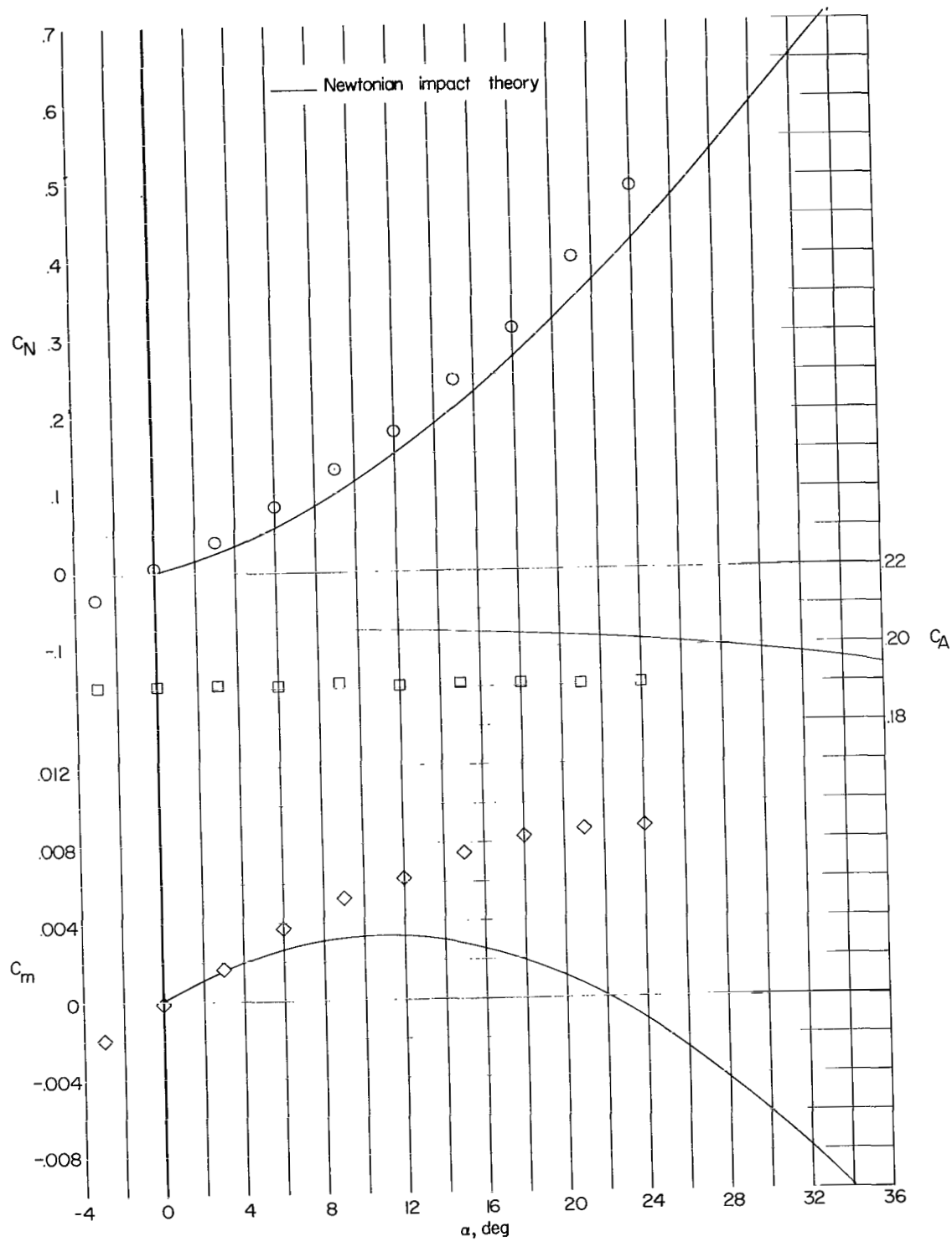

Figure 24.- Basic aerodynamic characteristics. t/c = 0.143; Λ = 45°.

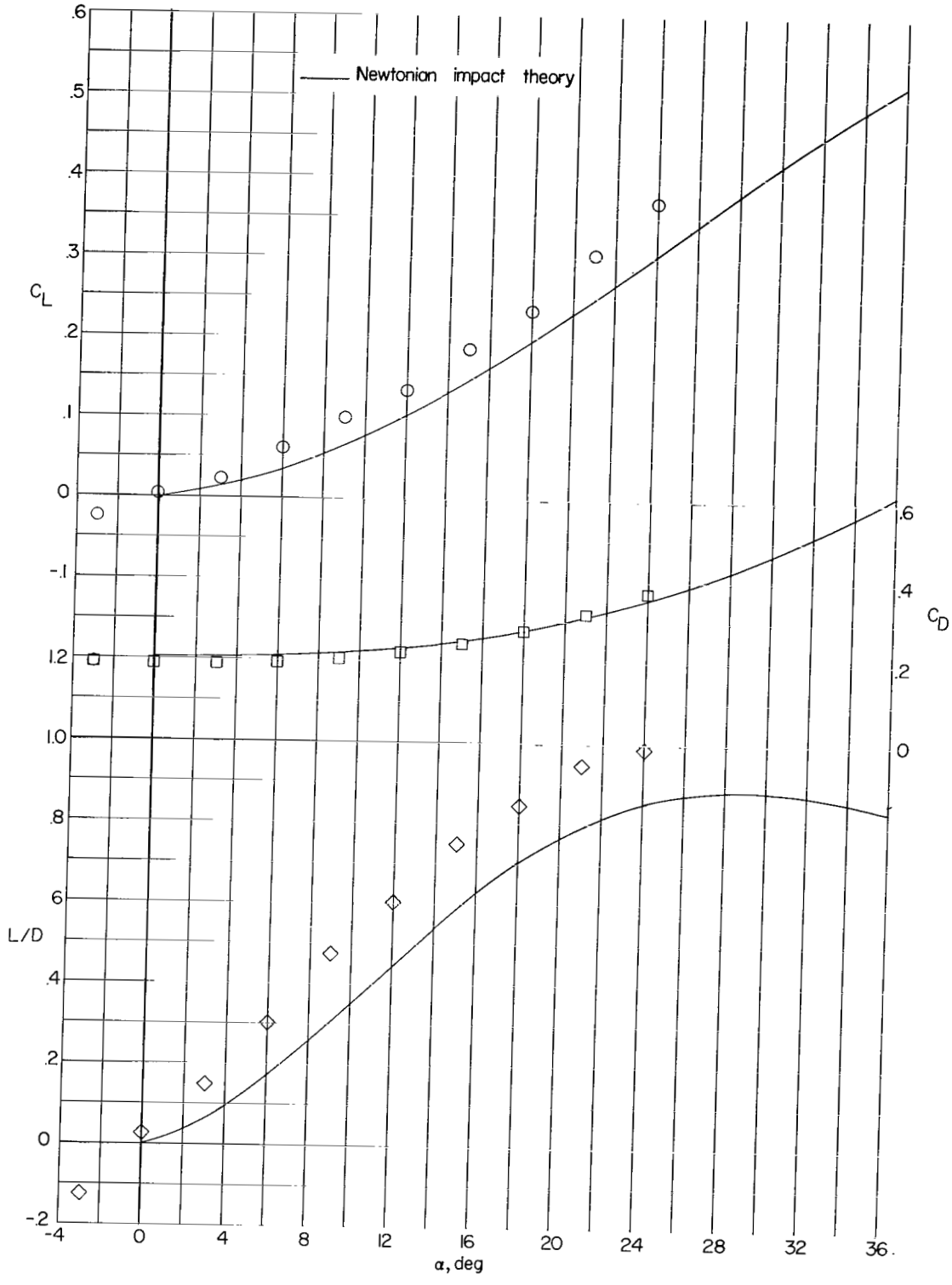

Figure 24.- Concluded.

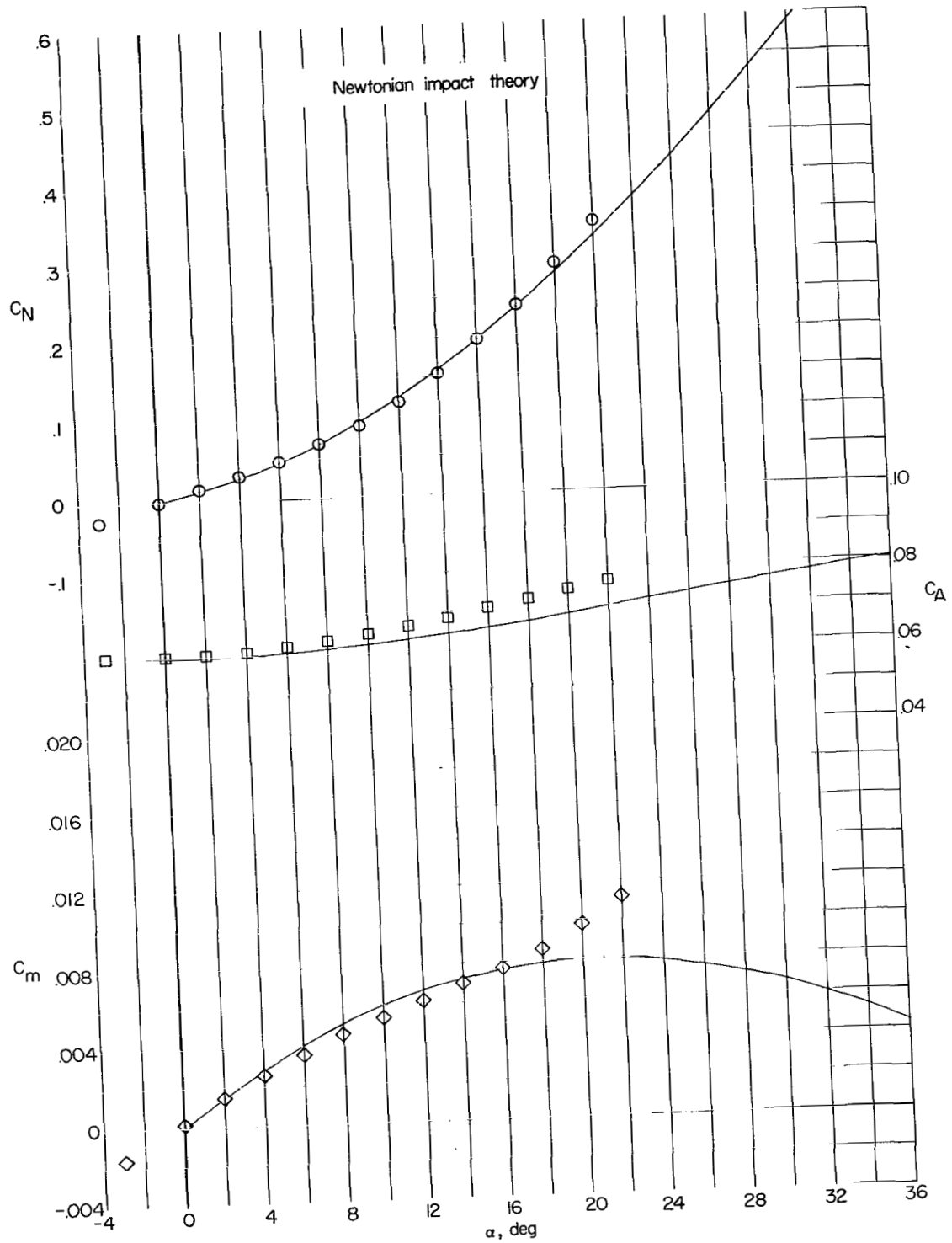

Figure 25.- Basic aerodynamic characteristics. t/c = 0.132; $\Lambda = 70^0$.

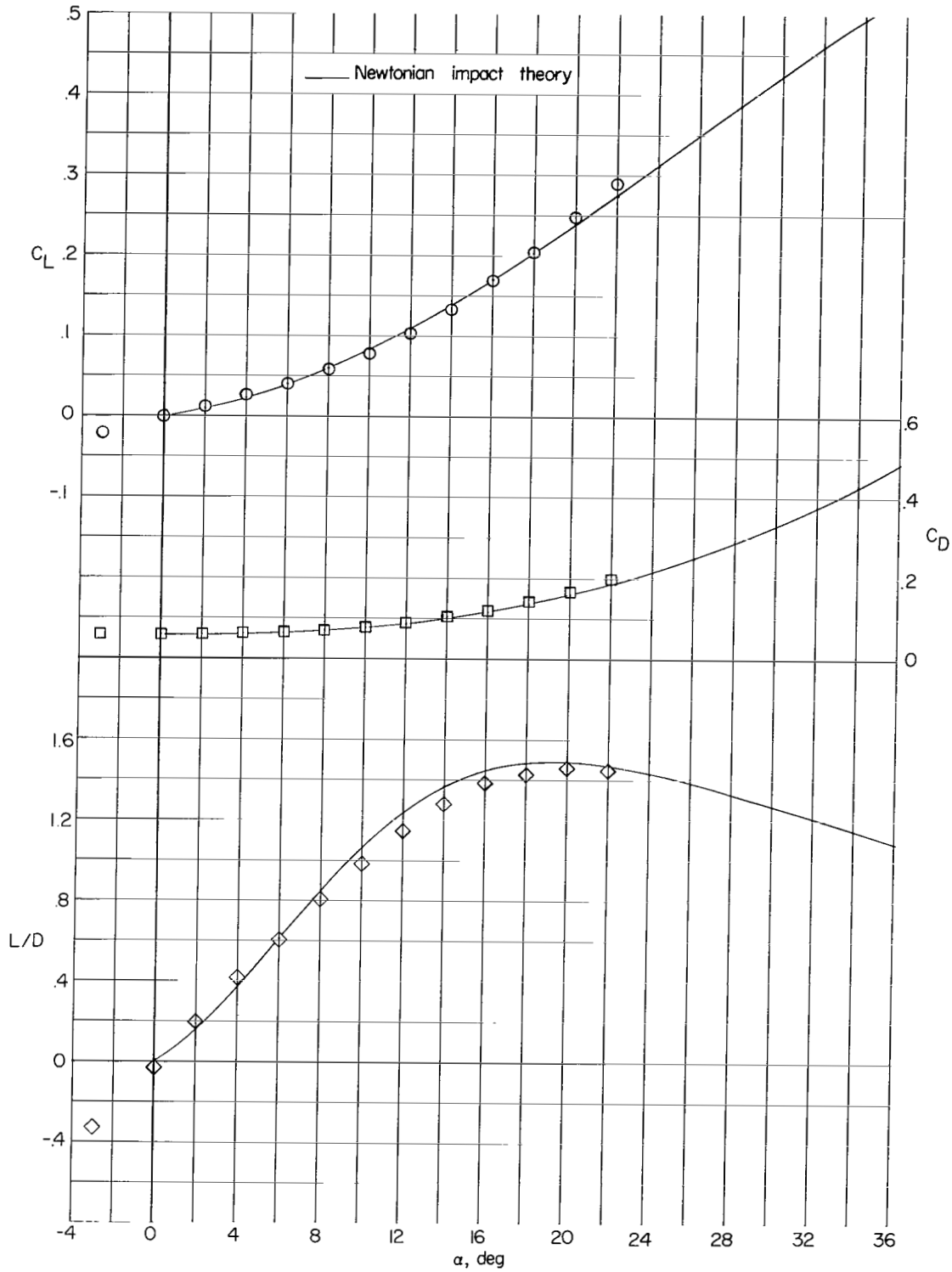

Figure 25.- Concluded.

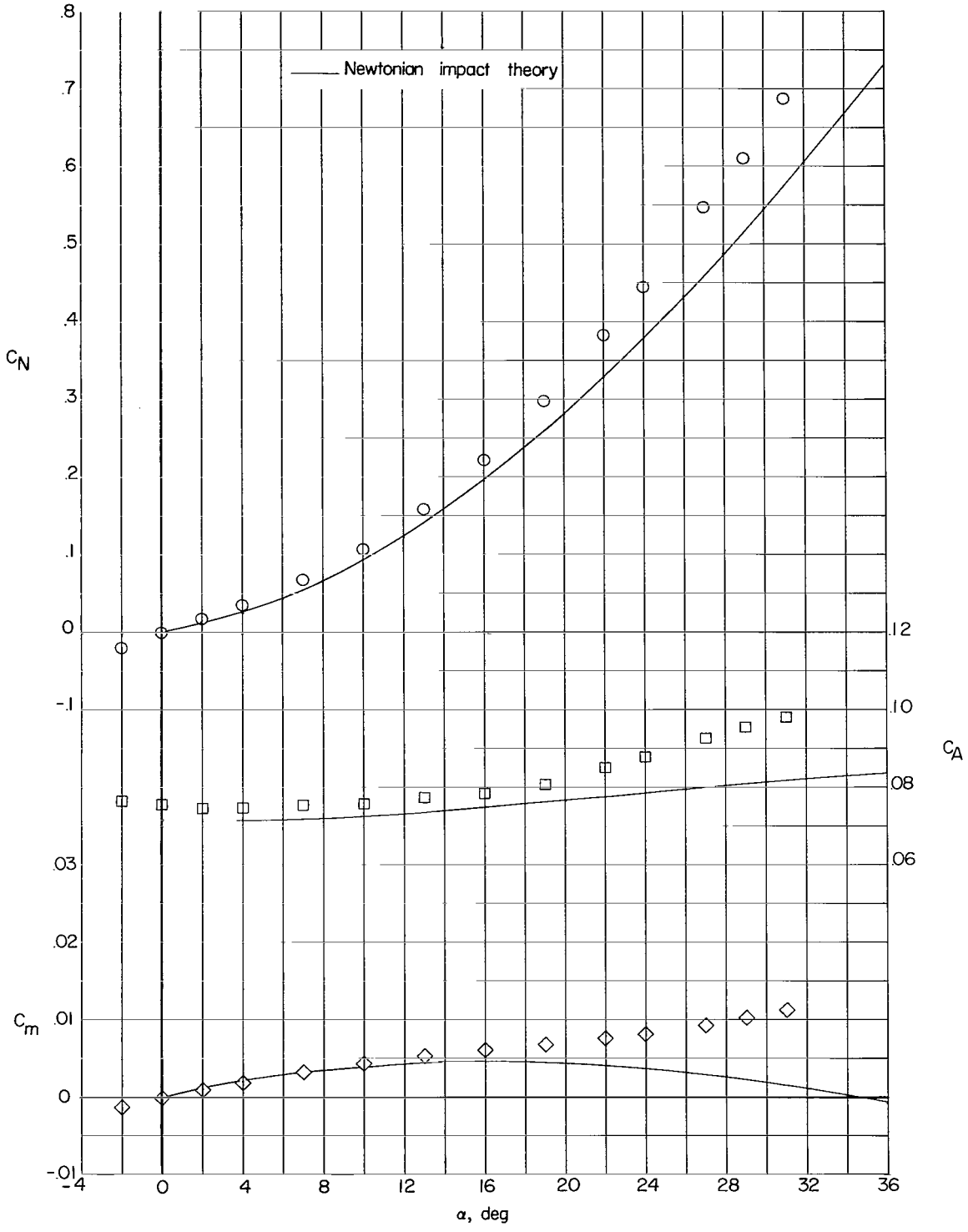

Figure 26.- Basic aerodynamic characteristics. t/c = 0.098; Λ = 60°.

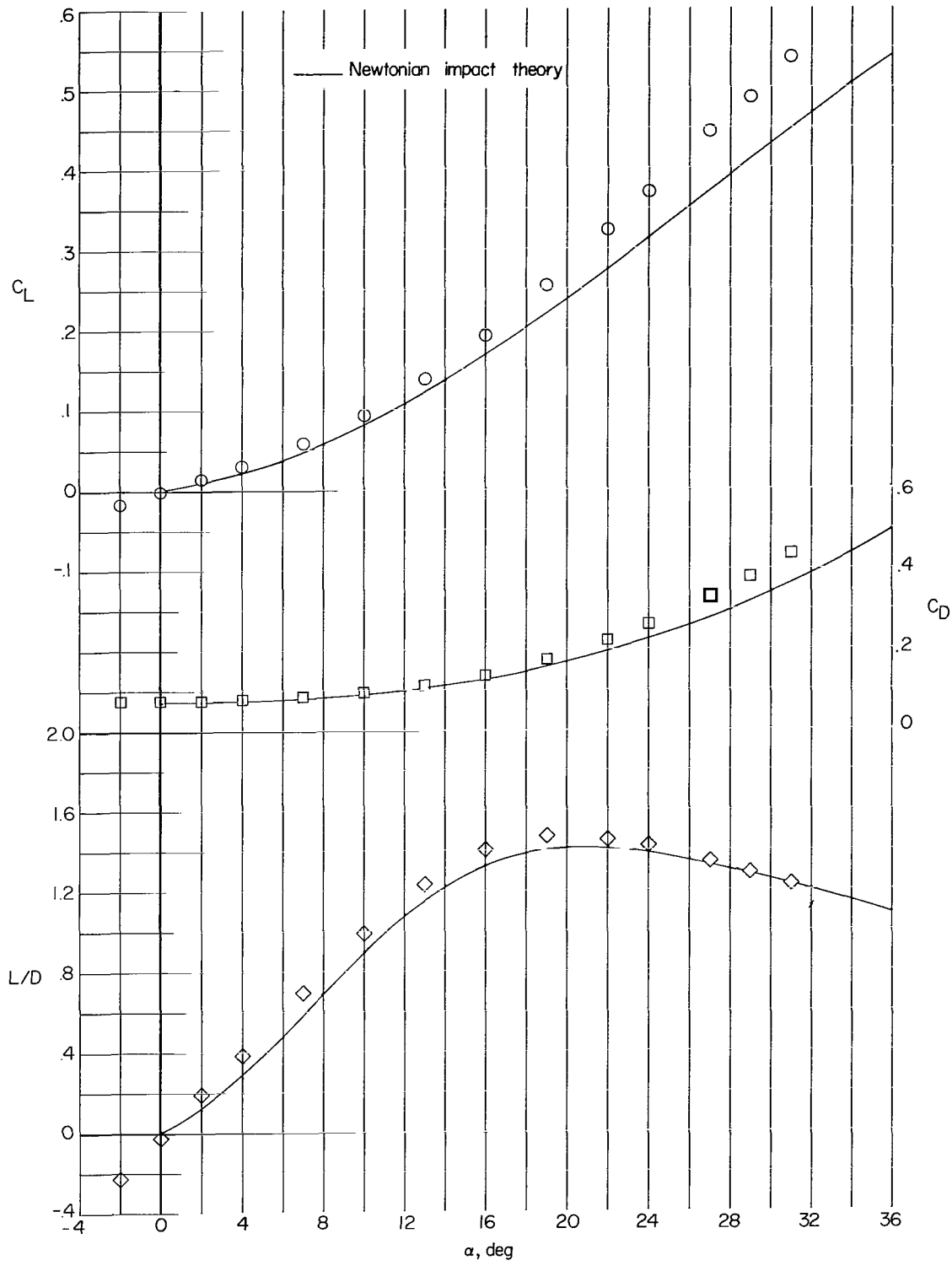

Figure 26.- Concluded.

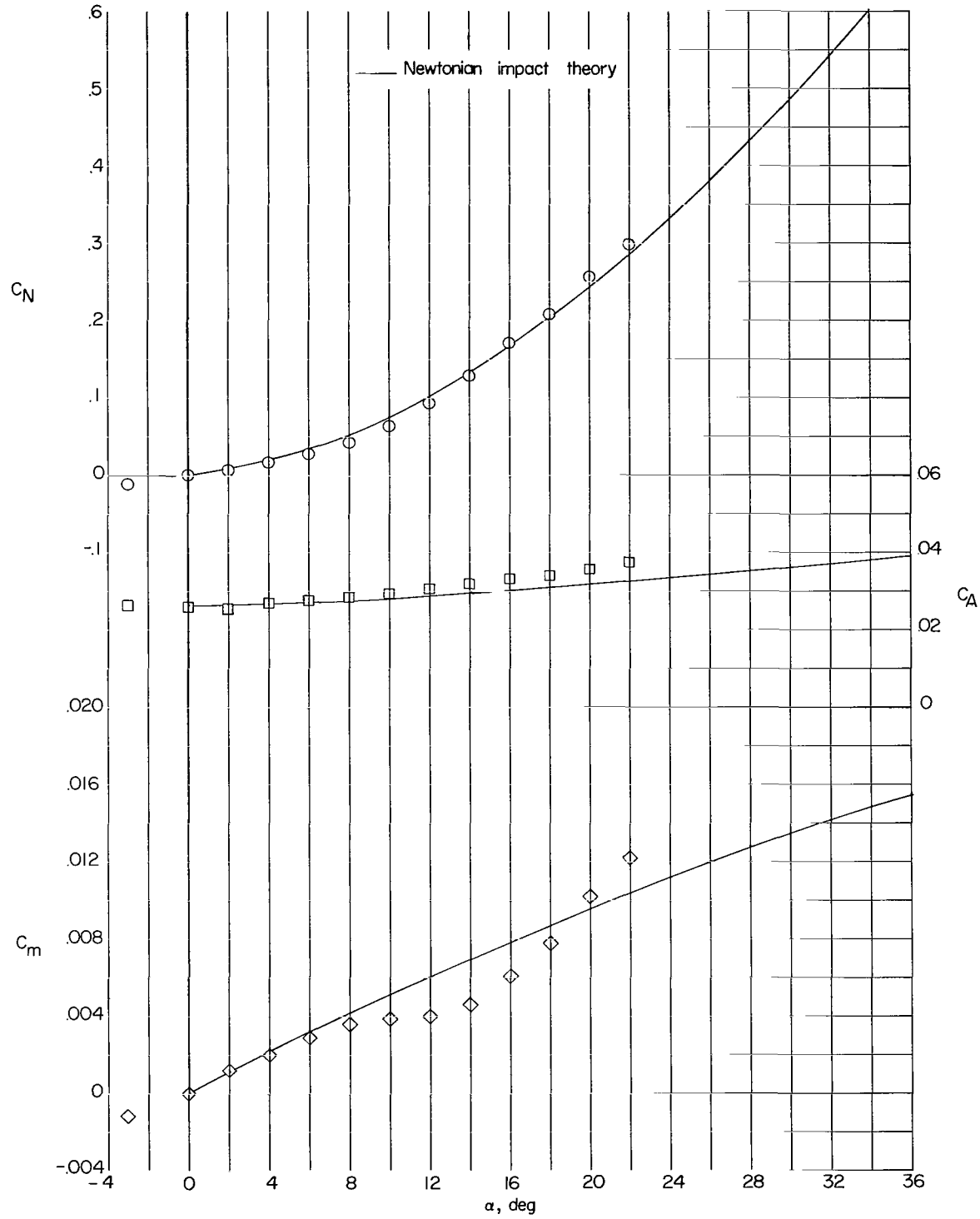

Figure 27.- Basic aerodynamic characteristics. t/c = 0.083; $\Lambda = 80^{0}$.

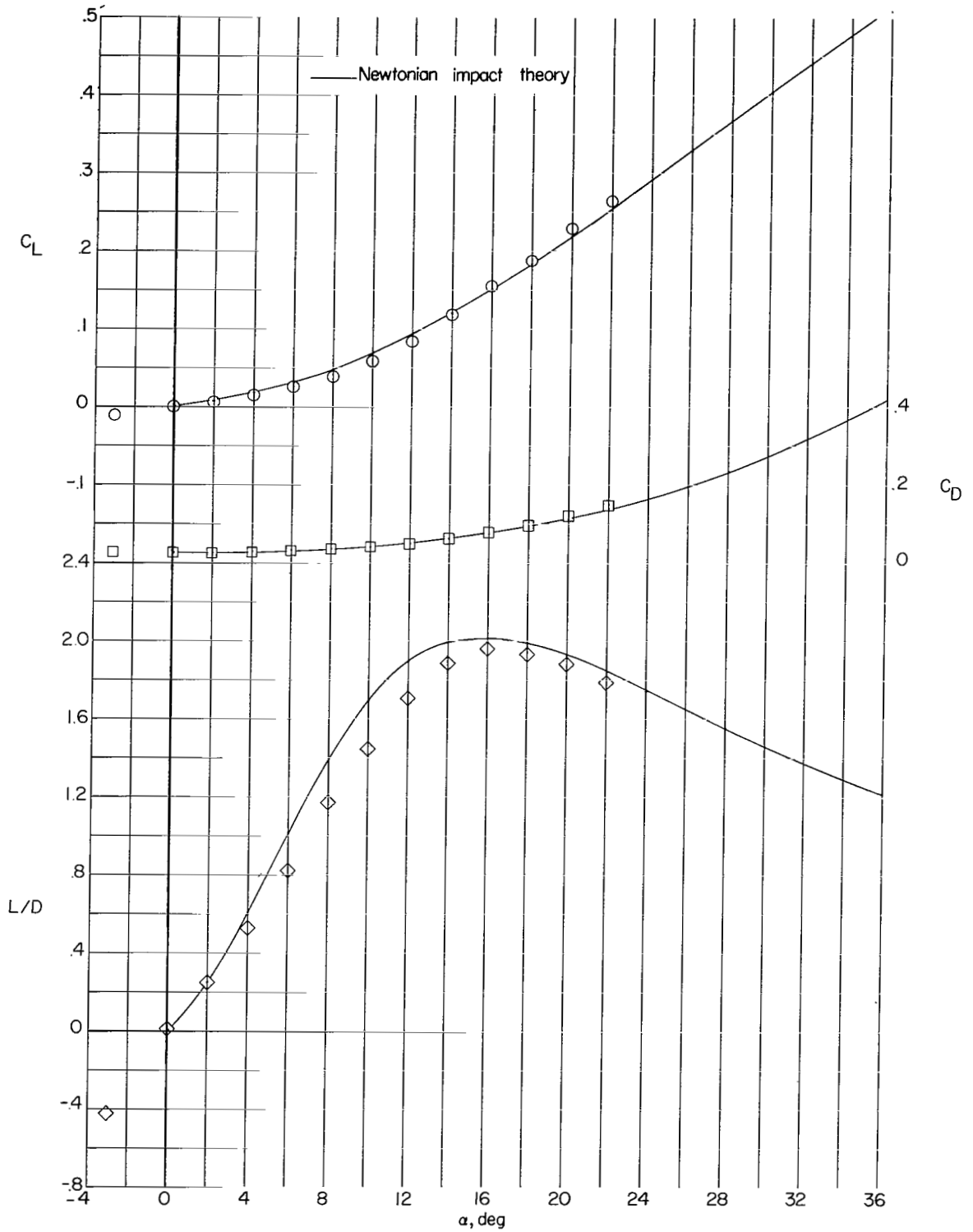

Figure 27.- Concluded.

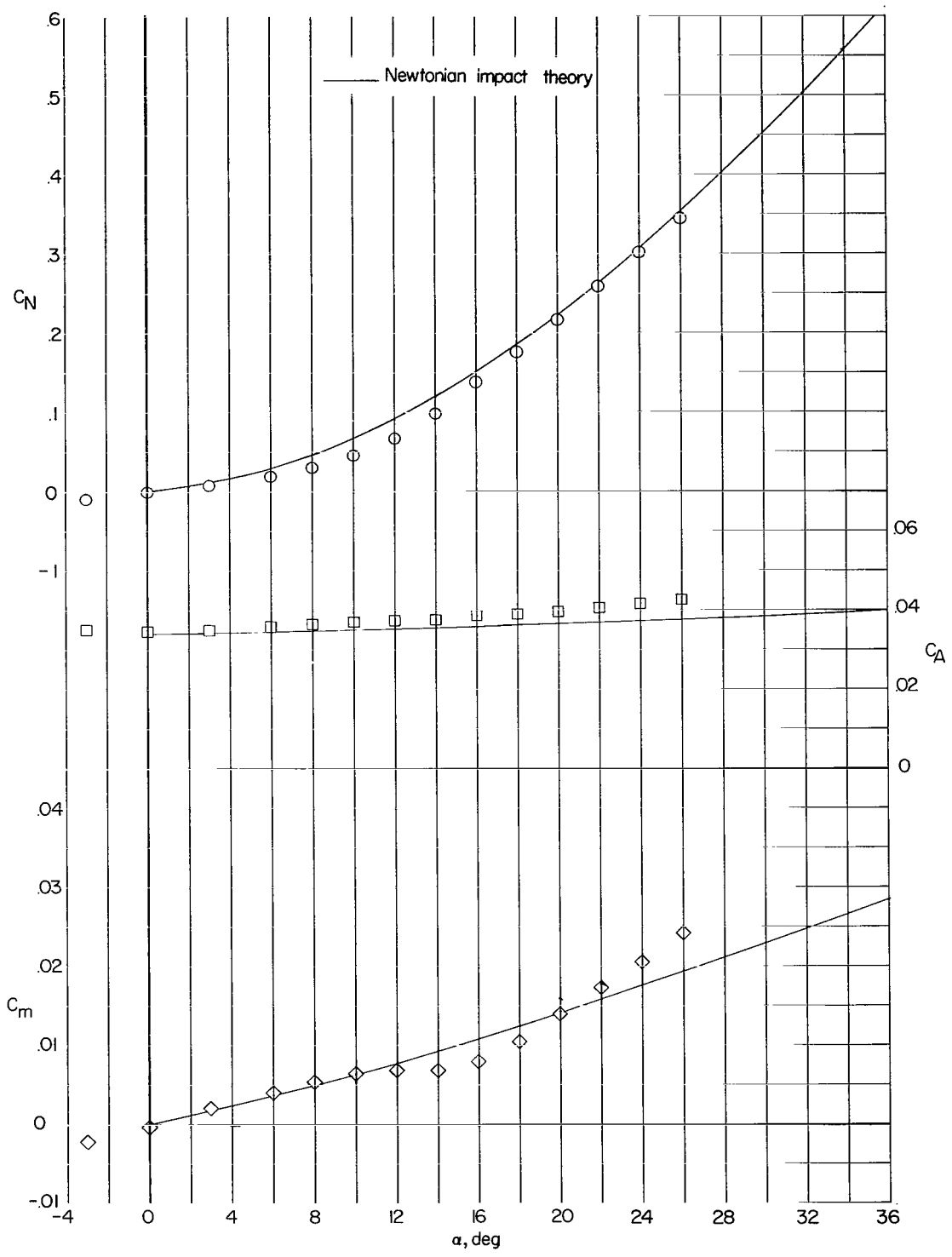

Figure 28.- Basic aerodynamic characteristics. t/c = 0.083; Λ = 85°.

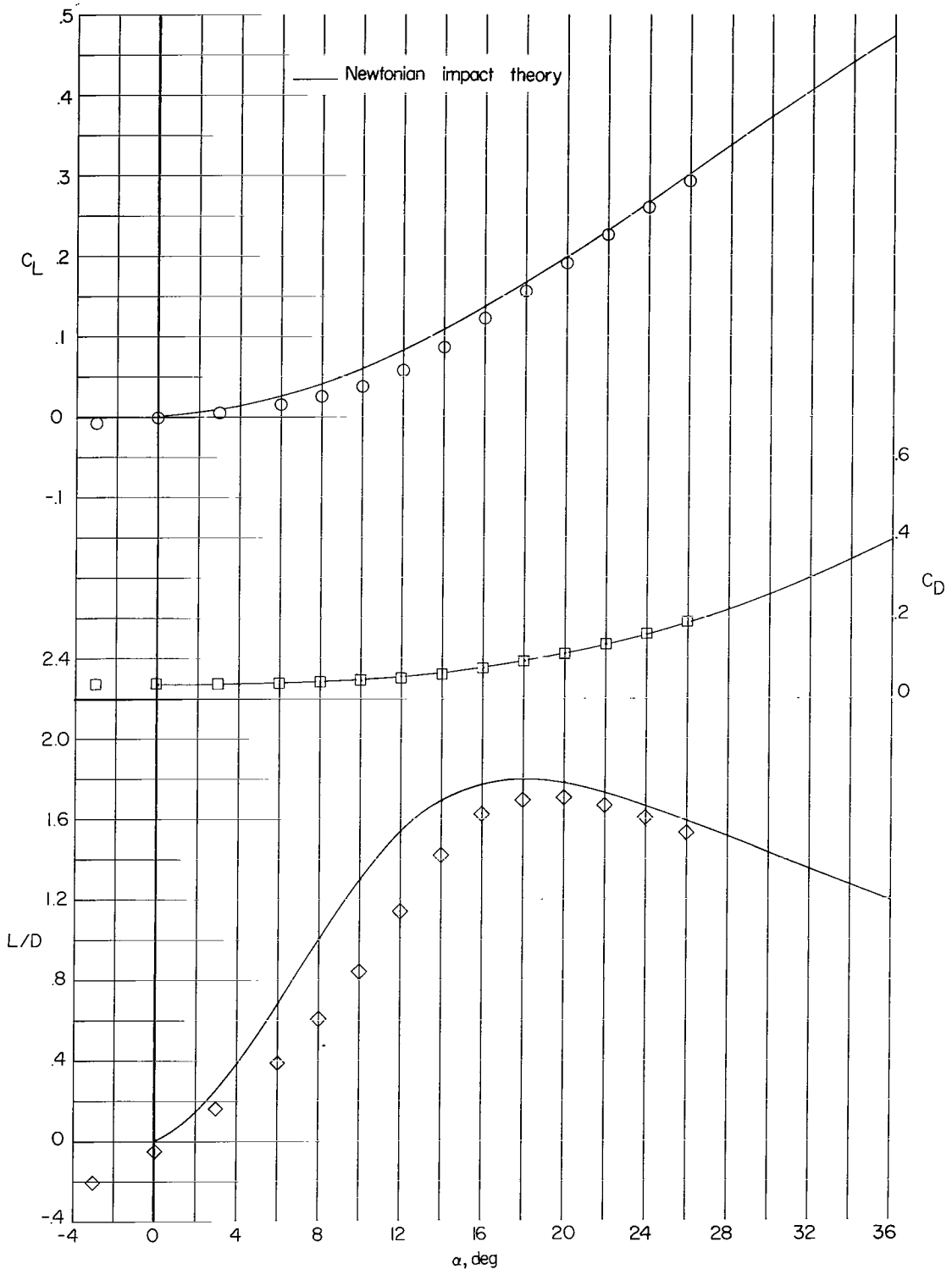

Figure 28.- Concluded.

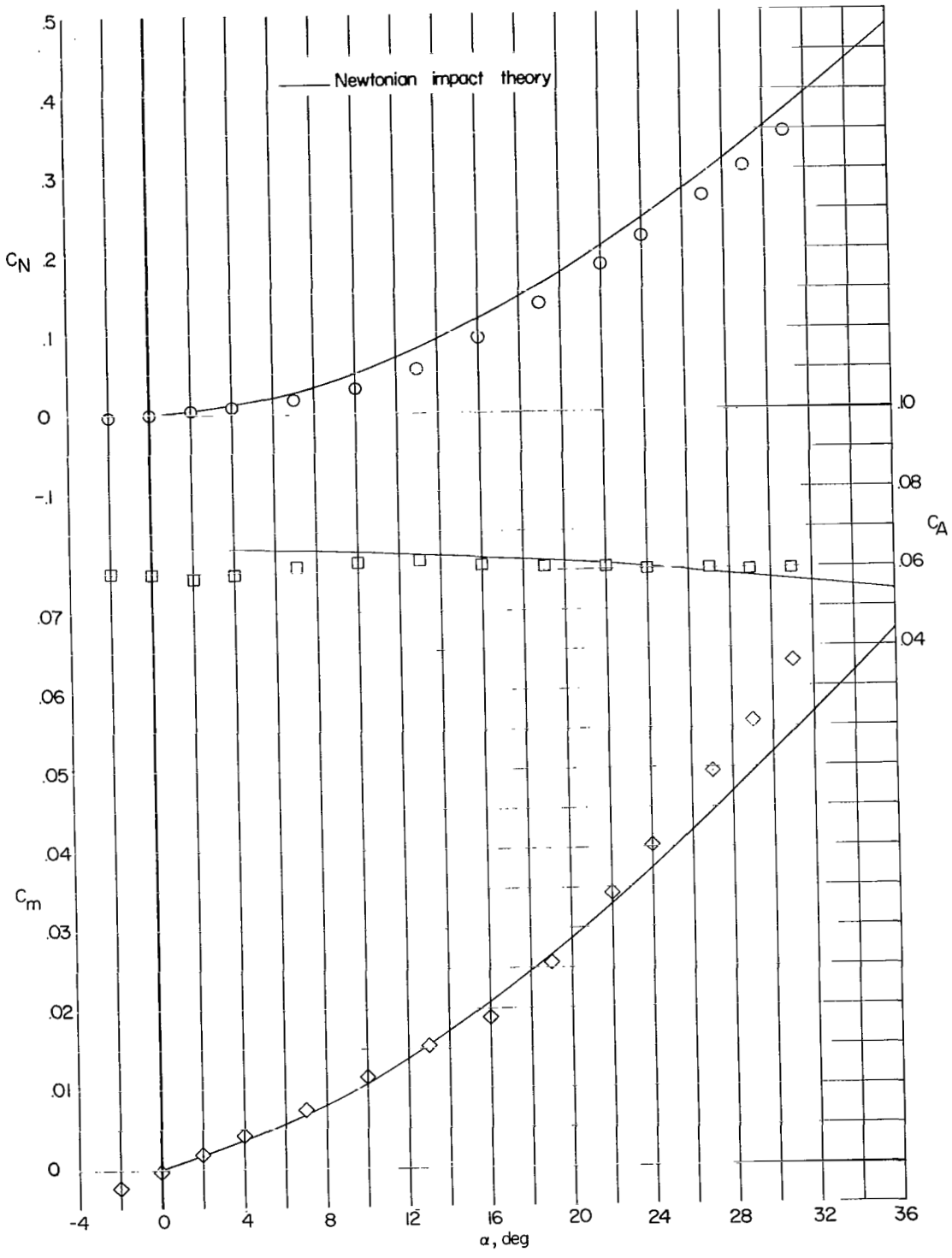

Figure 29.- Basic aerodynamic characteristics. t/c = 0.083; Λ = 90°.

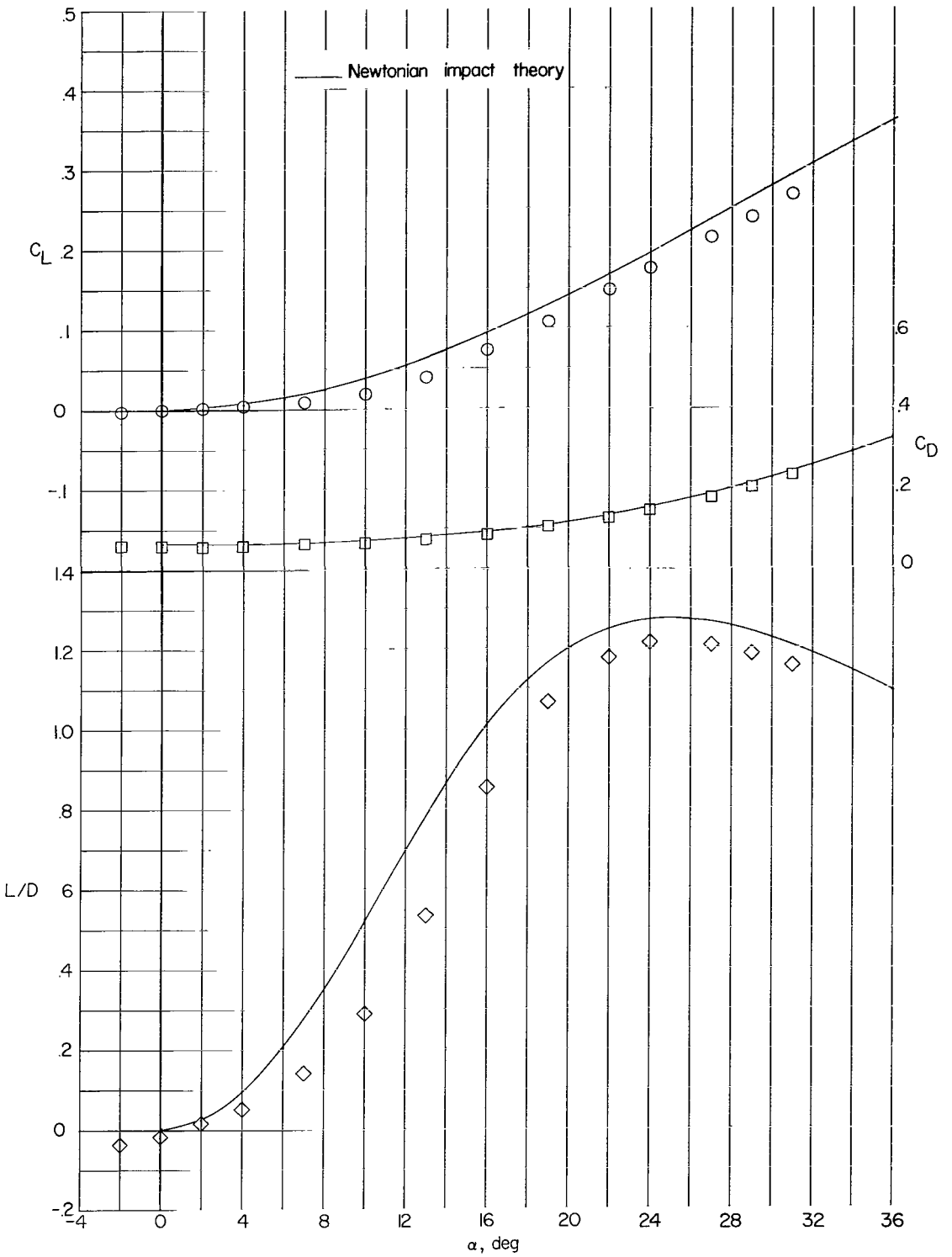

Figure 29.- Concluded.

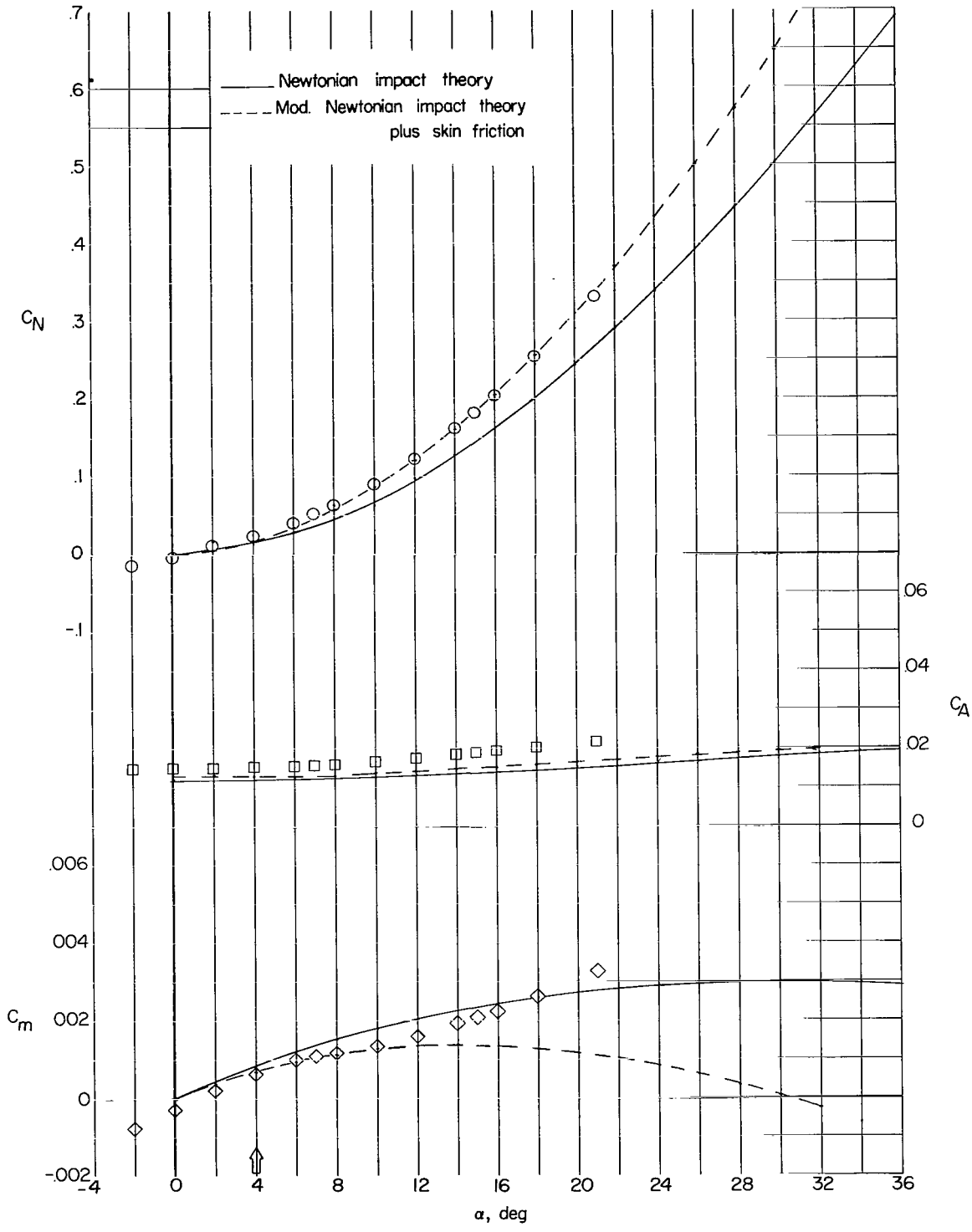

Figure 30.- Basic aerodynamic characteristics. t/c = 0.033; Λ = 70°.

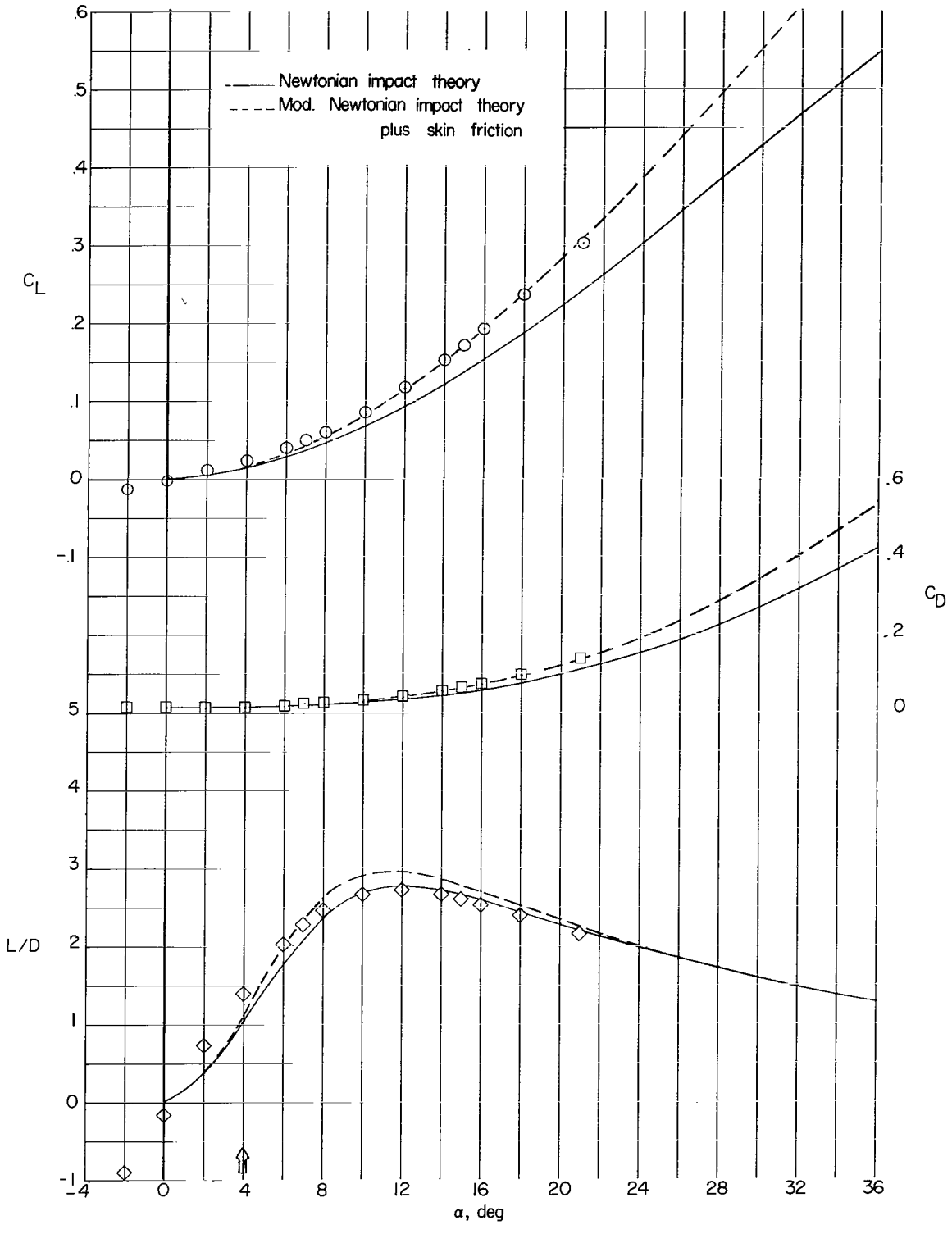

Figure 30.- Concluded.

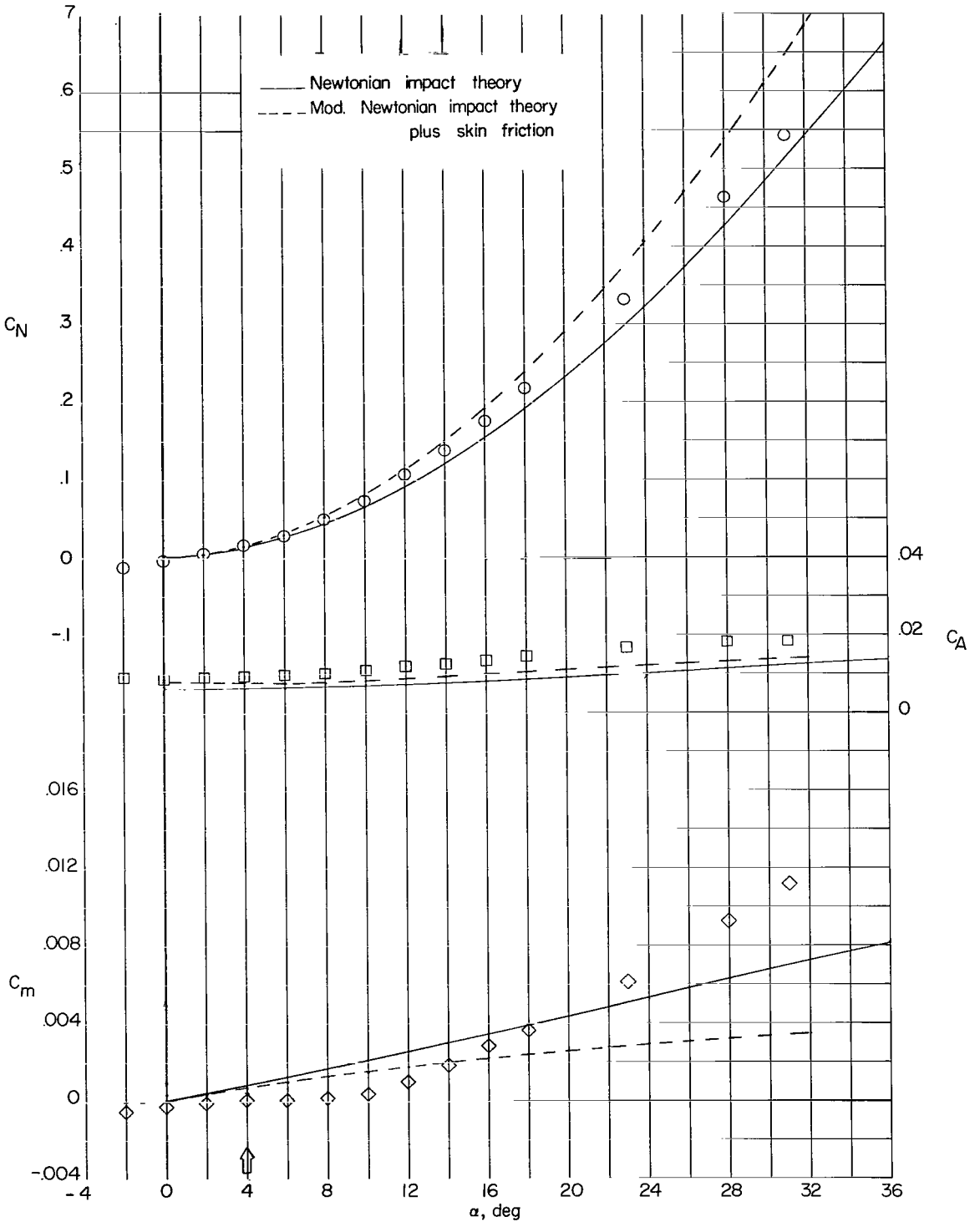

Figure 31.- Basic aerodynamic characteristics. t/c = 0.033; Λ = 80°.

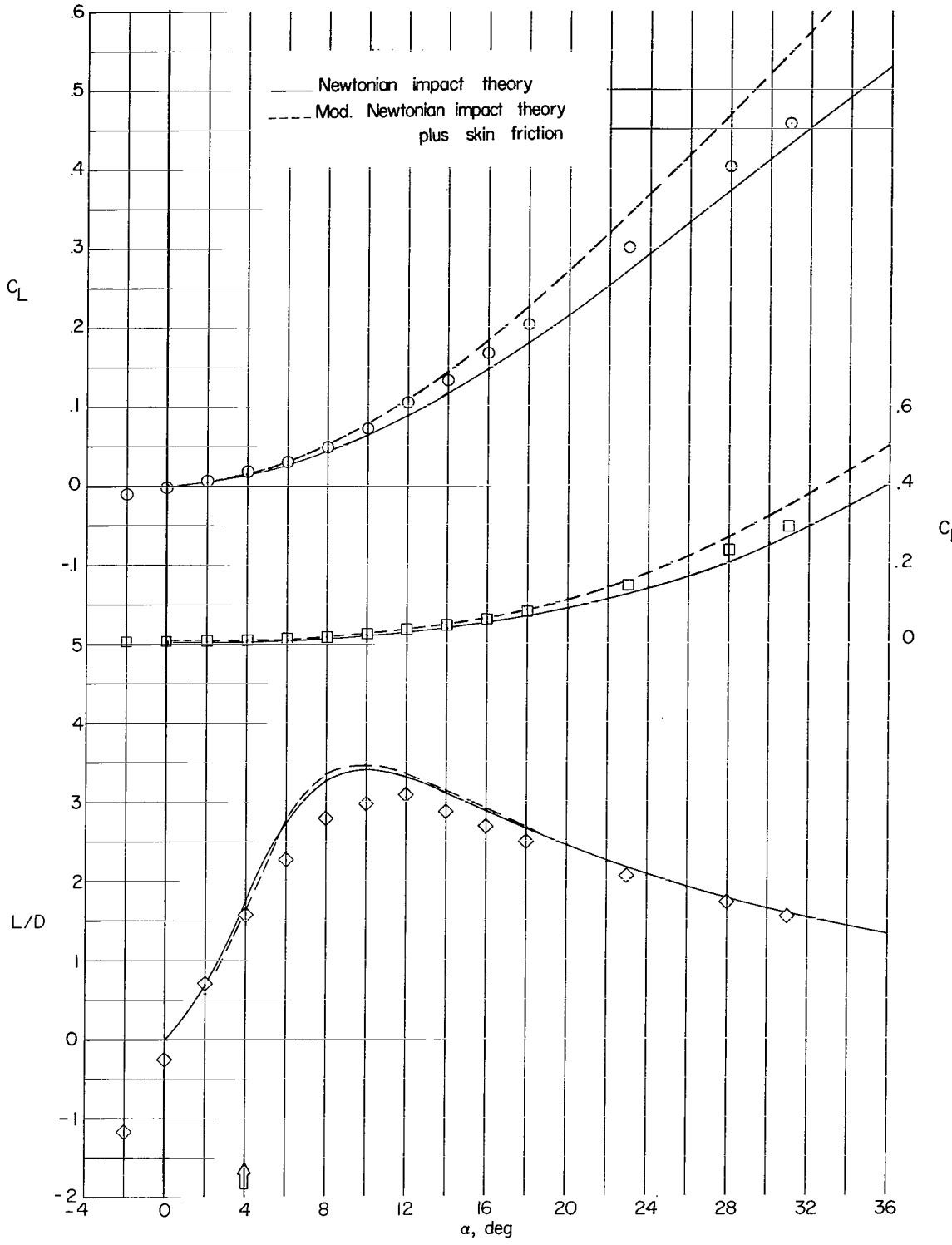

Figure 31.- Concluded.

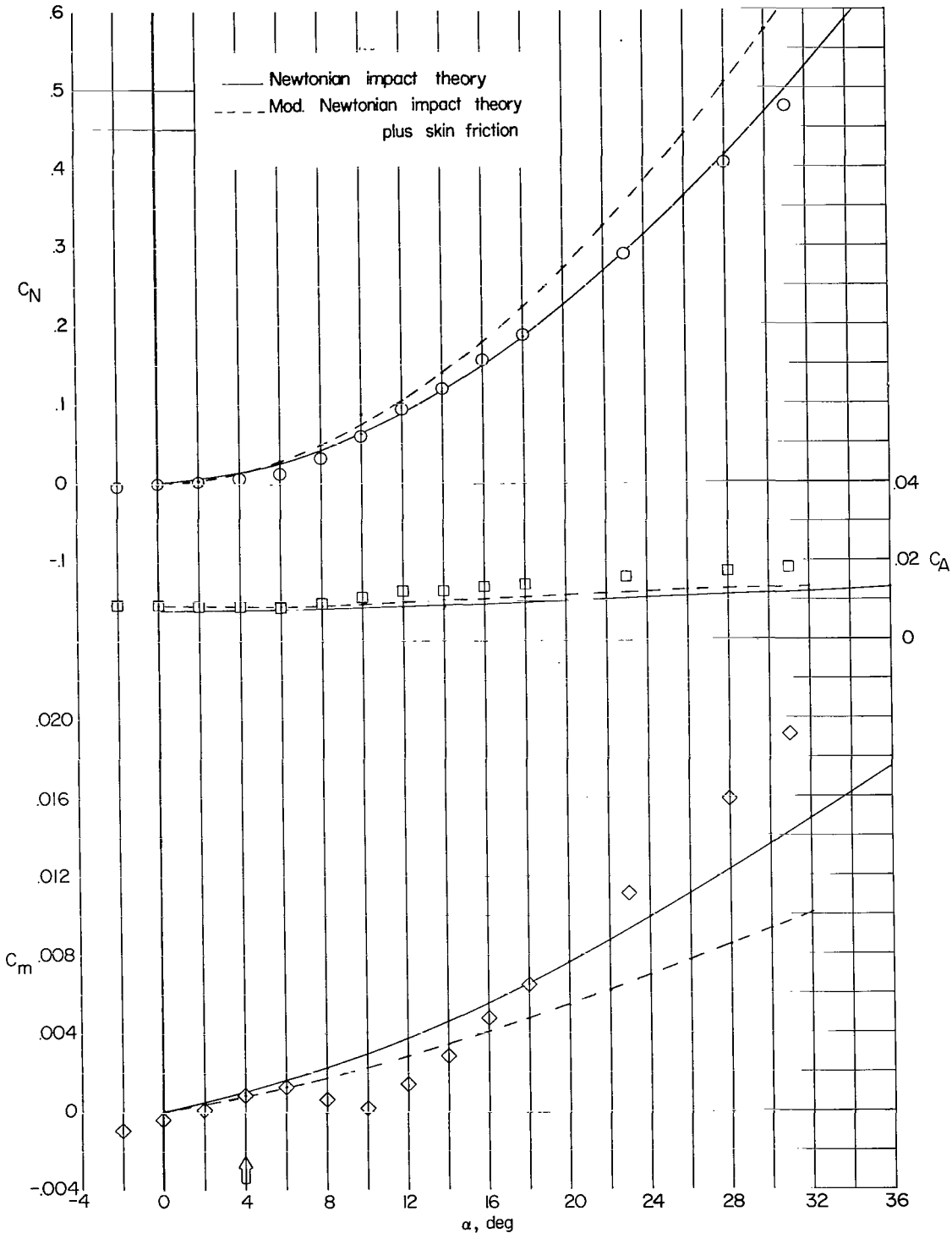

Figure 32.- Basic aerodynamic characteristics. t/c = 0.033; Λ = 85°.

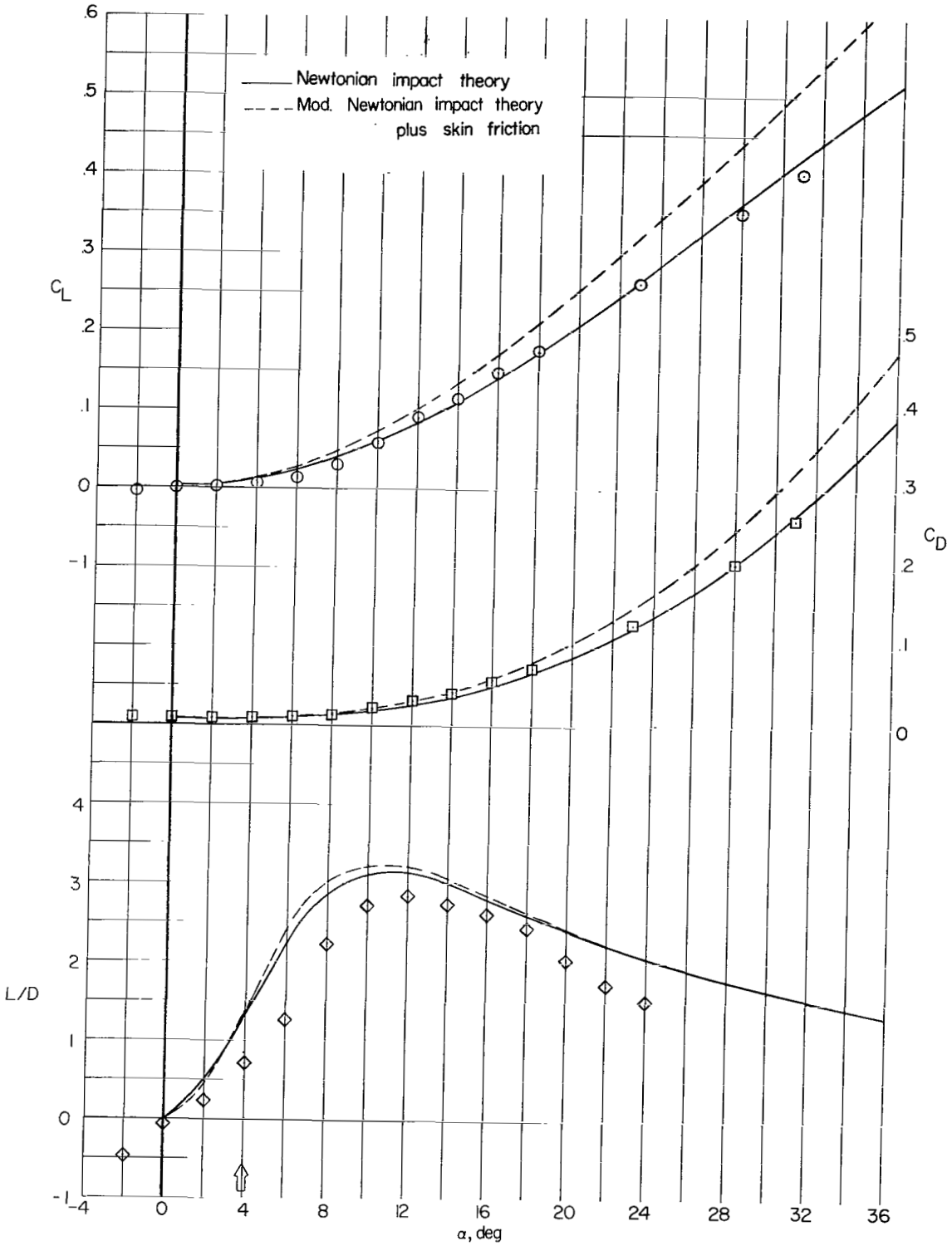

Figure 32.- Concluded.

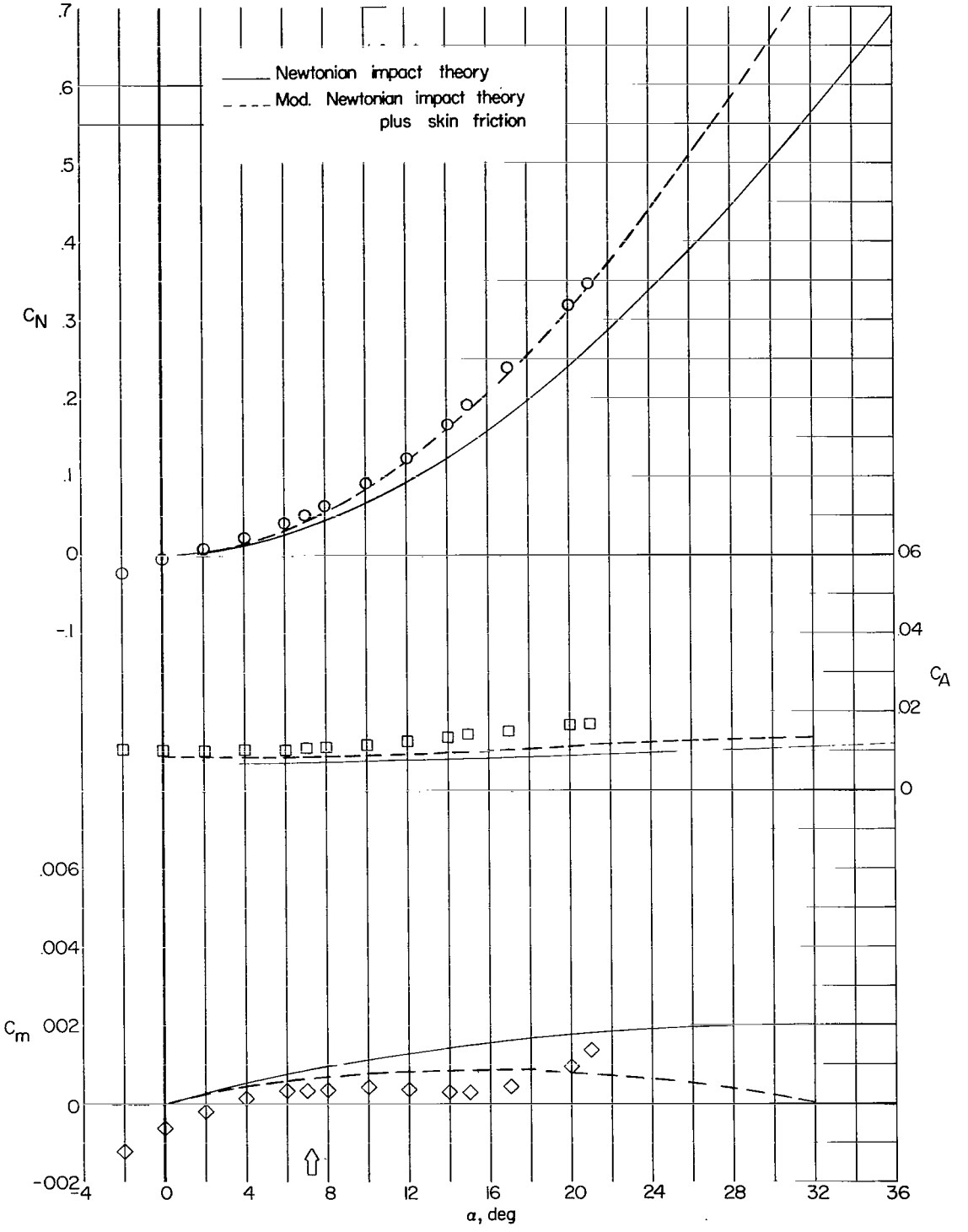

Figure 33.- Basic aerodynamic characteristics. t/c = 0.020; Λ = 70°.

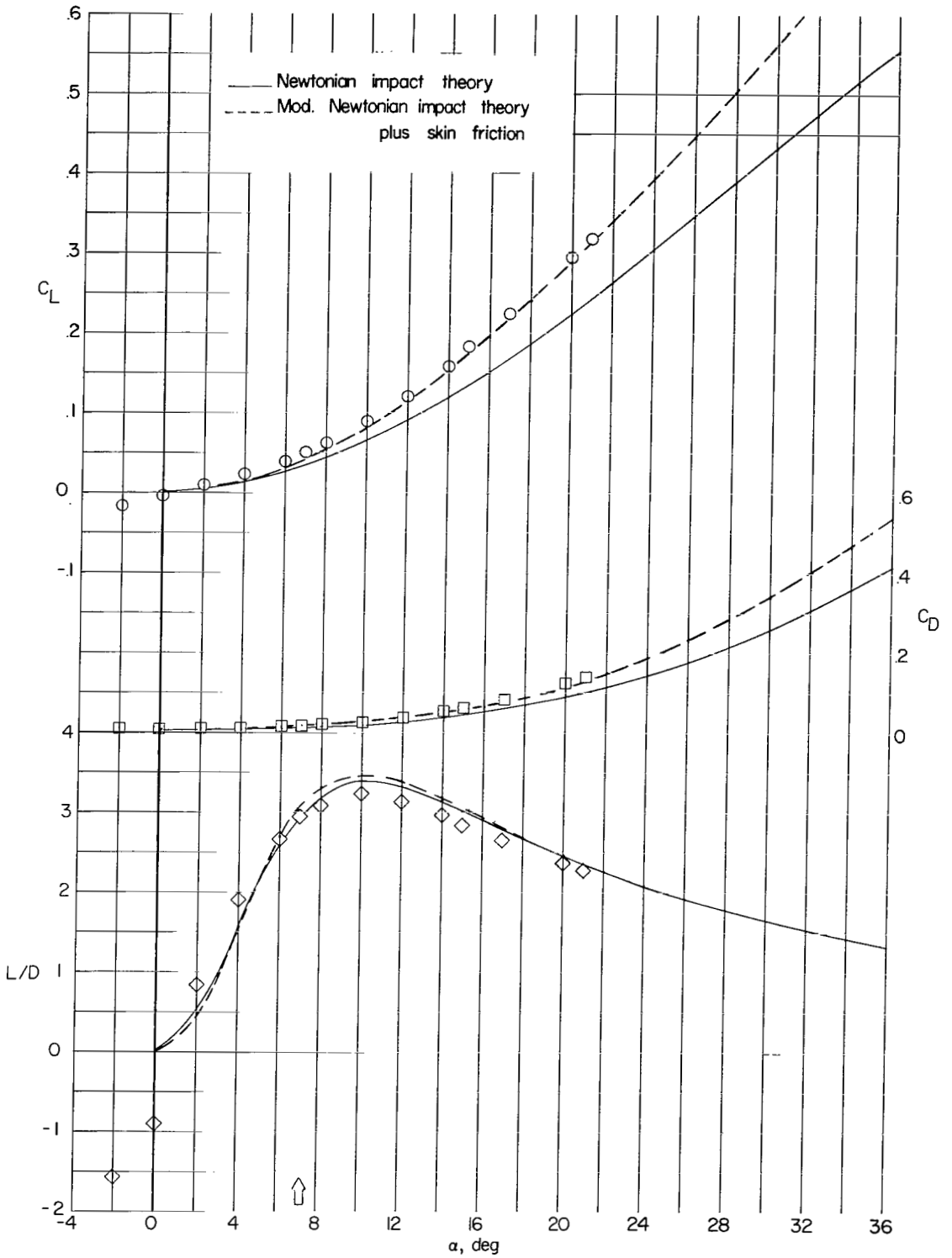

Figure 33.- Concluded.

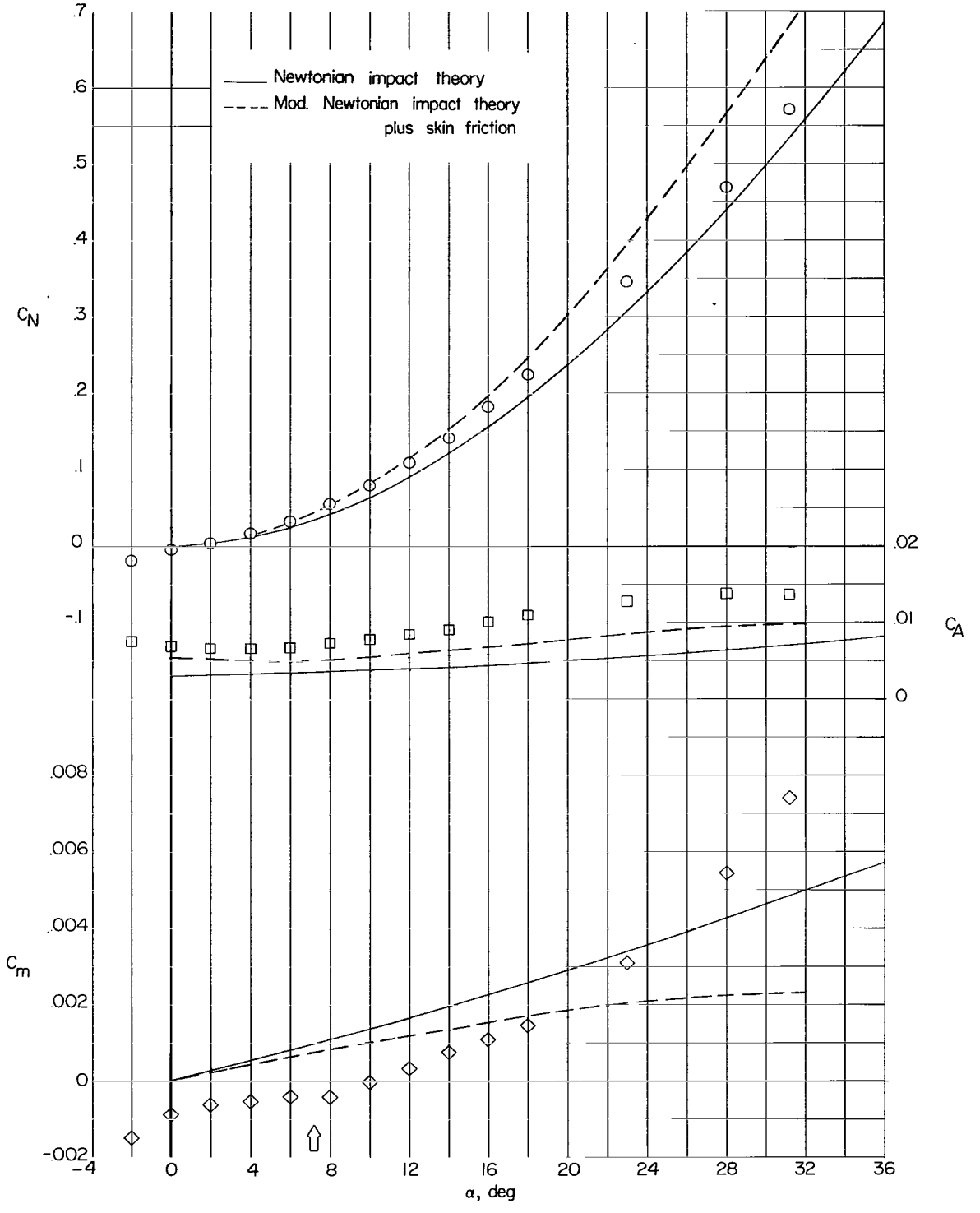

Figure 34.- Basic aerodynamic data. t/c = 0.020; Λ = 80°.

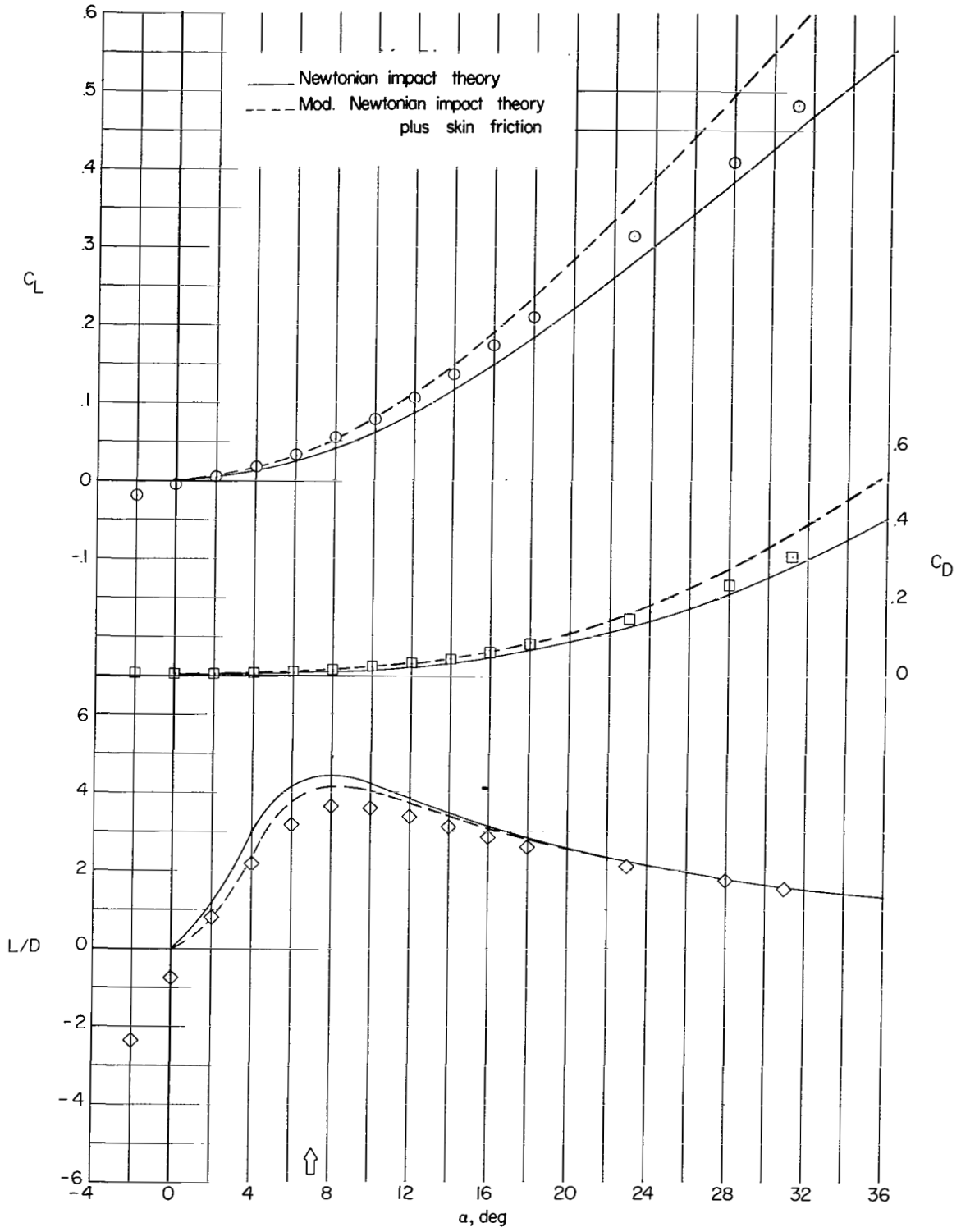

Figure 34.- Concluded.

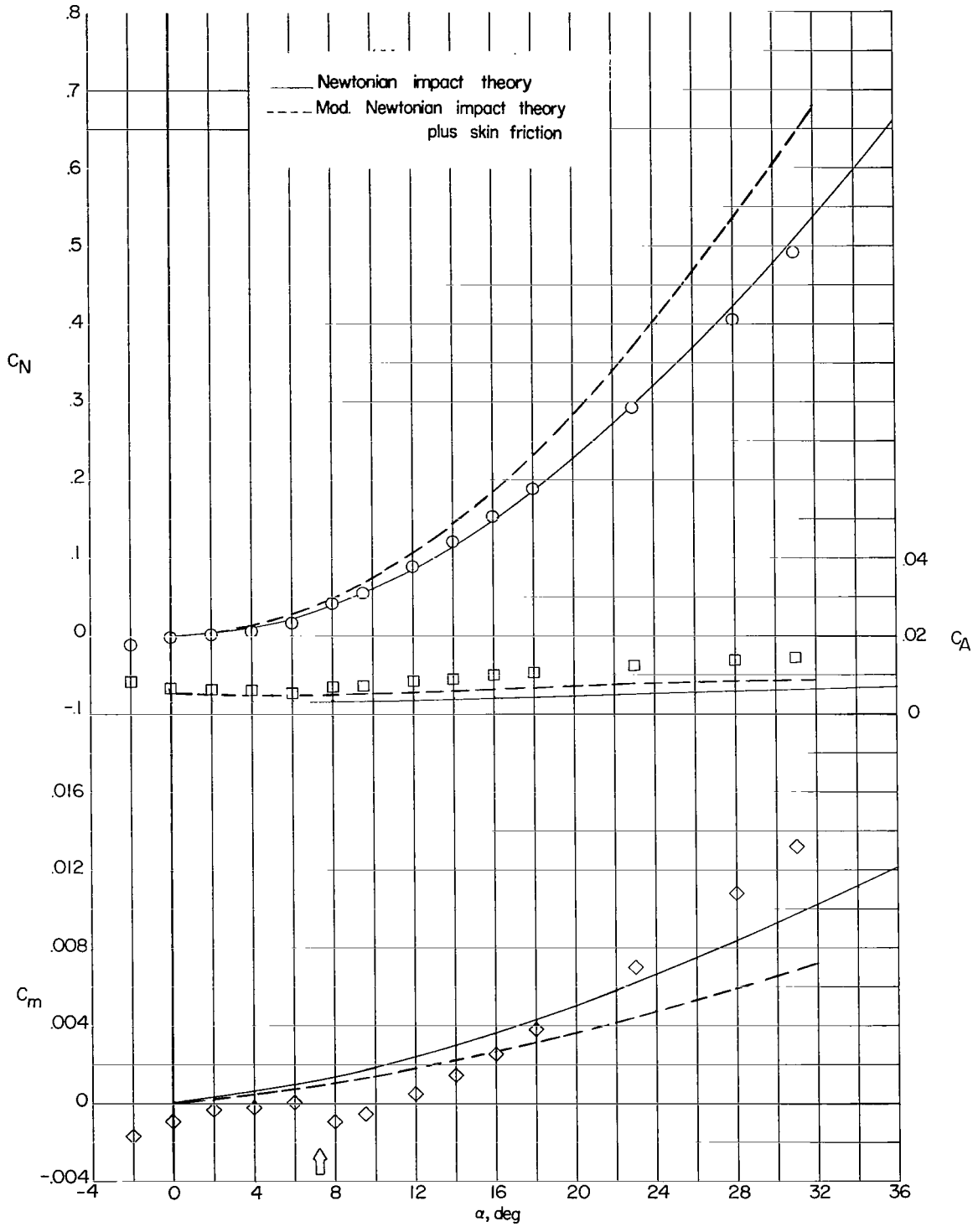

Figure 35.- Basic aerodynamic data. t/c = 0.020; Λ = 85°.

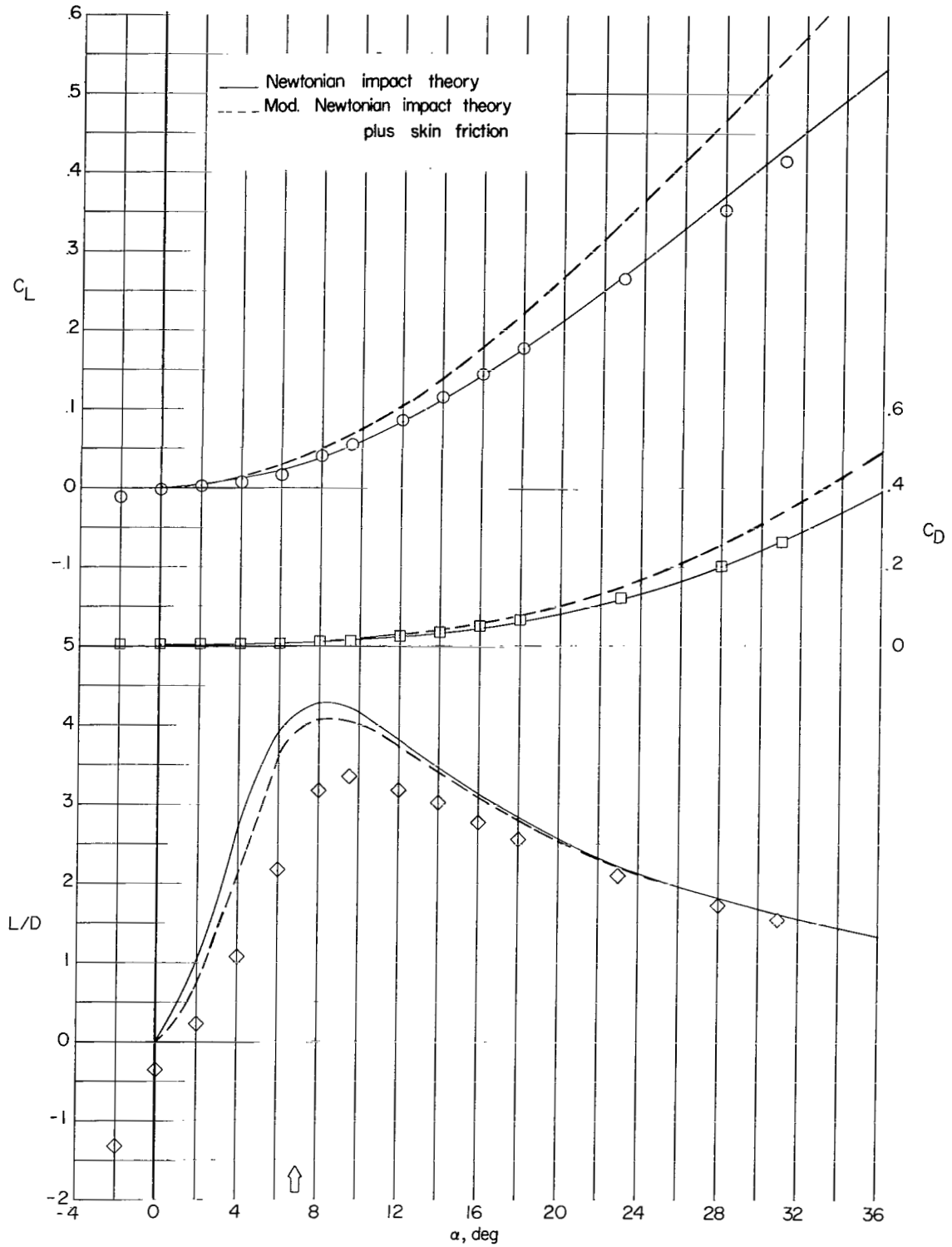

Figure 35.- Concluded.

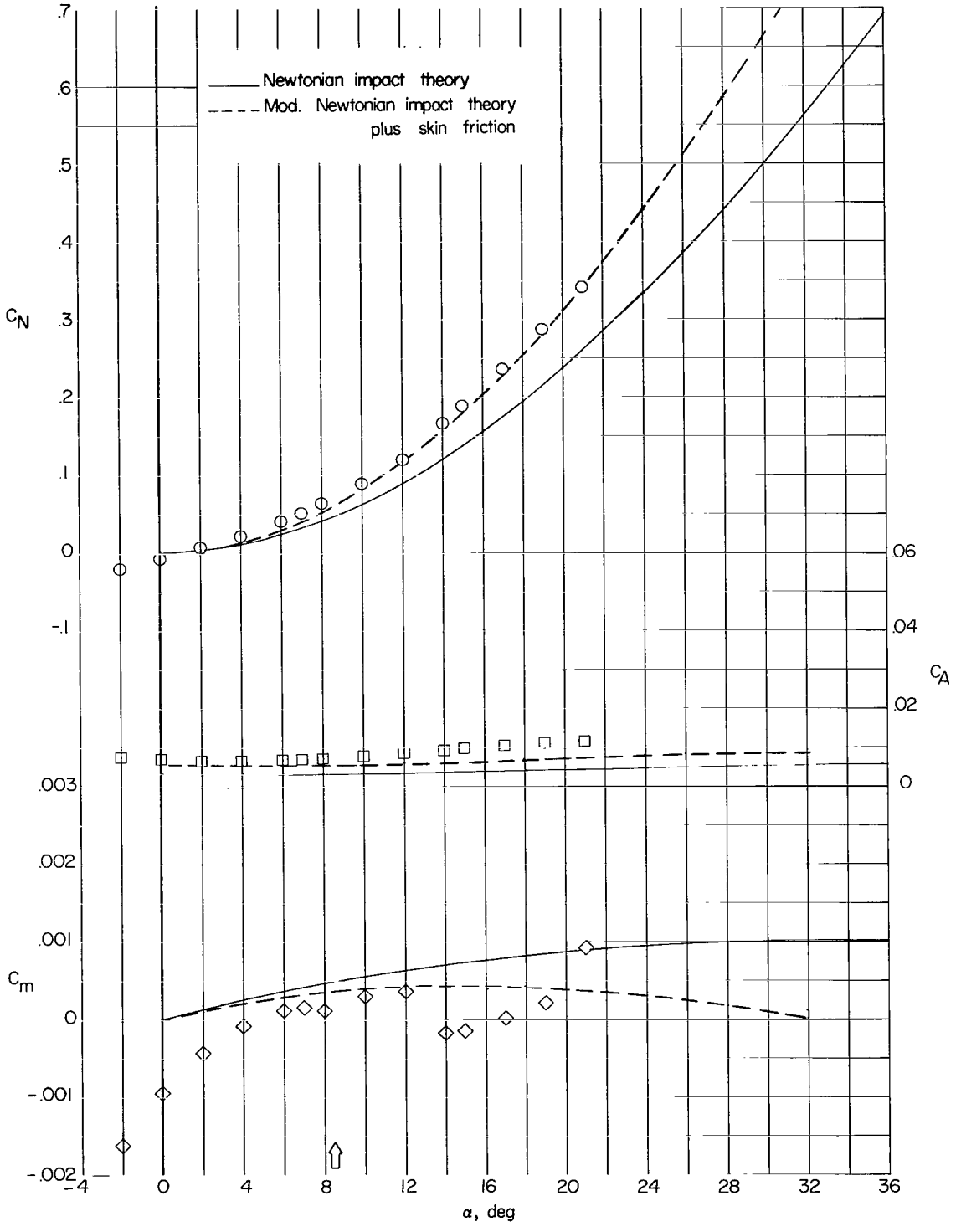

Figure 36.- Basic aerodynamic characteristics. t/c = 0.010; $\Lambda = 70^0$.

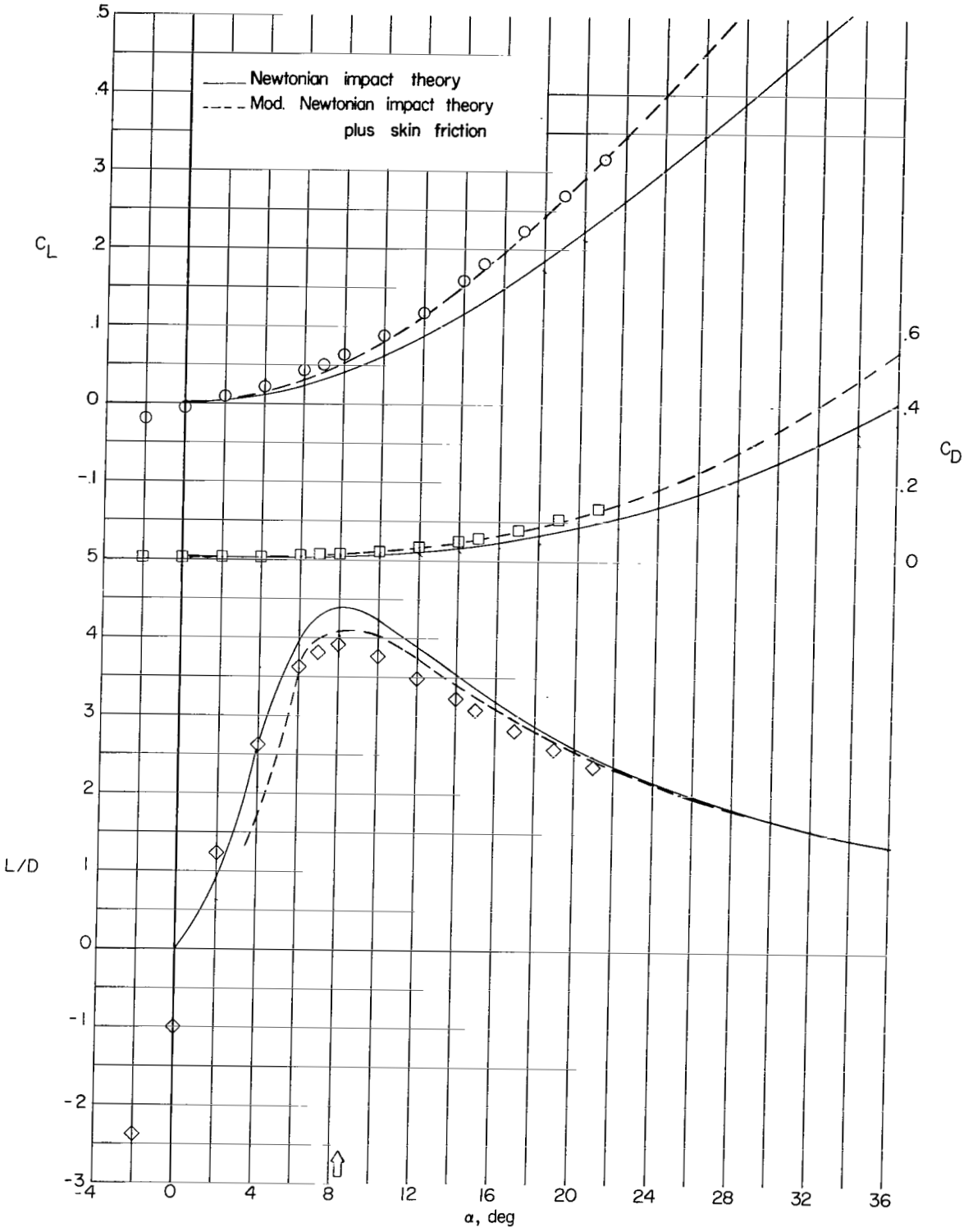

Figure 36.- Concluded.

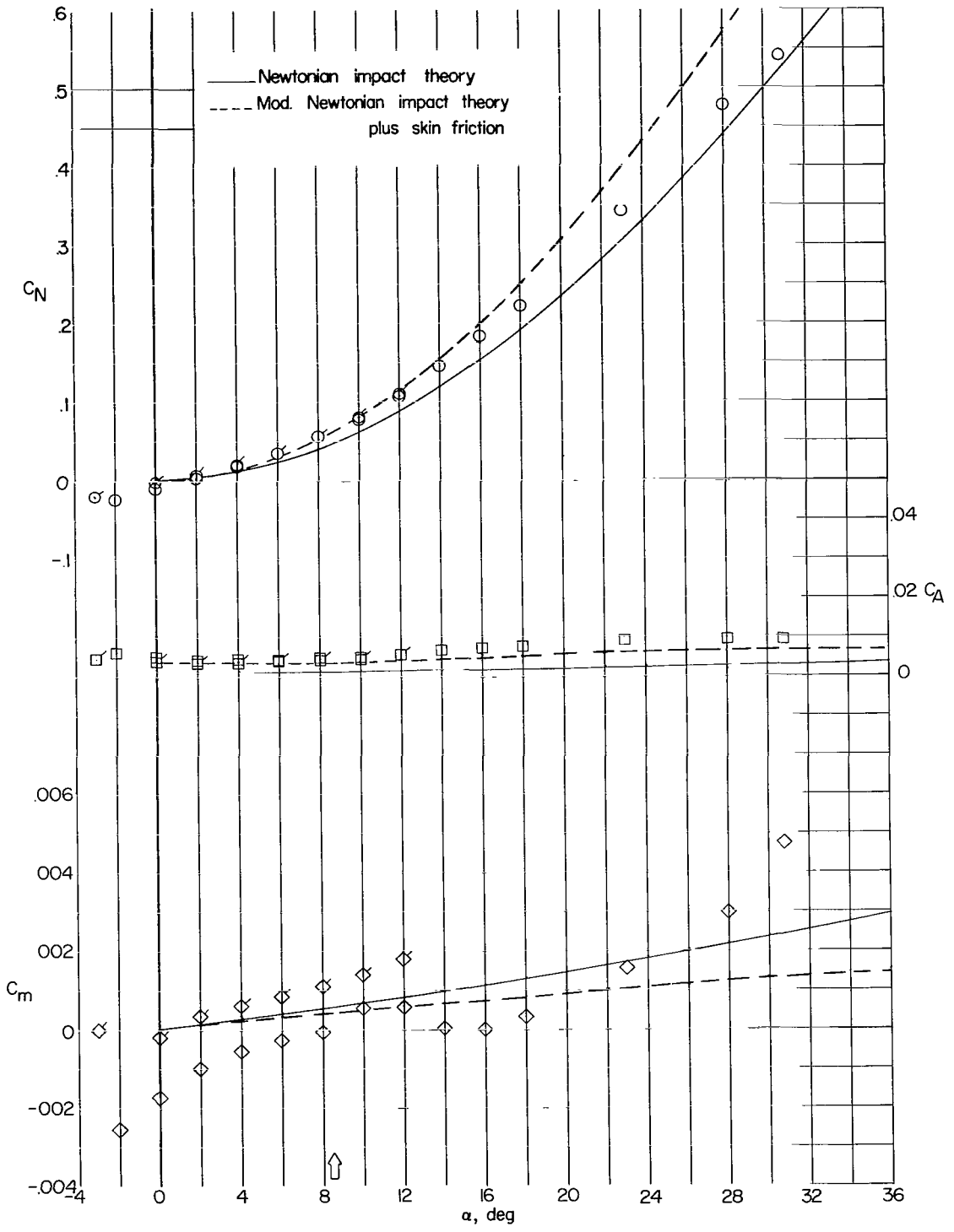

Figure 37.- Basic aerodynamic characteristics. t/c = 0.010; Λ = 80°. Flagged symbols denote use of small balance-housing body; unflagged symbols, of large balance-housing body.

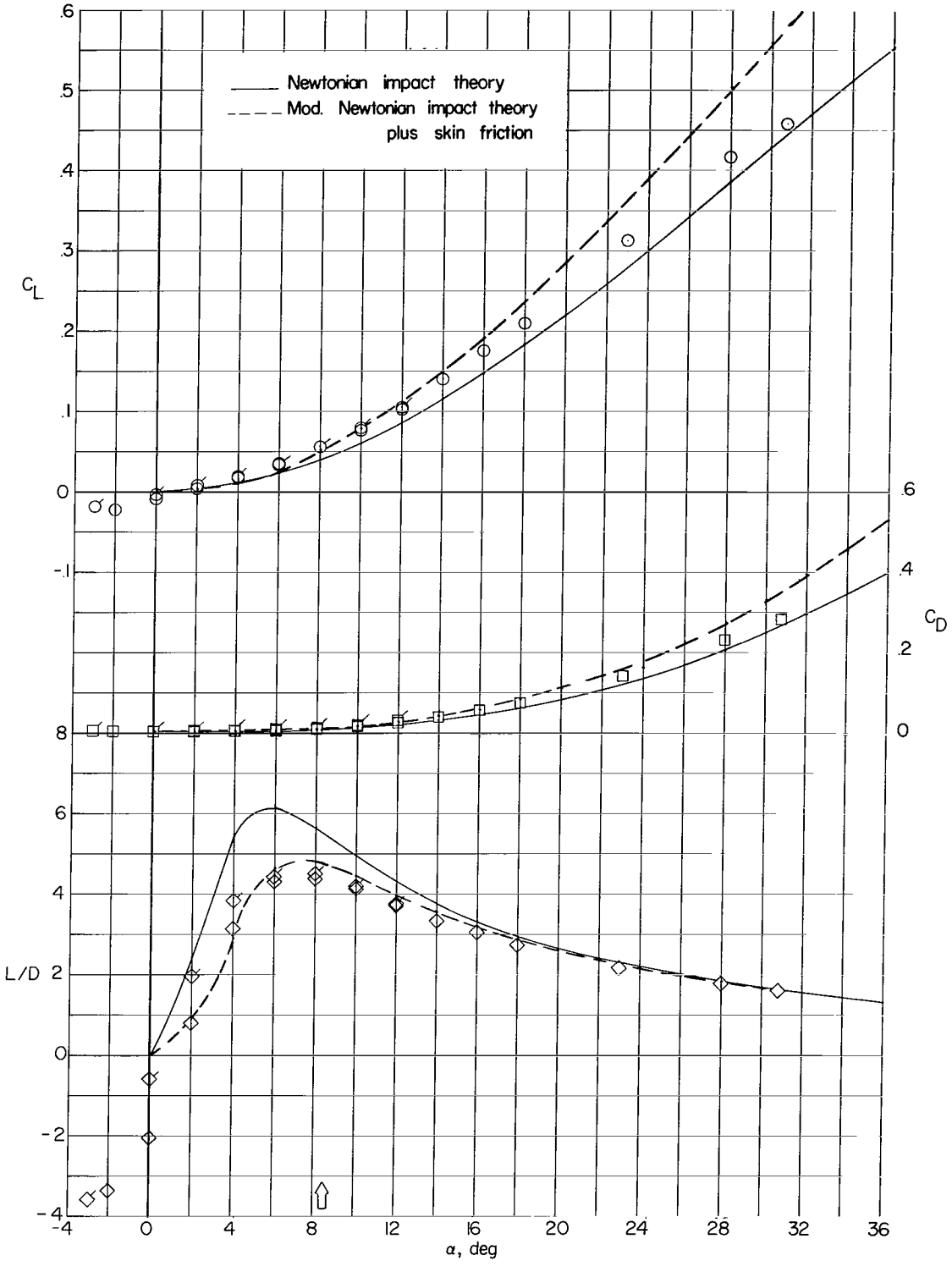

Figure 37.- Concluded.

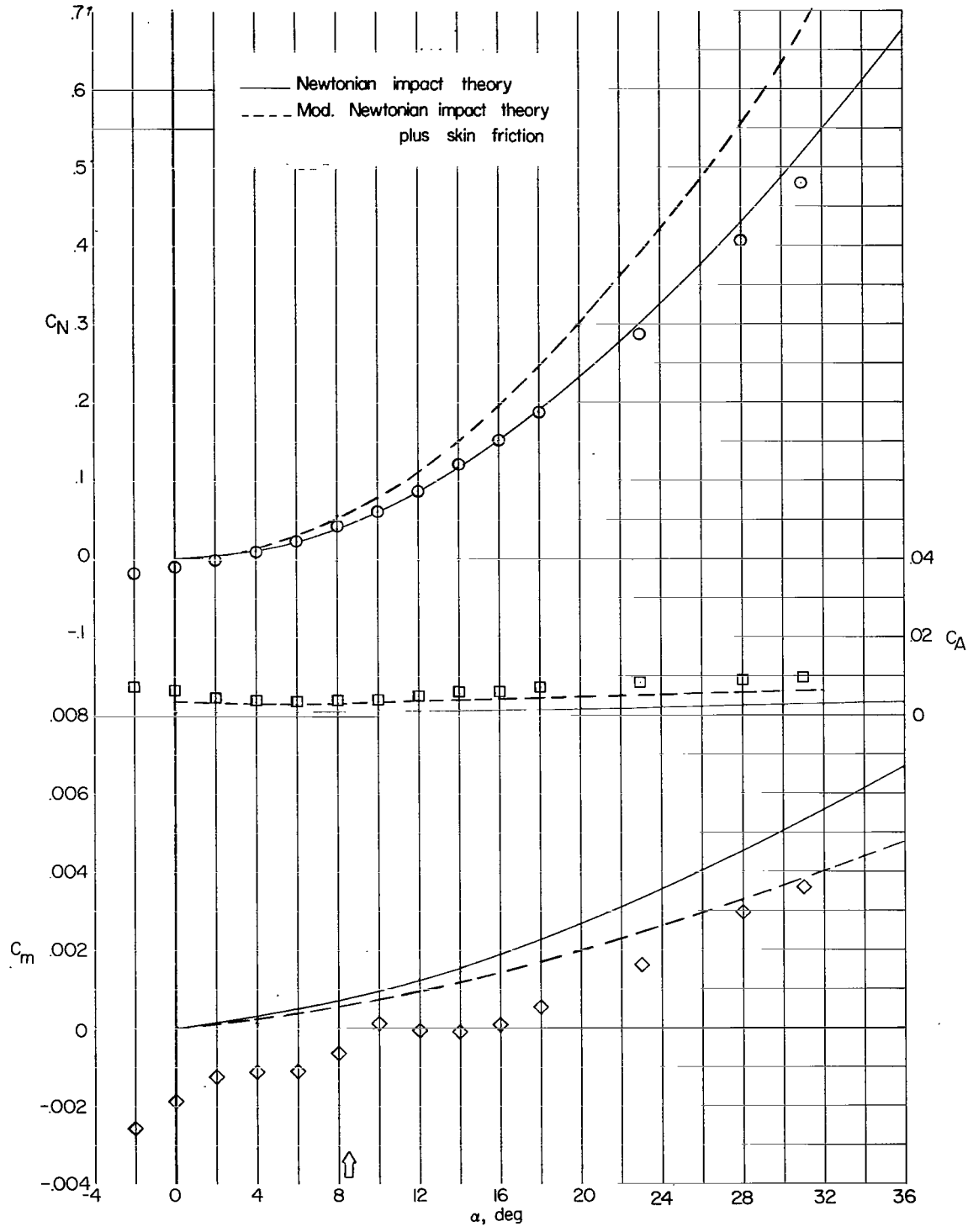

Figure 38.- Basic aerodynamic characteristics. t/c = 0.010; Λ = 85°.

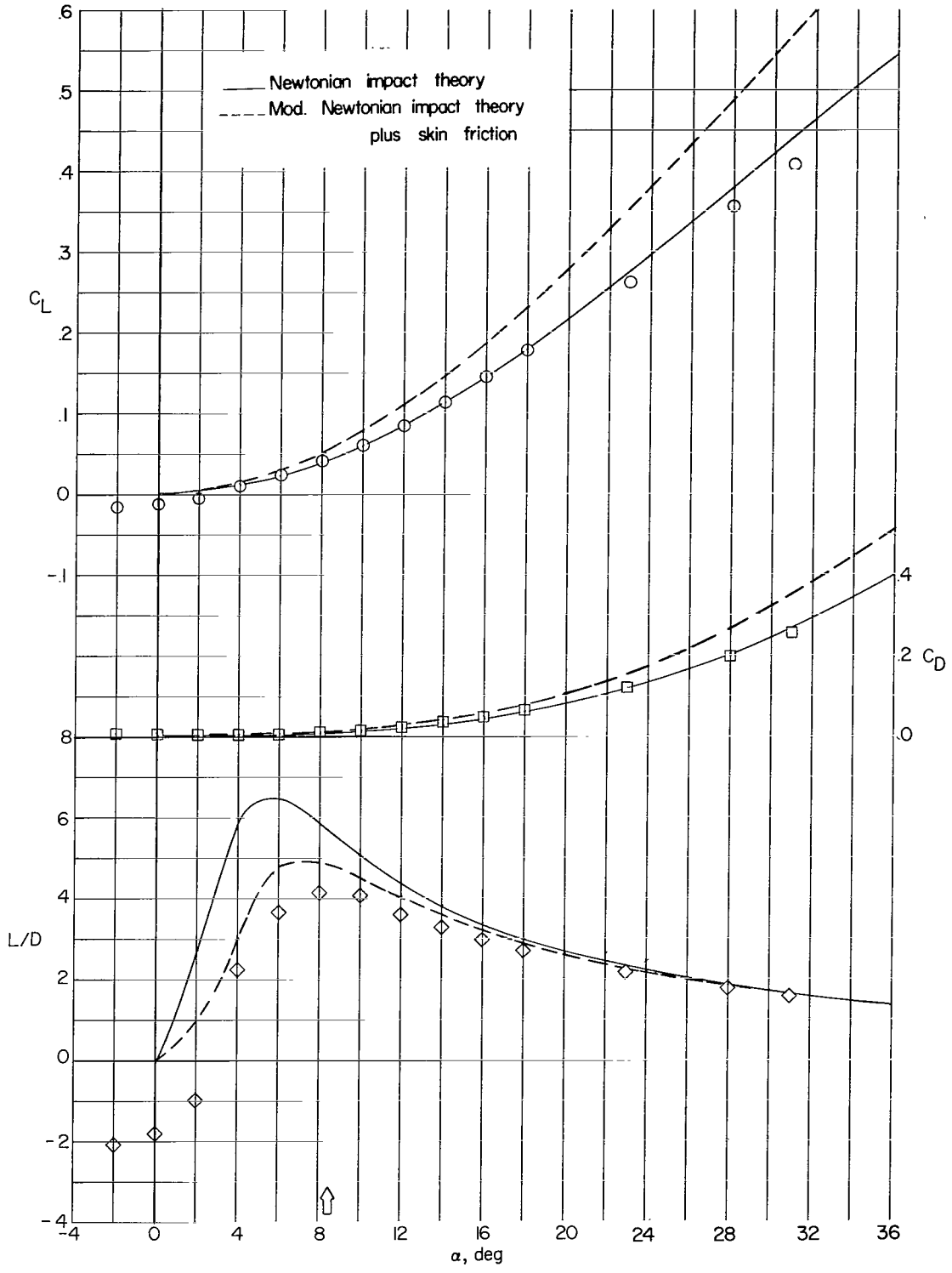

Figure 38.- Concluded.

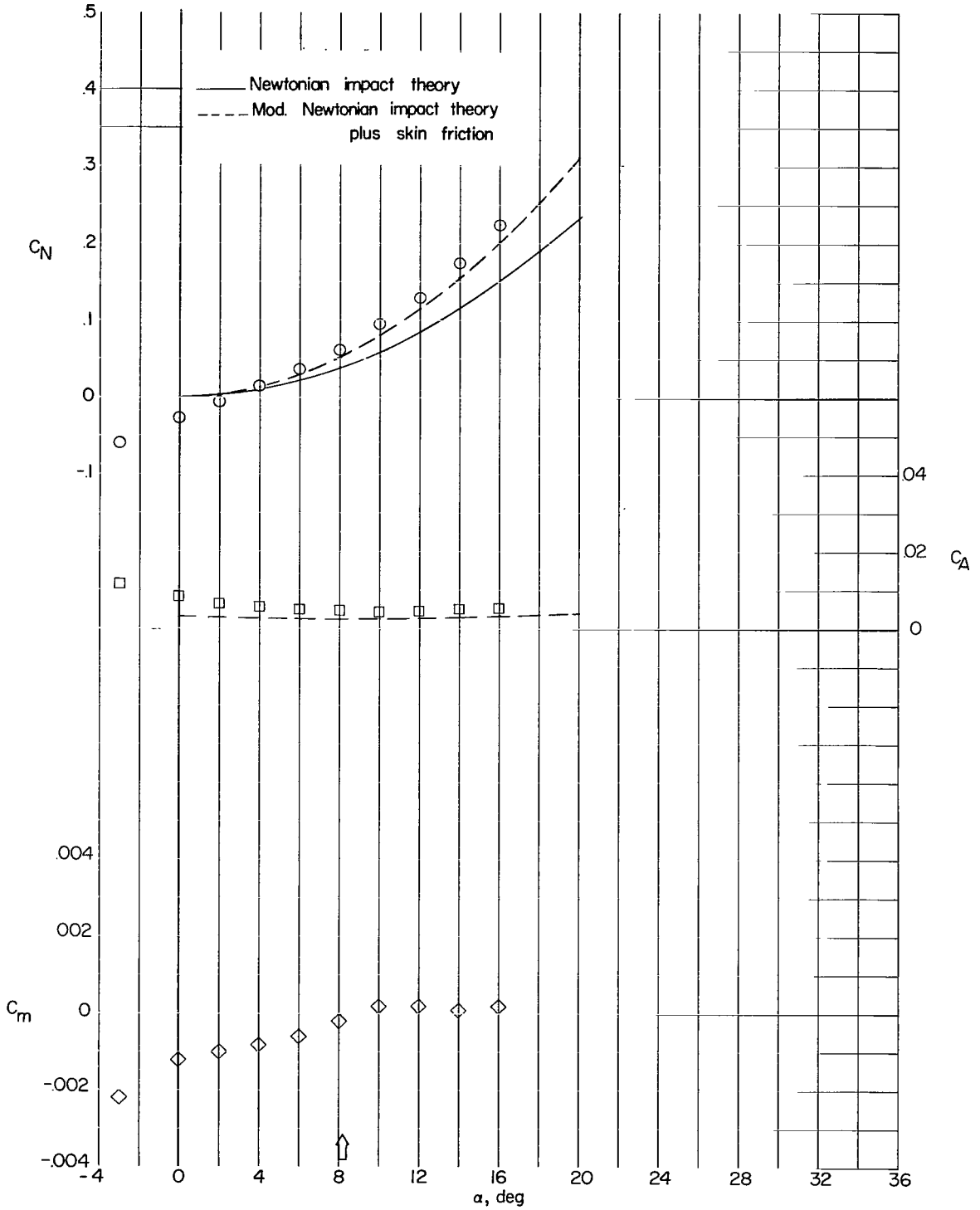

Figure 39.- Basic aerodynamic characteristics. t/c = 0; Λ = 60°.

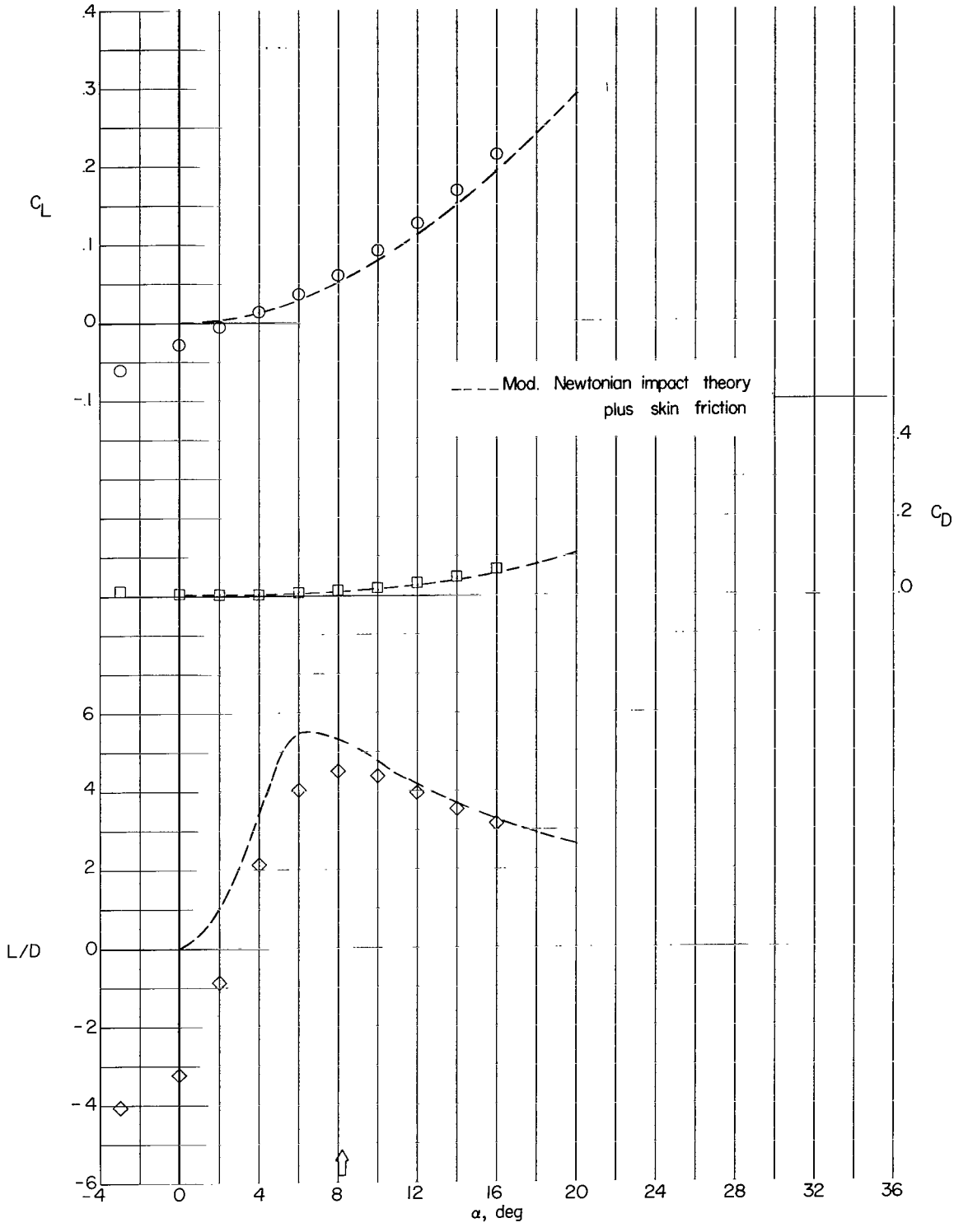

Figure 39.- Concluded.

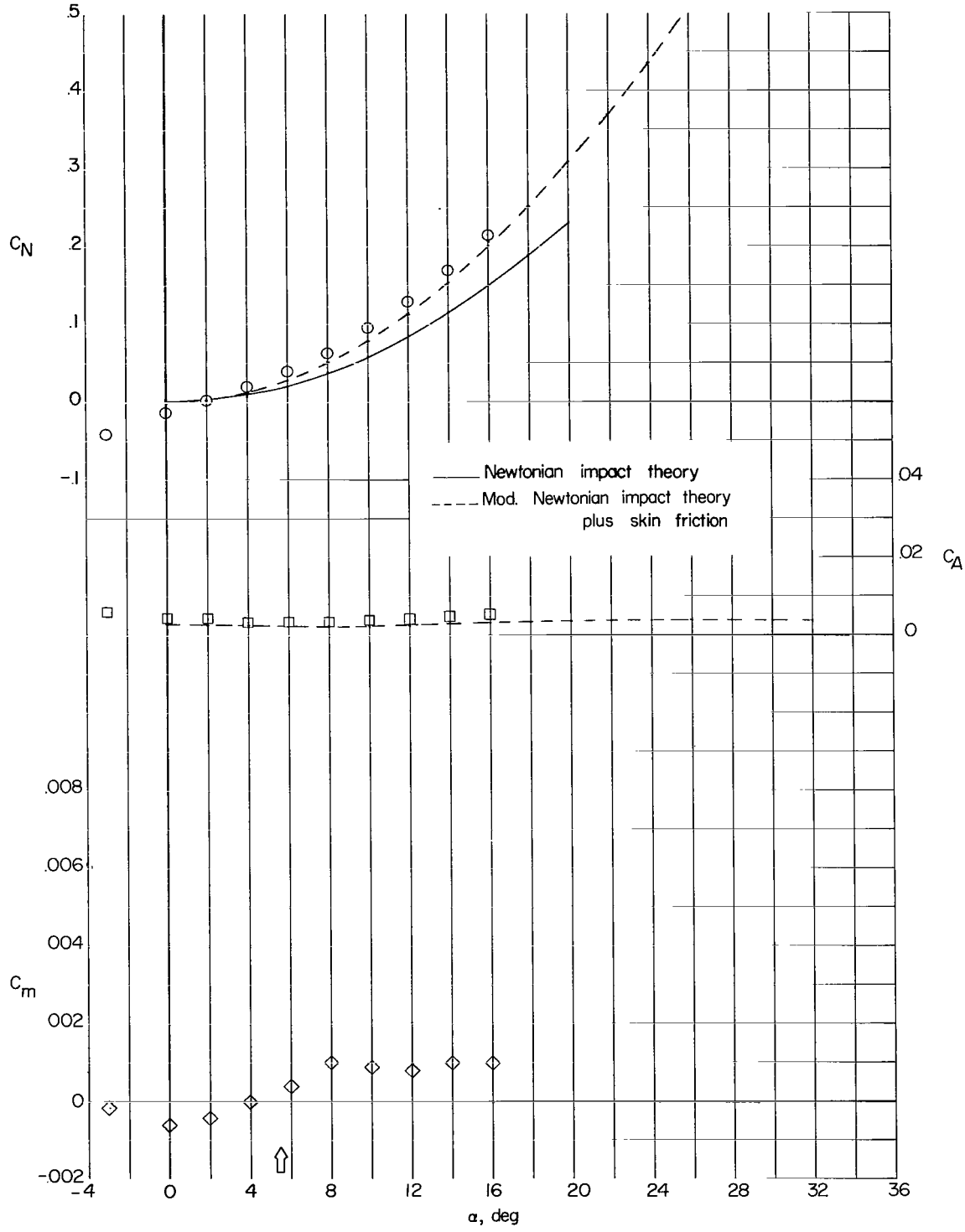

Figure 40.- Basic aerodynamic characteristics. t/c = 0; $\Lambda = 70^0$.

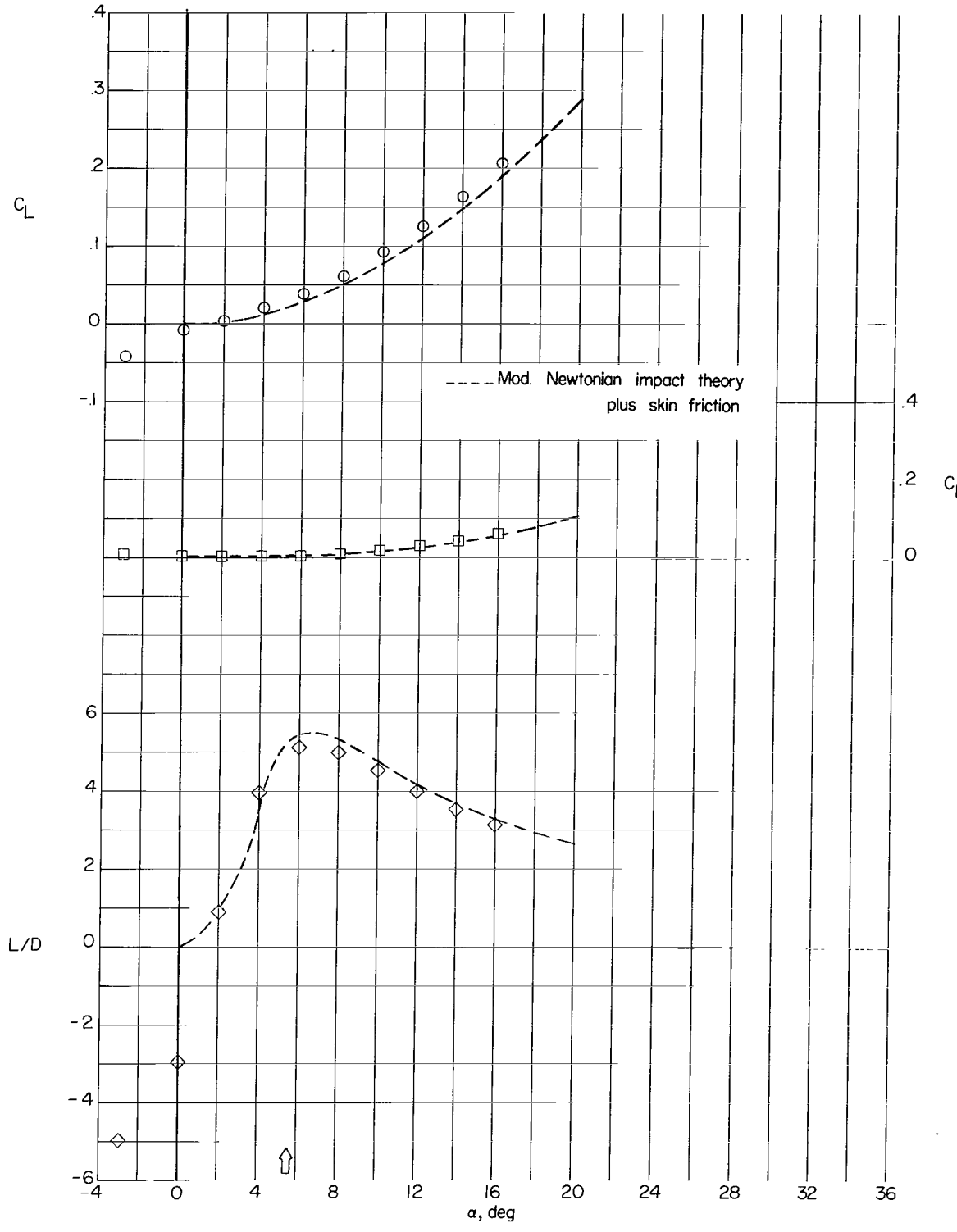

Figure 40.- Concluded.

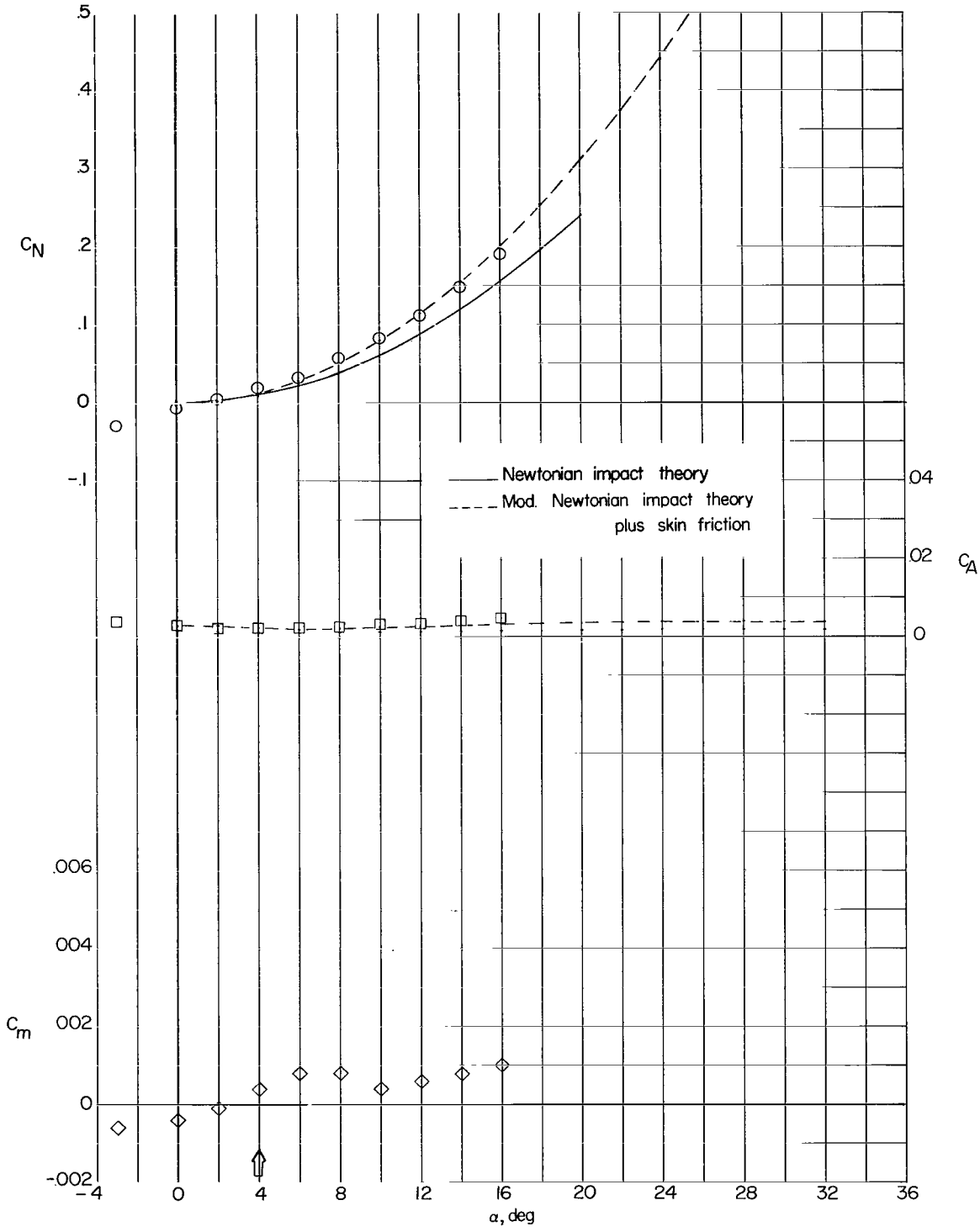

Figure 41.- Basic aerodynamic characteristics. $t/c = 0$; $\Lambda = 80^0$.

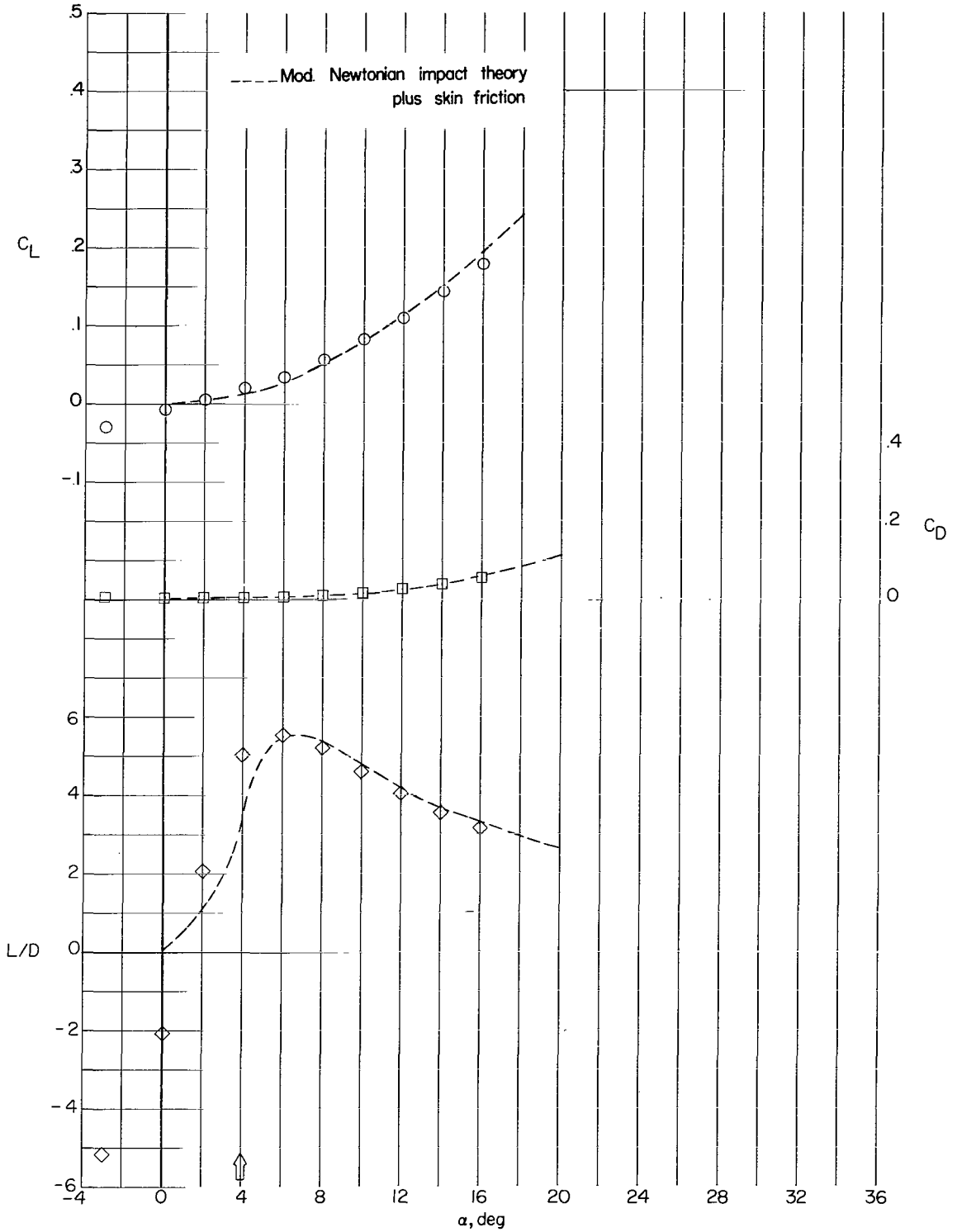

Figure 41.- Concluded.

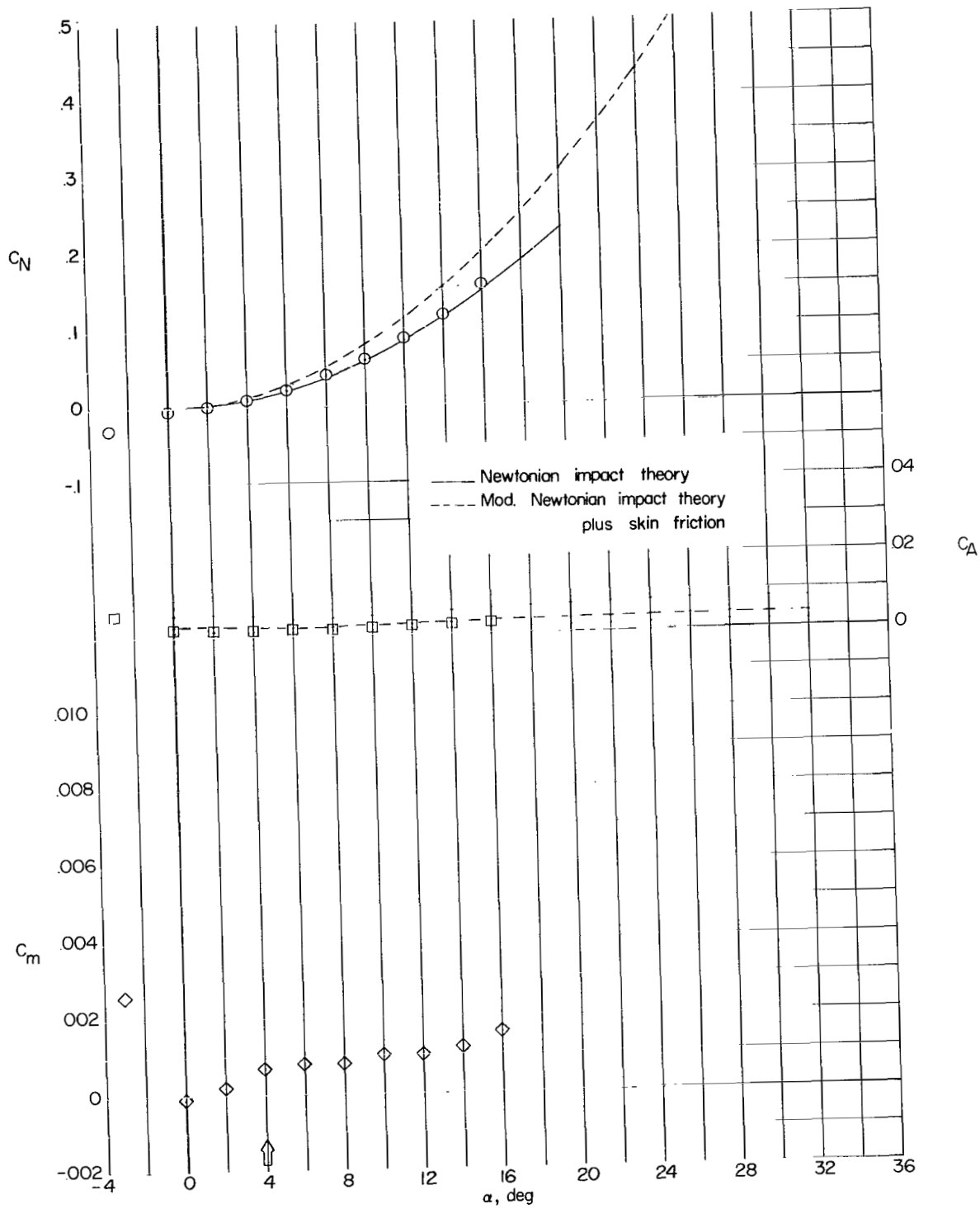

Figure 42.- Basic aerodynamic characteristics. t/c = 0; $\Lambda = 85^0$.

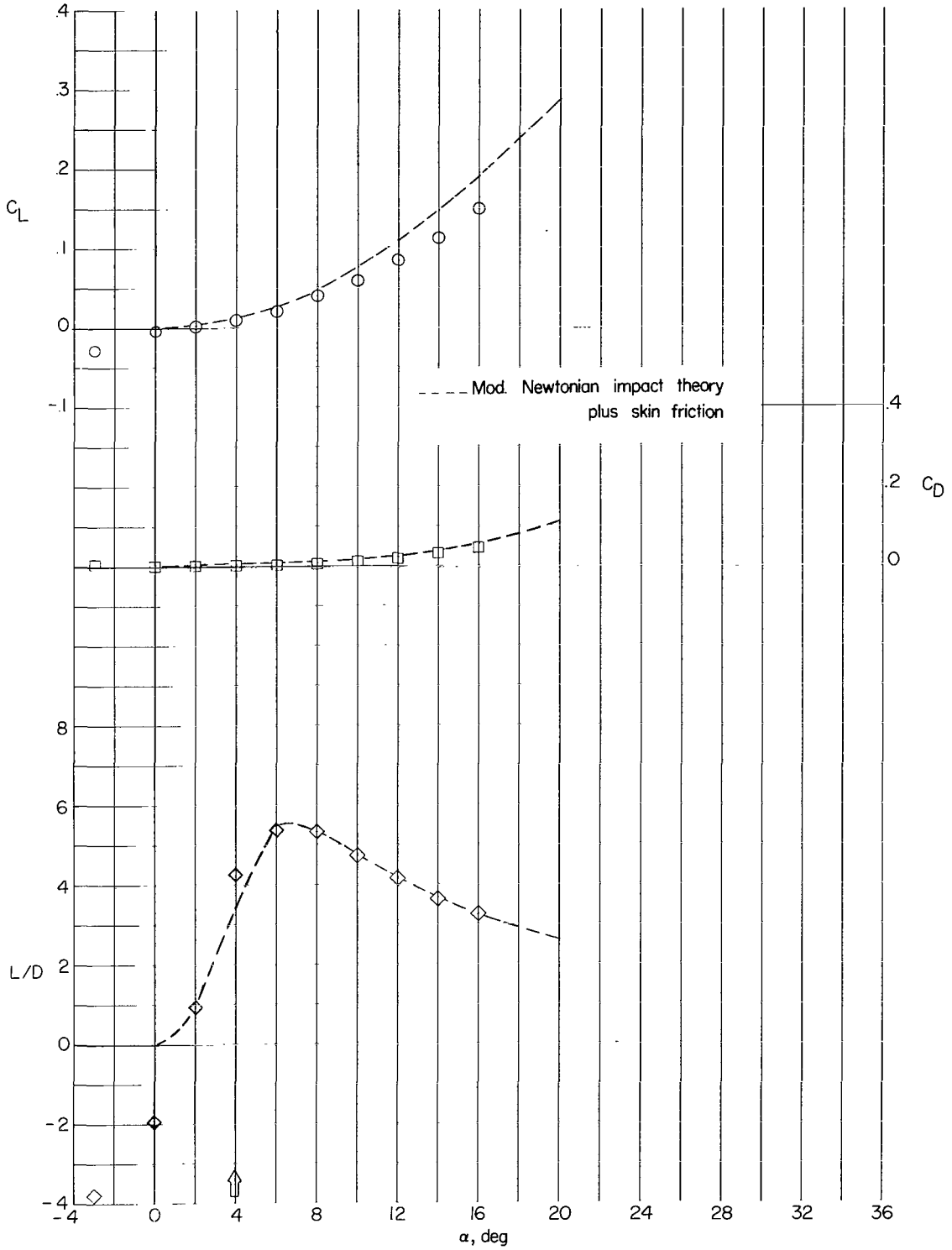

Figure 42.- Concluded.

"The aeronautical and space activities of the United States shall be conducted so as to contribute . . . to the expansion of human knowledge of phenomena in the atmosphere and space. The Administration shall provide for the widest practicable and appropriate dissemination of information concerning its activities and the results thereof."

—NATIONAL AERONAUTICS AND SPACE ACT OF 1958

NASA SCIENTIFIC AND TECHNICAL PUBLICATIONS

TECHNICAL REPORTS: Scientific and technical information considered important, complete, and a lasting contribution to existing knowledge.

TECHNICAL NOTES: Information less broad in scope but nevertheless of importance as a contribution to existing knowledge.

TECHNICAL MEMORANDUMS: Information receiving limited distribution because of preliminary data, security classification, or other reasons.

CONTRACTOR REPORTS: Technical information generated in connection with a NASA contract or grant and released under NASA auspices.

TECHNICAL TRANSLATIONS: Information published in a foreign language considered to merit NASA distribution in English.

TECHNICAL REPRINTS: Information derived from NASA activities and initially published in the form of journal articles.

SPECIAL PUBLICATIONS: Information derived from or of value to NASA activities but not necessarily reporting the results of individual NASA-programmed scientific efforts. Publications include conference proceedings, monographs, data compilations, handbooks, sourcebooks, and special bibliographies.

Details on the availability of these publications may be obtained from:

SCIENTIFIC AND TECHNICAL INFORMATION DIVISION

NATIONAL AERONAUTICS AND SPACE ADMINISTRATION

Washington, D.C. 20546